# Applicability of wireless injectable microstimulators based on volume conduction for high density neuromuscular stimulation

Ahmed Fayez Eladly

TESI DOCTORAL UPF / 2021

Director:

Dr. Antoni Ivorra Cano

DEPARTMENT OF INFORMATION AND COMMUNICATION TECHNOLOGIES

UNIVERSITAT POMPEU FABRA

This publication is part of a project that has received funding from the European Research Council (ERC) under the European Union's Horizon 2020 research and innovation programme (grant agreement No 724244).

# Acknowledgements

Firstly, I would like to express my sincerest gratitude to my PhD supervisor Dr. Antoni Ivorra Cano for granting me the opportunity to do what I love and pursue research under his tutelage in the exciting field of electrical stimulation. I am grateful for his patience, unwavering guidance and support that continued all throughout the course of my PhD and for the exciting scientific discussions we had which were a crucial part of my learning. I would especially like to thank him for creating a very interdisciplinary scientific environment that always challenged me and helped me navigate boundaries of different scientific fields with ease.

Secondly, I would like to thank Dr. Borja Mercadal, Marc Tudela-Pi, Dr. Jesús Minguillón, Dr. Tomás García-Sánchez and Dr. Laura Becerra-Fajardo, and Aracelys Garcia for their invaluable input, guidance, support and the scientific discussions I had the pleasure of having with them. I would also like to give special thanks and appreciation to Prof. Patri Vergara from the Universitat Autonoma de Barcelona for her support in providing rabbit carcasses so I could practice my surgical techniques on, Ms. Vera Lukesova for her technical assistance with the histochemical staining, and everyone in the Biomedical Electronics Research Group for the fun times I had during our coffee breaks, lunches and dinners.

Lastly, I would like to sincerely thank my beloved partner, Constantina, whom my PhD had taken the greatest toll on, for her support, kindness, and understanding. I would also like to thank my mom and dad for always championing me and for their never ending emotional/financial support. I dedicate this PhD to you!

*To Amr Kandil*

# Abstract

Wirelessly powered single-channel injectable intramuscular (IM) microstimulators represent an attractive approach for delivering multi-site stimulation needed to restore functional movement to paralyzed limbs since they can be implanted in a minimally invasive way. Currently available injectable wireless microstimulators for neuromuscular stimulation are bulky (diameter, ⌀, ~ 2 mm) because they contain large onboard power supply parts that increase their size and therefore can only be used to target whole large muscles, and not small muscles or individual within-muscle compartments. To overcome this issue, single channel wireless very thin (⌀ < 1 mm) microstimulators are under development in our lab. These devices are called eAXONs and operate by rectifying externally applied high frequency current bursts thereby avoiding the need of incorporating bulky power supply components within the device. This thesis explores the applicability of building an injectable wireless multichannel motor prosthetic system from individual eAXONs. Herein, it is demonstrated *in vivo* that multi-channel IM stimulation of a single muscle produces contractions that are fatigue-resistant, while single-channel IM stimulation does not. Moreover, evidence is provided that seem to suggest that mammalian skeletal muscles partition into successively smaller independent muscle compartments as their nerve supply divides. Meaning that, the number of within-muscle compartments seems to be far larger than what was previously thought. This confirms the need for thinner IM microstimulators like the eAXONs and confirms that the wireless high density networked neuroprosthetic system we envision to build from the eAXONs suits muscle's extensively segmented nerve supply.

The eAXONs have thin diameters because they rely on direct rectification of externally applied ac volume conducted currents alone for neurostimulation and thus the bulky power circuits that impede miniaturization are excluded. However, we numerically demonstrate that this unprecedented miniaturization comes at the cost of lower stimulation efficiency when compared to bulkier stimulators which can internally generate the stimulus pulses.

Abstract

This is the first account where the feasibility of establishing a dense distributed network of injectable wireless microstimulators in skeletal muscles is evaluated. It is a first step in developing bioinspired motor prostheses that can artificially produce naturalistic movements to recover lost motor functions in paralyzed patients.

# Contents

# Acronyms and Abbreviations

| | |
|---|---|
| ac | Alternating current |
| AP | Action Potential |
| CNS | Central Nervous System |
| dc | Direct current |
| eAXON | Electronic AXON |
| ES | Electrical Stimulation |
| FI | Fatigue Index |
| FNS | Functional Neuromuscular Stimulation |
| FT | Fatigue Time |
| GC | Galvanic Coupling |
| HF | High Frequency |
| IC | Inductive Coupling |
| IM | Intramuscular |
| LF | Low Frequency |
| MG | Medial Gastrocnemius |
| MP | Motor Point |
| MU | Motor Unit |
| NMC | Neuromuscular Compartment |
| RF | Radiofrequency |
| RMS | Root Mean Square |
| SEM | Standard Error of the Mean |
| WNZ | White New Zealand (Rabbit) |
| WPT | Wireless Power Transfer |

# Introduction

CHAPTER 1

## 1.1 Introduction

We humans can only interact and make changes in the world we live in by means of muscle contractions. In spinal cord injury, stroke and other neurological disorders leading to paralysis, communication between the central nervous system (CNS) and skeletal muscles becomes disrupted. Depending on the site of the injury in the CNS, the control signal may either fail to initiate, such as in the case of stroke or, in case of successful initiation, to propagate, as in the case of spinal cord injury. In either scenario, patients lose volitional control over their skeletal muscles. The loss of volition over movement in paralyzed patients renders them unable to perform common daily tasks, like standing up or pouring a glass of water, resulting in a poor quality of life. Patients who suffer from paralysis more often than not have intact peripheral motor nerves that can be artificially excited to elicit functional movement. Thus electric currents can be used to bypass the defective area in the nerve pathway and create proxy signals to drive skeletal muscles. The use of electrical stimulation to restore function in paralyzed muscles is known as functional neuromuscular stimulation (FNS) and has found several applications in helping patients suffering from paralysis such as to ambulate[1]–[4], to breathe[5]–[7], to control their bladder[8],[9], and to regain their sexual functions [10]. Rather than acting directly on the muscles, FNS generally works by exciting the peripheral nerves which in turn synaptically activate the muscles causing them to contract. (It must be noted that the amplitude of the current required to directly activate muscle fibers is very high compared to that required to activate the nerve fibers that supply those same muscle fibers [11].)

Electrical stimulation can be delivered through an electrode that is either placed on the skin overlying the target muscle or through an implanted one. Implantable systems are preferred over non-invasive ones for their higher stimulation selectivity, superior aesthetics, and the fact that they do not need to donned and doffed. Implanted electrodes lie much closer to the target nerve in comparison to superficial ones and therefore the electric fields can be focused on the neural structure that requires stimulation (i.e. the motor nerve) while sparing those that do not (i.e. superficial skin receptors that are associated sensation of pain)[12]. Currently available implantable FNS systems can be classified as either wired or wireless. Wired implantable FNS systems consist of electrodes implanted at the site where stimulation is needed and a relatively bulky pulse generator that is connected to those electrodes via electrical cables, which are known as 'leads' in the field. Typically the pulse generator is implanted subcutaneously and is usually located remotely in the chest or abdomen region for safekeeping away from the skeletal muscles where significant motion occurs during stimulation. In implantable systems. the electrodes can be in direct contact with the nerves, for instance, surrounding them as in the case of nerve cuff electrodes[13] or can be implanted within the muscles[14] or on the muscles[15] to activate nearby nerves. An advantage of implantable nerve over muscle based FNS systems is that they provide access to multiple muscles needed to perform complex movements from a single stimulation site, but they involve the risk of causing permanent nerve damage. In any case, wired FNS systems (nerve or muscle based) require complicated and invasive surgeries for their installation, which deters many patients from using them.

On the other hand, in wireless implantable FNS systems, the leads are avoided (the term 'leadless' is also used). The wireless implantable stimulators incorporate both the pulse generator and electrodes on the same implantable unit and have significantly smaller sizes compared to their wired counterparts[16][17][18]. As

a result, these microstimulators can be deployed wholly at the stimulation site and cause significantly less trauma during their implantation. Despite this reduction in size, achieving sub-millimetric wireless microstimulators is still a challenge [17]. This is because bulky onboard power sources in the forms of coils or batteries are required to ensure that the current requirements needed for neurostimulation are met, which are generally higher for intramuscular stimulation (few mAs) than nerve stimulation (few tens of µAs) since the IM electrodes do not directly contact the nerves [19]. To our knowledge, the only wireless implantable microstimulators that reached the clinics and were tested in humans were called the BIONs developed by G.E. Loeb *et al*.

Unfortunately, paralyzed patients cannot benefit from the application of FNS for functional movement restoration through the use of the above mentioned FNS systems. This is mainly because none of them can be used to provide a high density of stimulation sites to activate skeletal muscles in a selective, spatially distributed, asynchronous way (i.e. similar to the way the CNS produces natural muscle contractions), while avoiding complicated and invasive implantation surgeries. High-density nerve ‘electrodes’ (i.e. a single wired device carrying a large number of independent electrical contacts, the actual electrodes, implanted on the nerve to access different muscles or even different parts of the same muscle) that can artificially achieve physiological recruitment of skeletal muscles have been successfully developed and assayed[20], [21], but require highly invasive implantation surgeries that hinder their widespread use and their translation to the clinics.

Due to the lack of appropriate minimally invasive neuromuscular interfaces, conventional FNS is performed in a conservative manner by using a low density of stimulation channels to limit potential tissue trauma. This results necessarily in the use of unnaturally high stimulation frequencies to obtain a smooth contraction from the

activated muscle. Such high stimulation frequencies produce contractions that fatigue very quickly. The early appearance of muscle fatigue during conventional electrical stimulation places a limit on the duration of the functional tasks that can be performed with an FNS system, resulting in little clinical benefit to patients.

It was implicitly mentioned in the literature that for a FNS system to be successful, it has to include the capability of being able to provide multi-channel stimulation. High density FNS is favorable compared to low density FNS since several characteristics of the resulting contractions such as fatigue-resistance [22], [23], smoothness [24], [25] and stability[26][27][18] are significantly enhanced. It was reported that the larger the number of stimulation channels, the more physiological (i.e. fatigue-resistant and graceful) the elicited movements were [22][20][28][29], insofar as the channel density is not too high that it leads to excessive electrical interactions (overlap) between the stimulus channels.

To make the use of FNS more widespread and to make it a practical solution for restoring lost motor functions in paralyzed patients, the issue of rapid rate of electrical stimulation (ES) induced fatigue must be overcome. To address this, an alternative method of delivering electrical stimulation to skeletal muscles called interleaved or asynchronous stimulation has been proposed by other authors and has been shown to be effective in delaying the onset of ES-induced fatigue. Interleaved stimulation is based on the muscle activation pattern the CNS uses to produce natural contractions [30], and thus contractions obtained with interleaved stimulation resemble physiological ones compared to single site conventional FNS. Interleaved stimulation reduces ES-induced fatigue by utilizing a high density of stimulation channels and low stimulation frequency per channel (instead of high stimulation frequencies used in conventional FNS) to evoke smooth muscle contractions. Interleaved stimulation can be accomplished with electrodes placed on or inside the nerves (i.e. nerve electrodes), on the skin over

skeletal muscles (i.e. skin electrodes), or inside the skeletal muscles (i.e. intramuscular (IM) electrodes). IM electrodes are the most attractive configuration because they achieve very good spatial selectivity needed for selective recruitment of different muscles and even muscle compartments that are involved in complex movement patterns with the least possible invasiveness (implantation via injection)[31]–[33]. Interleaved stimulation is not widely used in the clinics since there are no currently available FNS systems that can provide multiple stimulation sites without needing extensive surgeries to implant them.

Therefore, the ideal FNS system should have the following design features: 1) implantable, 2) minimally invasive, 3) wireless, 4) flexible, 5) sub-millimetric, and 6) allow for multichannel operation. All these desirable criteria are met by the neural neuromuscular interface we are developing in our lab for which we have coined the name eAXON (short for electronic AXON). The eAXONs are a single-channel flexible microstimulators that are cylindrical in shape with a very thin cross-section ($\varnothing < 1$ mm) allowing them to introduced in skeletal muscles via simple injection, potentially in an outpatient clinic with help of local anesthesia.

The eAXONs are mechanically flexible owing to their limited onboard electronics which are envisioned to be housed inside a compact hard capsule whose length will be only a small fraction of the entire stimulator length (i.e. except for the electronics, the eAXON is mainly composed of soft medical grade silicone). It is noteworthy to pay attention to the flexible mechanical features of the eAXON, since this will greatly reduce scarring likely to occur post-implantation due to micromotion [34], [35]. Compared to currently available wireless [18], [36] or wired [14][37][38] IM electrode designs, the eAXON is extremely thin. These bulky IM interfaces are too large to selectively activate the small motor unit

(MU) groups in the muscle, while such fine selective access will be possible with thin microstimulators like the eAXON.

This reduced diameter of the eAXON (⌀ < 1 mm) is a consequence of using instantaneous and direct rectification of bursts of high frequency (HF) current, which flows through the tissues where the devices are deployed by volume conduction, as the method for performing neurostimulation. Since the eAXON does not generate stimulus pulses and relies on an external system to do that, the complex large power supply (which represent the main onboard components that limit miniaturization) and pulse generating circuits are excluded and therefore extremely thin microstimulators can be realized. This approach (also referred to herein as rectifying method) was proposed early in the 60s and abandoned thereafter, but it was *in vivo*-tested by our lab more recently and it was further developed by us so that the microstimulator included a digital unit to permit addressability to allow for multichannel network operation [39]–[41]. eAXON method is simply the rectifying method complemented by the addressability feature. The submillimetric dimension of eAXONs (as well as their addressability) allows us to satisfy criterion #6 (see above paragraph) which is multichannel operation. The thin cross-section of the eAXON would allow inserting them in large numbers (i.e. as a network) to access and control small clusters of MUs in skeletal muscles needed for the selective and asynchronous activation of muscles, without significantly increasing the complexity of implantation and associated surgical trauma.

Although the application of the eAXONs that is investigated in this thesis is one pertaining to muscle stimulation for motor function restoration in muscle paralysis/weakness, the use of the eAXONs can extend to many other applications, for instance, neuromodulation[42], [43].

## 1.2 Research questions

Interleaved stimulation or some optimized variant of it is the method by which we envision to deliver electrical stimulation to skeletal muscles with our multichannel eAXON FNS system. While there was considerable literature on the use of interleaved stimulation to minimize ES-induced muscle fatigue with surface and nerve electrodes, very few studies exist on the use of interleaved stimulation to reduce ES-induced fatigue with IM electrodes. Not only were those reports scarce, but they also reported conflicting results (i.e. some studies reported reduced fatigue and another reported no fatigue reduction with IM interleaved stimulation). In addition, in those limited number of studies that were carried out so far, authors reported the use of two IM electrodes per muscle to perform interleaved stimulation. It is not clear to us why a large number of IM electrodes were not assayed in those studies.

Moreover, because neurostimulation through direct rectification of volume conducted ac currents (i.e. the rectifying method) is a relatively new and heterodox method in which neural stimulation is brought about by half rectified stimulus signals instead of conventional square waveforms, its stimulation efficiency was yet to be determined. Thus, we compared the stimulation efficiency and the miniaturization potential of two possible approaches for developing microstimulators based on volume conduction as a wireless power transfer (WPT) method; the rectifying and the regular method. In the rectifying method, very thin microstimulators can be realized and in this method, the microstimulators do not incorporate a pulse generating circuit and rely on the direct and instantaneous rectification of externally applied volume conducted ac currents for neurostimulation [44] (i.e. the eAXONs). Moreover, the microstimulator delivers half-rectified stimulus signals (that still

contain the oscillations of the transmitted ac currents) which have been shown to be able to induce nerve activation. In the regular method, the microstimulators are bulkier since they have to include a component (e.g. capacitor) to store the electrical energy received from the externally transmitted volume conducted ac fields to power an onboard pulse generating circuit that produces square stimulus waveforms [45].

Therefore, the following are the questions that were posited and addressed by the work carried out in this PhD.

Firstly, the fatigue reduction associated with interleaved stimulation commonly observed with surface or nerve electrodes could not be consistently achieved with IM electrodes. We hypothesized that this inconsistency was caused by the fact that it is difficult to know the locations in the muscle for placing the IM electrodes that would minimize stimulation overlap between the muscle fibers activated by the electrodes used in interleaved stimulation. So, we asked whether or not the uncontrolled stimulation overlap amongst the different IM electrodes used in interleaved stimulation was the cause of such inconsistency. In relation to this question, we asked what was the smallest compartment of the skeletal muscle that could be independently activated with an IM electrode. It was reported that mammalian skeletal muscles have a compartmentalized innervation and based on this compartmentalized innervation the muscle itself is compartmentalized into sections, i.e. when a single compartment is activated at low stimulus levels with an IM electrode, only that compartment is stimulated. It was reported in cats and rats that the muscle is coarsely compartmentalized, i.e. these compartments exist about primary IM nerve branches. So, we asked whether or not the muscle is finely compartmentalized, i.e. if each of the secondary and tertiary and subsequent IM nerve branches corresponded to progressively finer and more numerous compartments.

Secondly, it is known that the eAXONs provide wireless neurostimulation via a heterodox method (i.e. rectifying method) that passes to the nerve fibers half-rectified ac signals as stimulus waveforms that have different shape than square waveforms conventionally used in neurostimulation. So, we asked if those half-rectified signals associated with the rectifying method are as effective as their square waveform counterparts associated with the regular method in activating a nerve fiber. We also assessed the miniaturization potential of microstimulators based on the regular method by using the predicted energy required for neurostimulation to estimate the size of the internal storage capacitor.

.

## 1.3 Dissertation outline

The second chapter is an overview of the concepts and terminology that commonly appear in the field of electrical stimulation of peripheral nerves and muscles and that are crucial for understanding the content of this thesis. It also includes a brief introduction to the anatomy of the peripheral neuromuscular systems and common approaches used to modulate muscle force and recruitment by varying the features of the electrical pulses used in stimulation. It also includes a critical analysis of different designs of fully implantable FNS systems that were developed over the last several decades and emphasizes the need for a multichannel distributed wirelessly controlled system that can be implanted in a minimally invasive fashion for control of muscle contraction.

The third chapter details an experimental study conducted in an *in vivo* model (White New Zealand rabbits) where the amount of muscle fatigue and ripple (i.e. measure of contractile smoothness) induced by interleaved stimulation and conventional stimulation

was compared after it was ensured that the overlap between the electrodes used in interleaved stimulation was minimal.

The fourth chapter details a computational study that compares the stimulation efficiency and the miniaturization potential of two approaches for developing wireless microstimulators based on volume conduction. In rectifying method, the microstimulators bypass the need to incorporate onboard bulky power source and pulse generating circuits by relying on the rectification of externally applied volume conducted ac currents as means for obtaining the stimulus pulses. In the regular method, microstimulators carry an internal bulky storage capacitor to store the energy from the transmitted ac fields which is then used to drive a pulse generating circuit to produce the square stimulus pulses.

# Background

CHAPTER 2

## 2.1 Anatomy of the peripheral neuromuscular system

Neurons are the building blocks of the nervous system and they transmit information via the propagation of impulses known as action potentials (AP). Each neuron can vary in shape and in size depending upon their function and location in the body. Despite this variability, all neurons do hold a certain aspect in common, which is the fact that all neurons are composed of four anatomical parts, namely, the dendrites, the axons, the axon terminals and the cell body as shown in Figure 1. For the purposes of this thesis, we will concern ourselves with a specialized type of neurons called motoneurons that connect the CNS with the peripheral skeletal muscles and will focus only on the axons, and the axon terminals, since these are the two structures of the neuron that are commonly interfaced with when applying electrical stimulation peripherally.

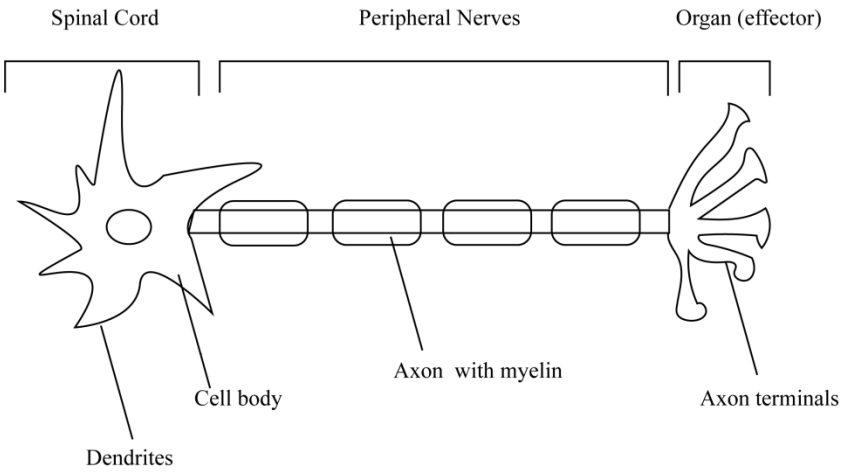


**Figure 1 schematic showing the different anatomical parts of a neuron and where each part of the neuron is located in the nervous system.**

Briefly, dendrites are the processes that emanate from the cell body whose function is to receive input signals from neighboring neurons and transmit them to the cell body. Once the input neural signals arrive at the cell body, they are integrated. Neural signals can be excitatory (induce depolarization) or inhibitory (causing hyperpolarization) in nature. The cell body will "decide" whether it should fire or not depending upon the net effect of the sum of all depolarization and hyperpolarization events. If the net outcome after all the input signals are integrated is excitatory, the cell body will fire and send an action potential down the axon (the longest projection). At its terminus, this axon divides several times to create a network of distributed branches that establishes multiple connections either onto other neurons or an organ (effector) it innervates. Signal transmission between two neurons or a neuron and the organ it supplies is accomplished through the release of chemicals called neurotransmitters into small microscopic clefts called synapses.

The main function of neurons is to generate and to transmit action potentials. The membrane of neurons contains ion channels whose open or close state is controlled by changes in membrane voltage. In its resting state, the membrane is negatively charged due to the fact that the positively charged sodium ions are constantly being ejected from inside of the neuron by active sodium pumps. When the membrane is electrically perturbed either due to a natural or an artificial electrical stimulus, its voltage will change accordingly. In the case of a hyperpolarizing stimulus, that is, a stimulus that decreases the membrane potential so that it becomes more negative compared to the resting state, the membrane potential will decrease in a relatively linear fashion without eliciting a unique response from the membrane. However, if a depolarizing stimulus is applied, the membrane voltage will increase linearly until a threshold value is reached beyond which an automatic nonlinear positive spike in membrane voltage is produced that quickly decays back to the resting voltage level. This characteristic transient response is what

is known as AP and it is the result of the sum of individual currents corresponding to different ionic channels in the membrane. The AP travels like a wave spreading from one location on the axon/dendrite/cell body to the next and is the building block of the language used by neurons to communicate with each other and with other organs that are innervated by them. The neuron that innervates the skeletal muscle fibers is called a motoneuron. The cell body of a motoneuron is located in the spinal cord, its axon in the peripheral nerve and its axon terminals inside skeletal muscles.

Axons of motoneurons exit the ventral horn of the spinal cord enroute to their target muscles in a form of bundles called the peripheral nerves. Those same peripheral nerves also contain the sensory fibers that carry information from the muscle spindles and tendon organs (located peripherally) back to the spinal cord i.e. afferent pathway. The sensory fibers enter through the dorsal horn of the spinal cord. The peripheral nerve begins as a thick nerve trunk proximally where it emerges from the spinal cord and then divides repeatedly as it travels distally distributing branches to the different muscles as it passes by them on its course. Once the peripheral nerve enters a specific muscle, it divides into spatially distributed finer nerve branches, each containing successively fewer numbers of axons. Simultaneously, as the IM nerve branches divide, the axons inside these IM nerve branches also divide giving rise to multiple collaterals (i.e. branches) until terminally each collateral branch of each axon forms a synapse or sometimes multiple synapses with a single and only a single muscle fiber [46]. It is through this organization that the smallest functional units of the neuromuscular system called the motor units (MUs) are constructed [47]. Thus the MU is constituted of a single motoneuron and all the muscle fibers it innervates. A schematic showing the afferent and efferent pathways connecting the skeletal muscle and the spinal cord is shown in Figure 2

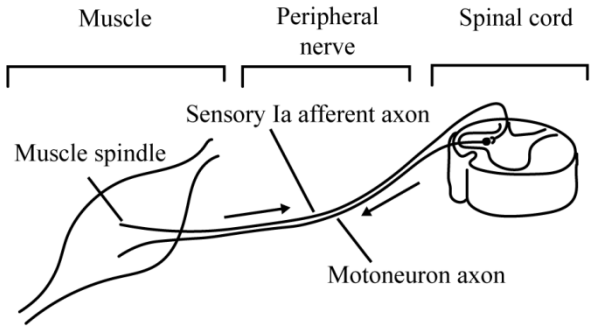


**Figure 2 Afferent and efferent connections between the skeletal muscle and the spinal cord (top). Arrows show the direction of information flow.**

When electrical stimulation is applied to peripheral nerves, both sensory and motor fibers are activated [12]. Sensory fibers, in particular, the large sensory Ia monosynaptic afferent fibers get activated at sub-motor excitation thresholds[48]. In fact, some stimulation protocols are designed to predominantly engage the large sensory Ia afferent fibers over motor fibers to indirectly evoke contractions by inducing reflexes with the purpose of generating muscle contractions that follow the normal order of motor unit recruitment (see later section 2.2.3) which are more fatigue-resistant than those obtained by purely recruiting motor fibers [49].

There are different types of motor units based upon the metabolic and force profiles of the muscle fibers that constitute them [50]. The first type is the fast motor units or fast glycolytic. These motor units are innervated by large diameter motor axons and consist of a large number of muscle fibers and therefore, when activated, produce rapidly rising large forces. They are characterized by their limited capacity for oxidative metabolism and high glycolysis rates. The fast motor units fatigue very rapidly and recover slowly. The second type of motor unit is known as the slow oxidative. These motor units are supplied by small diameter motor axons and consist of a small number of muscle fibers and produce small gradually developing forces when activated. These MUs depend more on

oxidative than glycolytic metabolism for their energy needs and when stimulated, they generate contraction that can be sustained for extended periods of time without fatigue and show fast recovery. The third class of motor units is the fast oxidative which corresponds to a motor unit type that falls somewhere in the middle of the spectrum if fast glycolytic and slow oxidative motor unit types represent the extreme and opposite points of that spectrum.

## 2.2 Factors influencing muscle recruitment by intramuscular stimulation

### 2.2.1 Effect of intramuscular stimulation site

FNS uses electrodes to deliver electrical stimulation to target nerves. These electrodes can be placed on the skin over a target muscle (i.e. non-invasively) or alternatively these electrodes can be implanted inside the muscle or in or on the nerve innervating that muscle (i.e. invasively). Regarding the electrodes that target the muscles, electrical stimulation during FNS is applied at special sites in the muscle called motor points[51]. The motor points are defined as the locations in the muscle that require the least current to elicit a contraction and these typically correspond to the sites where the nerve enters the muscle [52]. The motor point serves as a preferred site for applying neuromuscular stimulation as the excitation threshold of a muscle can be reached with relatively low currents[53]. While there is a clear benefit to placing IM electrodes near or at the motor point, there is a downside to this, namely, that this electrode placement results in a steep rate of muscle force recruitment i.e. every small step increase in the magnitude of the injected electric pulse produces a corresponding large step increase in the force output from the muscle [54]. Such input-output relationship result in ballistic or jerky movements that are highly

problematic in FNS applications where fine and gradual control over muscle force is desired[55]. For most FNS applications, it is desirable that the difference between the stimulus strength that achieves threshold muscle activation and that which produces maximum muscle activation is sufficiently large so that muscle force can finely be modulated with high resolution by varying the strength of electrical stimulation. Muscle force recruitment obtained with an IM electrode placed distally (downstream from the motor point) is much shallower compared to that observed with an IM electrode placed at the motor point [56][15]. Therefore, choosing sites other than motor points in the muscle to deliver stimulation may be advantageous when graded slowly rising forces are desired.

Moreover, the site of stimulation can have significant consequences on the characteristics of the muscle contraction elicited with electrical stimulation. MUs belonging to the same histological class have shown a tendency to aggregate in localized regions of the muscle. Therefore, by varying the location of the electrode in the muscle, one can expect to produce contractions with different rising and fatiguing characteristics depending on the type of MUs predominantly present near the electrodes [57][24][58]. Contractions caused by mainly recruiting the fast motor units will be characterized by rapidly developing and deteriorating forces. On the other hand, a contraction resulting from the activation of mainly slow motor units will show gradually rising and prolonged forces.

### 2.2.2 Effect of electrode-nerve distance

Neural structures that are close to the electrodes will be recruited at lower stimulus strengths than structures that are further away from the electrode. This is because tissue acts as a volume conductor and the strength of an externally applied stimulation field diminishes with distance [50]. Therefore, the excitation threshold of the motor

axon will depend on the physical position of the electrode with respect to it. The closer the electrode is to the excitable axon the higher its excitability and lower the current required to activate it [12]. Different neural structures lying at the same distance from the electrode could not be selectively activated, since the effect of the electric field on them would be the same, unless they have different geometries (different geometries can lead to different charge densities accumulating on the surface of neural structures which can lead to a difference in excitability despite being under the same electric field strength)[59]. Thus, selectivity of stimulation can be substantially improved by correctly placing the electrode as close as possible to the element that needs to be stimulated. The closer the electrode is to the target nerve the more selective the stimulation becomes as the electric field can be pinpointed on the target nerve without reaching or activating the innervation of non-target muscles.

### 2.2.3 Effect of motor axon diameter

As alluded to in the previous paragraph, the anatomical geometry of the neural structures being stimulated can determine their threshold of excitation i.e. how excitable they are. Structures having different shapes can have very different excitation behaviors even under the same electric field strength. This fact underlies one of the most persistent problems in FNS, which is that contractions evoked with electrical stimulation fatigue significantly faster compared to natural ones [60][61]. Recall that slow (fatigue-resistant) muscle fibers are innervated by motor axons of small diameters while fast (fatigable) muscle fibers are innervated by axons with large diameters. Because of this difference in the diameters of the axons controlling fast and slow muscle fibers, an electric field applied via an electrode selectively excites the large motor axons (since they

have lower resistance) over thin motor axons. So, for stimulation of gradually increasing strength, the large motor axons are recruited first at lower stimulus strengths and the small motor axons and their slow muscle fibers would only be activated after a sufficiently strong stimulus is applied and after most of the large axons have been recruited [62]–[66].

## 2.2.4 Effect of stimulation parameters

In FNS, muscle tension depends on the number of active MUs and the frequency at which they are stimulated, both of which can be controlled by varying the amplitude, the pulse duration, or the frequency of the stimulus pulse.

In *amplitude modulation,* the amplitude of the applied current pulses can be varied to provide control over the strength of contraction of a muscle. For a fixed pulse width, at low amplitudes, none of the motor units are recruited. As the amplitude of the injected current pulse is stepped in small increments, more and more axons and the muscle fibers they supply become recruited until a point where any further increase in amplitude caused no further effect on muscle force [67].

In *pulse width modulation,* similarly for a fixed amplitude value, the number of recruited motor units and therefore muscle force can be modulated by changing the duration of the pulse. By gradually increasing the pulse duration, the threshold of more and more motor axons is reached until the muscle is fully recruited. Moreover, pulse width modulation has been reported to influence the shape of the electric field. Setting the pulse width to very small values has been demonstrated to achieve a more spatially focused stimulation with nerve cuff electrodes so that a unique set of axons in a collection of axons found in a compound nerve can be selectively recruited [68].

With respect to *frequency modulation*, recruited muscle force can be increased not just by increasing the number of activated MUs but also by making a fixed number of MUs fire at a higher rate. Therefore when the frequency of stimulation is increased, the magnitude of the evoked force and its smoothness also increase. When a single pulse is delivered to a muscle an individual twitch is produced. In that twitch, the muscle momentarily contracts and then relaxes. When the rate of stimulation (i.e. frequency) is slightly increased, the successive twitches begin to progressively overlap. The partial overlap of the consecutive twitches causes an oscillation in muscle tension and produces a rippled tension. Any further increase in frequency will cause the complete fusion of the individual twitches after which point oscillations disappear and contraction becomes smooth. At such high frequencies the muscle engages in a new twitch before it begins to relax and thus smooth force level is sustained. Frequency where summation of twitches takes place is known as tetanic or fusion frequency. Frequency is usually not used to modulate muscle force. It is usually set to a value at which fused contractions can be obtained [69][66].

## 2.3 Limitations of functional neuromuscular stimulation

The main challenges that hinder the use of most FNS systems clinically are 1) the early onset of fatigue [70][71] and 2) the difficulty to produce graded and refined movements [54], [61], [72], [73]. Both of these challenges are believed to stem from the fact that extraneural stimulation causes the preferential activation of fast fatigable motor units. The gracefulness of natural contractions is accomplished by recruiting the slow motor units first when

relatively small forces are needed and progressively larger motor units with larger force outputs if a demand for larger forces develops. The order of recruitment is reversed in FNS as the external electric field is more likely to activate the large axons (low threshold) controlling the fast fatigable motor units than the small axons (high threshold) innervating the slow motor units. Since artificial stimulation has a greater propensity to activate the large fatigable motor units, usually the resulting contraction shows a quickly fatiguing behavior. The inverse order of recruitment underlies the steeply rising fatigable forces seen in FNS and overcoming it will allow the production of graceful naturalistic movements. A networked neuroprosthetic system such as the one we envision to construct with the eAXONs can potentially help overcome these two main limitations of FES. Because of the eAXON system's ability to provide a large number of stimulus channels, low frequency-multichannel (i.e. interleaved) stimulation can be used to reduce ES-induced fatigue. Moreover, since each eAXON is thin enough to selectively control a fine group of MUs in the skeletal muscle with small force outputs, gradually larger forces can be obtained in small steps by sequentially increasing the number of active eAXONs, thereby overcoming the problem of poor motor control. In the next section, the major stepping stones in the history of the development of fully implantable FNS systems designed for movement restoration in paralysed individuals will be discussed and a special emphasis will be placed on the expected contributions of the eAXONs to the field.

## 2.4 Fully implantable intramuscular functional neuromuscular stimulation multi-channel systems

### 2.4.1 Freehand® system

In 1998, the first 8-channel fully implantable FNS system that utilized IM electrodes for restoration of upper hand function in paralyzed patients was developed and manufactured by NeuroControl Corporation [74]. The system consisted of: 1) eight IM electrodes that were implanted inside different muscles of the forearm and the hand, 2) leads that connected the electrodes to the central generator, and 3) a central pulse generator as shown in Figure 3. The stimulation parameters are fed to the implanted pulse generator through inductive coupling with an external system. The electrodes tips are located inside the muscles, the central pulse generator is implanted remotely in the chest region (far away from possible movements) and the leads had to be routed subcutaneously from the site of the electrodes to connect them to the pulse generator. This system came with several drawbacks. The large and bulky size of the hardware that needed to be implanted called for highly complicated and invasive surgeries which in many cases deterred patients from using it. The leads were subject to significant mechanical stresses due to muscle contractions elicited by the stimulation. Those leads could be easily displaced or fractured, which resulted in an increase in the number of revisit surgeries to replace worn down parts.

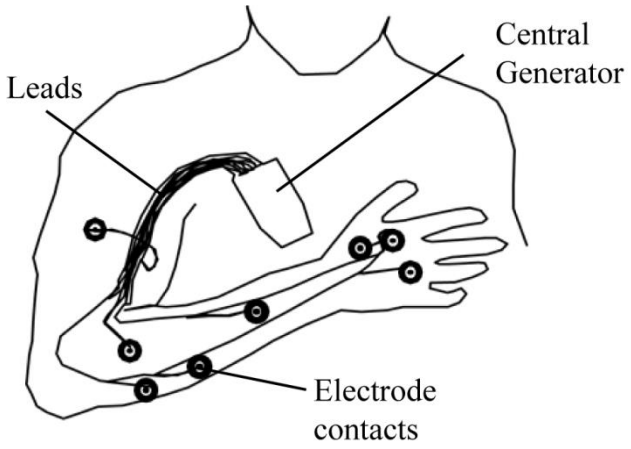


**Figure 3 A schematic of the implanted components of the Freehand® system.**

The leads provided a large surface area over which bacteria and other pathogens could grow and so risk of infection post-implantation is high [75]. Those disadvantages created the motivation for the development of a fully implantable wireless system that consisted of a network of single channel microstimulators called the BIOnic Neurons or BIONs to provide multiple point stimulation with the smallest amount of implanted hardware possible at the time and the least possible invasiveness.

## 2.4.2 BIOnic Neurons or BIONs.

In FNS, multiple stimulation channels are needed to selectively excite the large number of muscles involved in the execution of complex motor tasks like walking or standing up. Generally, the larger the number of stimulus channels that are employed by an FNS system, the greater the number of the neural structures that can

be controlled and the more accurately the movement produced by the FNS system can approximate the natural one[28].

Prior to the BIONs, the implantation of wired intramuscular electrodes required complex surgeries as the connecting leads needed routing over considerable distances to a pulse generator that is normally positioned in the chest or the abdomen. Implantation becomes more challenging if the number of sites that require stimulation is large. Usually, the durability of these wired systems is limited due to vulnerability of the leads to displacement and fracture caused by the excessive bending during movement [76], [77] [14].

Thus, there was a clear clinical need for a new neural interface design that would be wireless and much smaller in size than the FreeHand System to sidestep any complicated surgeries that would be needed to implant it. The BIOnic Neurons or simply the BIONs are single channel miniature stimulators that were conceived and developed by G. Loeb *et al.* [78]. Each BION contains the electronics needed to generate pulses as well as the electrode contacts through which stimulation is delivered to the tissue. The BIONs have an elongated cylindrical geometry which is a geometry that is conducive for implantation via injection compared to other geometries like discs, for example. The BIONs are cylindrical in shape and thin enough (2 mm in diameter) to be injected using a hypodermic needle in a minimally invasive technique Figure 4 in an outpatient clinic. The BION microstimulators are deployed at the locations in the body that require precise and selective stimulation. The energy and stimulation parameters are fed to the BIONs by an external system through inductive coupling (IC) with an externally generated RF magnetic field. Each BION can be addressed individually to selectively control the devices that are active. The maximum number of BIONs that can be controlled and powered by the external system is 256.

The BION are designed for permanent implantation and thus their migration tendency, biocompatibility and functionality has been evaluated in rats [79], cats [80][81][45] before being trialed in humans [82]. Despite being initially developed to treat muscle weakness and paralysis, the BIONs use have expanded to treating a wide range of neurological disorders that require neuromodulation like obstructive sleep apnea, shoulder subluxation in stroke patients, osteoarthritis, and for correcting foot drop [83]–[86]. In recent clinical studies, the BIONs showed several adverse effects including device migration and increased pain at implant site [85].

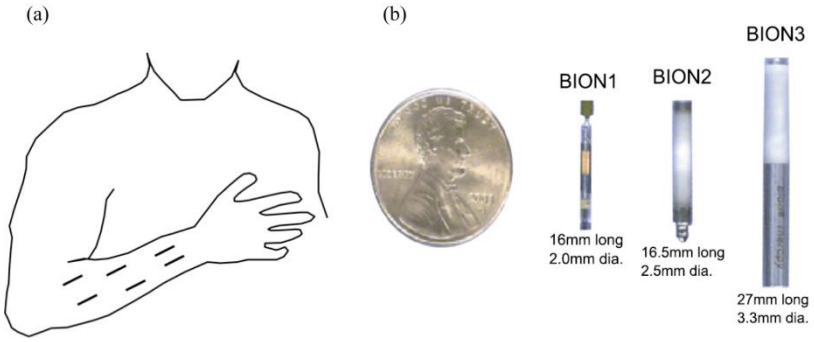


**Figure 4 BIONs or Bionic Neurons. (a) schematic of how the implanted BIONs would look like in human arm. (b) sizes of different generations of the BIONs with a US penny as a scale (taken from** [78]**).**

The electronics inside the BIONs are housed within a rigid outer case made of hard materials like ceramic or glass that can possibly erode and scar the soft tissues that surround them once the BION is implanted. This presents a much bigger problem for BIONs implanted intramuscularly where mechanical stresses caused by the muscle contraction they themselves elicit can produce excessive scarring[87],[49]. Their rigid mechanical properties can cause increased local inflammation and poor integration in the surrounding tissues and ultimately their rejection. Furthermore, the formation of very thick scars around the BIONs would result in

their functional deterioration i.e. very high stimulus strengths would be needed to evoke very small responses. The very high stimulus strengths required to counter the effect of increased scarring would overwhelm the power generation capacity of the BION neurostimulators resulting in their failure [88].

Of course, implant miniaturization is critical because the smaller the size of the microstimulator the less the trauma that would result from its implantation [89] and the greater its spatial selectivity since the it will approach the size of individual nerve fibers instead of a collection of them. Although the BIONs system can achieve electrical access to multiple sites in the body at only a tiny fraction of the required implantable hardware if the Freehand® system was used, the BIONs are still too bulky. This is because, the high power demands of neurostimulation imposes that the BIONs contain a large diameter metallic coil or a bulky battery as part of their electronic circuit to ensure an adequate power supply, which results in an increase in their overall diameter. Because of the way they are powered, further miniaturization of the BIONs is hindered. Therefore, alternative powering solutions or stimulation approaches that do not require bulky parts to be present in the implantable micro-stimulator are needed. In the following section, our envisioned solution to this problem is presented and discussed.

## 2.4.3 eAXON Project

The eAXON project is aimed to develop very thin injectable wireless single-channel microstimulators called the eAXONs that could be implanted in large number as a network to provide multisite selective electrical stimulation to skeletal muscles to restore functional movement to paralyzed limbs. The eAXONs represent a new generation of injectable wireless microstimulators

undergoing development in our lab to overcome two shortcomings of the BION system; namely, its bulkiness and mechanical rigidity.

In contrast to the BIONs, the eAXONs use volume conduction as a wireless power transfer (WPT) method. Volume conduction does not require the implanted microstimulator to incorporate internal bulky components for sufficient power transfer and thus allow for significant microstimulator miniaturization compared to inductive coupling. With volume conduction as a WPT method, we envision two different approaches for developing wireless microstimulators.

The first approach consists of developing implants that act as rectifiers of volume conducted high frequency current bursts. By rectifying pulses of high frequency currents across the implant, low frequency currents are generated that can cause local stimulation [41]. We will refer to this approach as the ***rectifying method*** (for developing microstimulators using WPT based on volume conduction). This approach was first conceived and demonstrated in 60s by two independent research teams[92], [93]. However, those studies are barely cited and, in fact, no references to them are found after the 80s. In those studies the rectification circuitry simply consisted of a diode and, therefore, no control capabilities were possible. It was never shown the use of more advanced circuits than a diode for rectifying ac currents flowing through tissues. These microstimulators would only be applicable to scenarios in which a single target needs to be stimulated. In the early 2010s, we [44] and others [94] unaware of those pioneering studies in the 60s, obtained analogous results using diodes. However, we later demonstrated that it is possible to implement digitally addressable and controllable rectifying implants [39], [40]. In essence, the electronics of these addressable rectifiers consists of a digital unit that via transistors controls the flow of rectified current through the implant. The digital unit is powered by WPT based on volume

conduction. It must be noted, however, that the power used for stimulation does not originate from the implant but directly from the passive transformation the high frequency current bursts that flow through the tissues where the implant is located. When this approach includes a digital unit to control the flow of rectified current [39], [40], we refer to as the ***eAXON method***, where eAXON stands for "electronic axon" in reference to their intended application. The eAXON method is a subclass of the rectifying method.

The second approach would consist of using WPT based on volume conduction to power a conventional pulse generator incorporated inside the implant. This generator would then deliver the stimulation pulses either through the same pair of electrodes used for power capture or through another pair of electrodes on the surface of the implant. We will refer to this approach as the ***regular method*** (for developing microstimulators using WPT based on volume conduction). The high frequency currents would not only be used for power transfer but would also be used to transmit commands from the transmitter to the implant thus allowing the development of smart networks of microstimulators. To the best of our knowledge, although this approach has been implicitly or explicitly proposed in different studies on WPT based on volume conduction [90], [91], it has never been experimentally tried for stimulation.

In contrast to the BION microstimulator, the eAXONs (based on the eAXON method) is envisioned to have the shape of a very thin (ø < 1 mm) flexible tube. Internally, this tube will contain an assembly which consists of: 1) a compact hard hermetically sealed capsule (housing all the electronic components that are needed for neural stimulation and/or recording) at the center, and 2) two coiled metallic wires that flank the central capsule. The coiled wires have two distinct regions. The part of the coil that is loosely wound will serve as a miniature lead and will occupy most of the length of the

eAXON, while the other much shorter part that is tightly wound will serve as the electrode. A photo of a prototype of a non-addressable eAXON is shown in Figure 5. This prototype was demonstrated in [41]. The eAXONs have these unique geometrical and mechanical properties because they avoid the need of bulky components for powering. Instead of delivering monophasic waveforms, versions of the eAXONs have been successfully developed that achieve biphasic waveforms that are less likely to cause electrochemical damage [53] to the tissue [41], [97].


**Figure 5 Dimensions and flexibility of a prototype of a non-addressable eAXON.**

The system needed to perform wireless stimulation of excitable tissues with an implanted eAXON is shown inFigure 6. The fact that the eAXONs are very thin opens up the possibility of implanting a large number of them in a single muscle, without significantly increasing the complexity of implantation procedure. Additionally, their small diameter allows them to selectively target and activate not just whole muscles but sections of muscles. Thus we envision with eAXONs that one can achieve a very fine level of electrical access to regions or sub-regions of the neural circuitry of

the muscle; similar to the level of access that CNS has to skeletal muscles.

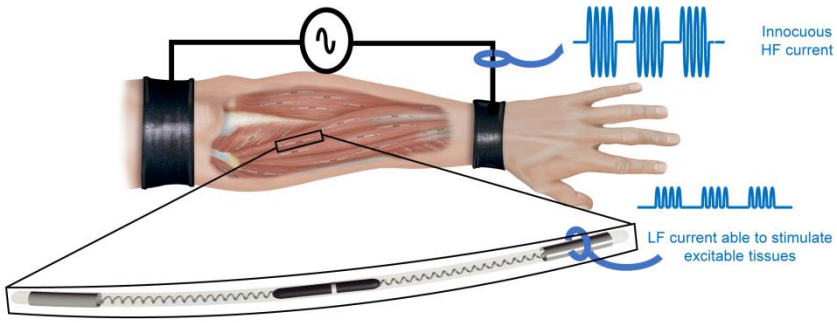


**Figure 6 Stimulation of excitable tissues via eAXONs. Bursts of high frequency HF currents are delivered wirelessly through external skin electrodes (black bands) that then pass through the tissue without exciting any neural structures in its path. However, when the HF currents reach the the eAXON and are rectified by them, tissues near the eAXON are excited.**

## 2.5 Skeletal muscle compartmentalization

In the case of nerve electrodes, the nerve, nerve fascicle or a nerve sub-fascicle may serve as potential neural anatomical targets for electrical stimulation. For IM electrodes, the neural targets are not as well defined in the literature as they are for nerve electrodes. This was a pressing issue since we envision establishing a network of the eAXONs where not only whole muscles, but also finer parts of muscles, are targeted to control paralyzed limbs. Therefore, defining the number, sizes, and locations of fine muscle compartments was critical.

All the published work on the neuromuscular organization of mammalian skeletal muscles suggested that they are anatomically divided into different compartments or partitions based on the extramuscular nerve branches that enter the muscle [106] [107][108][91],[92] [111] [112]. Each neuromuscular compartment (NMC) receives innervation from the CNS independently from the other through a single primary nerve branch. This partitioning of the nerve supply of the skeletal muscle is believed to play a critical role in how the CNS generates natural muscle contractions i.e. contractions that are smooth and fatigue-resistant. Physiologically, a contraction is achieved through the asynchronous and selective activation of different NMCs at relatively low firing rates [22], [113]. It is through the temporal summation of multiple out of phase NMC outputs that fatigue-resistant and graceful contractions are produced at the level of the muscle. The larger the number of NMCs that are asynchronously activated, the smoother and more fatigue-resistant the resulting contraction becomes [29].The fact that muscles naturally consisted of multiple NMCs that are electrically isolated from each other suited the design of a multi-channel networked neuro-prosthetic system like the one we proposing to construct from individual eAXONs. However, because these NMCs seemed to exist only about the primary extra-musuclar nerve branches and not about higher order IM nerve branches[114], it was anticipated that there would only be a few NMCs available in a muscle that can serve as targets for electrical stimulation with the individual eAXONs (since skeletal muscles naturally contain few primary IM nerve branches [115], [116]). Therefore, our initial hypothesis was that the partitioning of the skeletal muscles was not so extensive to justify the implantation of the large number of eAXONs we envisioned to deploy since there are only few NMCs to control. However, it will be discussed in chapter three of this thesis that this is not the case.

## 2.6 Fatigue reduction via interleaved stimulation

The frequency by which electrical pulses are presented to the skeletal muscle during FNS determines two important properties of the resulting contraction; its smoothness and its fatigue rate. It is known that the higher the stimulation frequency that is used, the smoother the resulting contraction becomes, but this comes at the cost of a higher rate of muscle fatigue [117]–[119].

In FNS, muscle contractions elicited must be smooth and fatigue-resistant so that they can be used to produce functional movement like standing up or walking. However, with currently available minimally invasive FNS neuromuscular interfaces, stimulation strategies such as multi-site interleaved stimulation which are based on natural muscle activation mechanism cannot be used.

Conventional FNS neuromuscular interfaces offer only a single active site for stimulation delivery. With only a single stimulation site, high stimulation frequency also known as the 'fusion frequency' must be used in order to obtain a fused contraction from the activated muscle which leads to high fatigue rate. This is because this fusion frequency (~ 80-100 Hz)[69] is several times higher than the natural firing rate of a MUs (~20 Hz)[120][121]. This unnatural rate of firing overwhelms the MUs resulting in their early fatigue. This produces a situation known as a 'trade off' where in order to gain more contractile smoothness, some fatigue-resistance must be sacrificed and vice versa.

In interleaved stimulation, the single electrode (which is what is conventionally used in FNS) is replaced by many electrodes and the frequency of the stimulus pulses applied to each electrode is set to a fraction of that required to achieve a fused contraction (i.e. fusion frequency) [29], [109], [122]–[125]. In addition, the train of

stimulus pulses applied to each electrode is delivered such that it is temporally out of phase with the other trains applied to other electrodes. This way, the force response evoked from each electrode is highly fatigue-resistant (because of the low stimulation frequency used) and the overall force response from the muscle is fused (because the rippled force outputs from the different electrodes are out of phase with each other, so they temporally add up to a smooth contraction). In other words, even though the force contribution from each electrode when considered in isolation contains a lot of oscillations (due to the low frequency), the overall contraction is a smooth one (due to the temporal summation of multiple non-synchronized force contributions).

## 2.7 Fine motor control

Although not investigated in this thesis, the miniature size of these eAXONs enables targeting of fine neural structures or motor unit groups that have small maximum force outputs. Having electrical access to the fine elements of the muscle refines the level of control that could be achieved with a motor prosthesis. The finer the NMCs that are targeted, the greater the resolution with which muscle force can be modulated between threshold and maximum activation. This can help overcome the sudden and steep activation of muscles often observed with currently available motor prosthesis. This steep recruitment and lack of graded control of muscle force represents another bottleneck of FNS (aside from early onset of muscle fatigue) and a neuro-prosthetic system that can access fine output elements of the skeletal muscle maybe the solution.

# Interleaved stimulation with minimally overlapping electrodes evokes smooth and fatigue resistant forces

CHAPTER 3

## 3.1 Abstract

It is known that multi-site interleaved stimulation generates less muscle fatigue compared to single-site synchronous stimulation. However, in the limited number of studies in which intramuscular electrodes were used, the fatigue reduction associated with interleaved stimulation could not consistently be achieved. We hypothesize that this could be due to the inability to place the intramuscular electrodes used in interleaved stimulation in locations that minimize overlap amongst the motor units activated by the electrodes. Our objective in the present study was to use independent intramuscular electrodes to compare fatigue induced by interleaved stimulation with that generated by synchronous stimulation at the same initial force and ripple.

In the medial gastrocnemius muscle of an anesthetized rabbit (n = 3), ten intramuscular hook wire electrodes were inserted at different distances from the nerve entry. Overlap was measured using the refractory technique and only three electrodes were found to be highly independent. After ensuring that forces obtained by both stimulation modalities had the same ripple and magnitude, fatigue induced during interleaved stimulation across three independent distal electrodes was compared to that obtained by synchronously delivering pulses to a single proximal electrode.

Contractions evoked by interleaved stimulation exhibited less fatigue than those evoked by synchronous stimulation. Twitch force recruitment curves collected from each of the ten intramuscular electrodes showed frequent intermediate plateaus and the force value at these plateaus decreased as the distance between the electrode and nerve entry increased.

The results indicate that interleaved intramuscular stimulation is preferred over synchronous intramuscular stimulation when fatigue-resistant and smooth forces are desired. In addition, the results suggest that the large muscle compartments innervated by the primary intramuscular nerve branches give rise to progressively smaller independent compartments in subsequent nerve divisions.

Part of this chapter was adapted from:

A. Eladly *et al.*, "Interleaved intramuscular stimulation with minimally overlapping electrodes evokes smooth and fatigue resistant forces," *J. Neural Eng.*, vol. 17, no. 4, 2020.

## 3.2 Introduction

Fatigue and ripple are two clinically important properties of artificially evoked forces that are influenced by stimulation frequency. We define force ripple as the degree to which a muscle contraction is not smooth. Lack of contractile smoothness arises when the delivered electrical pulses are widely spaced in time that the force twitches evoked by the individual pulses do not fully overlap or when individual twitches with unequal peak amplitudes summate [126]. Recall from section (2.6 in chapter 2)that high stimulation frequencies generate low ripple contractions that fatigue very quickly, while low stimulation frequencies yield fatigue-resistant contractions that contain high ripple [69], [127]. Because improvement in one property has to be traded for worsening in the other, clinically desirable forces that are low in ripple and low in fatigue are difficult to obtain with conventional synchronous stimulation (i.e conventional FNS).

Interleaved stimulation is a method of electrical stimulation of the muscle that attempts to combine the fatigue-resistance of low frequency stimulation with the low ripple of high frequency stimulation. It is believed that the low stimulation frequency, the reduced duty cycle of each motor unit group or muscle, and the improved blood flow are mechanisms by which interleaved stimulation delays muscle fatigue [128]. The fatigue benefit of interleaved stimulation over synchronous stimulation has been demonstrated using surface electrodes in humans [129]–[132], spinal cord [24], [25] and peripheral nerve electrodes [20], [22], [23], [133]–[135] in cats, and epimysial electrodes in frogs [28]. Yet, the enhanced fatigue-resistance often observed with interleaved stimulation could not be consistently shown with intramuscular electrodes. Intramuscularly, Lau et al. [136] and Peckham et al. [137] demonstrated that less fatigue occurred during interleaved

stimulation than synchronous stimulation, while Buckmire et al. [138] recently showed that both interleaved stimulation and synchronous stimulation induced the same amount of fatigue. We hypothesize that this inconsistency was due to excessive overlap between the motor unit groups activated by the electrodes within the interleaved protocol [22], [133], [134], [139]. That is, in the study by Buckmire et al. [138] it would be possible that almost the same populations of motor units were stimulated by the electrodes, thus causing the individual muscle fibers to be activated at a high frequency rather than at a low frequency. We consider that in order to isolate the effect of interleaved stimulation on fatigue, the overlap must be controlled.

While fatigue was used by many authors as the main outcome measure for comparing the benefits of interleaved and synchronous stimulation, ripple was used only by a few. Authors that quantified ripple showed that, for the same frequency, the amount of ripple obtained with multisite interleaved stimulation was always higher than when a single electrode stimulated at a high frequency was used [23], [140]. Downey et al. [141] showed that with surface electrodes, interleaved stimulation generally produced high ripple, but when optimal stimulation frequency was used, ripple as low as that obtainable with single site high frequency stimulation was achieved. Hughes et al. [142] demonstrated that epimysial multisite interleaved stimulation could not attain the same level of force smoothness achievable with single site high frequency stimulation. Because of the tradeoff that exists between ripple and fatigue when stimulation frequency is varied, it was unknown whether or not increasing the stimulation frequency of interleaved stimulation (to match itsforce ripple to that developed during synchronous stimulation) would undermine its fatigue resistance.

In this work, our objective was to fairly compare the effect of interleaved and synchronous intramuscular stimulation on fatigue by ensuring that forces obtained from both protocols were matched in terms of initial ripple and magnitude.

## 3.3 Methods

### 3.3.1 Animal Preparation and Electrode Implantation

The *in vivo* procedure was approved by the local Ethical Committee for Animal Research (CEEA- PRBB) and by the Catalan Government (application number: BPM-18-0028AE (project number: 10109)). Three adult male White New Zealand rabbits weighing 4.1-4.5 kg were used in three experimental sessions, one animal in each experimental session.

The animal was anesthetized by administering dexmedetomidine (0.1 mg/kg), ketamine (10 mg/kg), and buprenorphine (0.05 mg/kg) intramuscularly. Hair covering the right shank and thigh was clipped using an electric shaver. The animal was then intubated and anesthesia was maintained by 3-4% sevoflurane. The cephalic vein was cannulated and lactated Ringer solution was administered intravenously. The animal was monitored during anesthesia via pulse oximetry and capnography while the plane of anesthesia was assessed by checking for corneal reflexes. A 5 cm incision was made on the posterior surface of the shank from the popliteal fossa

intravenously. The animal was monitored during anesthesia via pulse oximetry and capnography while the plane of anesthesia was assessed by checking for corneal reflexes. A 5 cm incision was made on the posterior surface of the shank from the popliteal fossa all the way down to the calcaneus. The hamstring fascia was then cut to gain access to the medial gastrocnemius (MG) muscle. The MG was the muscle of choice because: 1) its intramuscular innervation pattern is known [115], 2) it has a relatively simple as well as easily accessible extra-muscular nerve supply, and 3) it is a mixed fiber type muscle. Multisite stimulation in a heterogeneous muscle, like the MG, is expected to produce more ripple than if a homogeneous muscle was used, such as the soleus. So the MG muscle model provided a worst case scenario for testing our hypothesis.

Carefully, the head of the gastrocnemius muscle was pried away using blunt dissection to reveal the site where the MG nerve entered the muscle. Once the motor point of the MG muscle was visualized as depicted in Figure 7 (a), a hook wire intramuscular electrode (Catalog number 003400160 by SGM d.o.o., Split, Croatia) was inserted approximately 10 mm deep into the muscle parallel to the projected path of the nerve. This electrode will be referred to hereafter as the motor point (MP) electrode. Subsequently, nine additional intramuscular hook wire electrodes (hereafter collectively referred to as non-motor point electrodes) were implanted at different predetermined locations away from the motor point according to the scheme shown in Figure 7(b). To do that, a punctured and wetted 5 cm × 2 cm paper grid with circular markings at 5 mm intervals was overlaid on the exposed surface of the muscle to guide the implantation as shown in Figure 7 (c). The hook wire electrodes which were housed in a 1.3 cm long 26G needle were inserted at an approximate 30° angle with respect to the muscle surface to approximately the same depth (~ 1 cm). The nine non-motor point electrodes were given an ID based on their position from the motor point; proximal-medial (PM), proximal-central

(PC), proximal-lateral (PL), central-medial (CM), central-central (CC), central-lateral (CL), distal-medial (DM), distal-central (DC), and distal-lateral (DL). This electrode arrangement, in which a separation distance of 5 mm was maintained between electrodes in rows and 10 mm between those in columns, was chosen because of the oblong shape of the muscle and our attempt to maximize the area of the muscle that could be explored with the nine electrodes that were available. The lower third of the muscle was spared as stimulation in this region evoked very weak force responses. Two small skin incisions about 1 cm apart were made on the thigh, creating a tunnel through which a short piece of silver wire (⌀ ~ 1 mm) was passed and served as a reference electrode. Once implantation of electrodes was completed, the muscle was covered with glycerin to prevent dehydration before the animal´s foot was mounted on the isometric force measurement system.

Upon postmortem examination, the tips of all the implanted hook wire electrodes were found to be entirely located within the MG muscle and not piercing the underlying musculature.

## 3.3.2 Isometric force measurement bench and stimulator/recorder

A system was implemented to measure isometric forces evoked from hind limb muscles of rabbits in response to electrical stimulation. A schematic drawing of the isometric force measurement set-up is shown in Figure 8Figure 8. It consists of a force measurement bench and a stimulator/recorder (i.e. electronics).

The force measurement bench consists of: 1) an acrylic baseplate on top of which a 1.5 mm thick iron sheet was screwed in with bolts to provide a strong ferromagnetic surface for the attachment of the rest of the components, 2) a height adjustable ankle steel clamp

equipped with a magnetic base and atraumatic 'cushioned' caps that are intended to go over and clamp the tuberosity of the tibia to

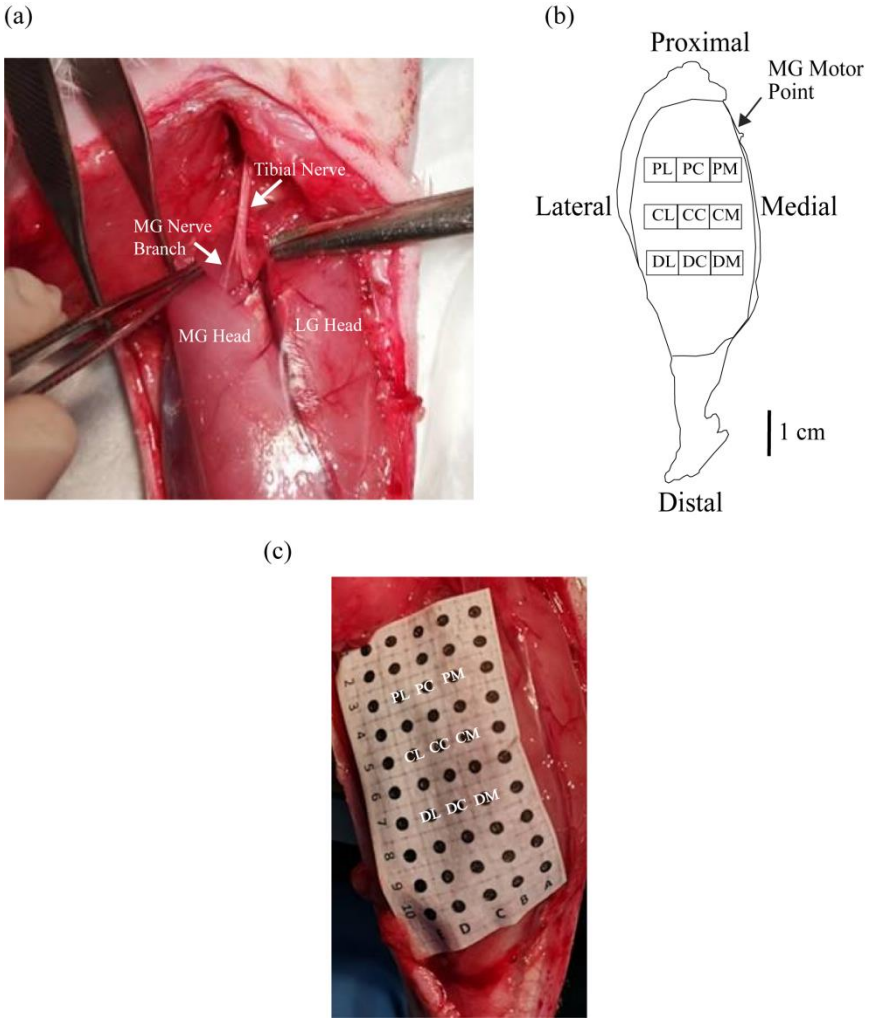


**Figure 7 Electrode implantation and experimental set-up. (a) The MG nerve branch of the tibial nerve was used to guide the insertion of the MP electrode. (b) Anatomical scheme (with scale bar) showing the final positions of the nine non-MP electrodes after their implantation in the MG muscle of the right leg with respect to the MP indicated by the black arrow. (c) Punctured grid paper used to ensure reproducible implantation across rabbits. The electrode IDs are overlaid on**

**the grid to mark the implantation site corresponding to each electrode.**

immobilize it, and 3) a metallic stand with a magnetic base for mounting the force transducer. The idea of using magnets for fixing the components was taken from [143]

The force transducer (STC-10kgAL-S by Vishay Precision Group, Malvern, PA, USA) was securely bolted to the metallic stand which in turn was affixed to the ferromagnetic surface via magnets. The animal was laid on its side with the leg to be tested being on the top. The leg was held above the surface of and parallel to the baseplate via the ankle clamp and then the foot was fastened via cable ties to a rigid plastic footplate which in turn was mechanically connected to the sensing element of the force transducer by a threaded rod at its center. The foot plate served as an interface between the animal's foot and the force transducer. The knee and ankle joint were flexed at approximately 90°. This ensured that the MG muscle was at the optimum length that produced the strongest response when it is electrically stimulated. The positioning of the foot resulted in a baseline force of approximately 1 N which was later subtracted from forces evoked by electrical stimulation. The distance between the ankle joint and the center of the footplate was approximately 8 cm.

In essence, the stimulator/recorder consisted in a computer controlled 16-channel current source able to generate monophasic pulses with a fixed duration of 250 µs and a programmable magnitude of up to 4 mA and a resolution of about 0.15 µA. Structurally, the core of the stimulator/recorder was a real-time controller (cRIO-9063 by National Instruments Corp., Austin, Texas, USA) that executed real-time algorithms uploaded from a PC laptop (Windows 10, model 532U3C Ultrabook by Samsung Electronics Co., Ltd, Suwon, South Korea) connected to it via USB. Two input-output modules were plugged into the real-time

controller: a signal conditioning and acquisition module for bridge sensors (NI-9237 by National Instruments Corp.) and a 16-channel voltage output module (NI-9264 by National Instruments Corp.). The input module NI-9237 was connected directly to the force transducer referred above. The output module NI-9264 was connected to a custom made 16-channel voltage to current converter. The real-time algorithms, which were specific for each one of the stimulation assays described below, were created in the instrumentation software platform LabVIEW (version 2017, by National Instruments Corp.). The LabVIEW platform was also used to record, pre-process and visualize the signal from the force transducer. The signal from the force transducer was acquired at a sampling rate of 1000 samples per second and low pass filtered by an $8^{th}$ order Bessel filter with a cutoff frequency of 100 Hz (unless otherwise specified in the assays described below).

In all assays, stimulation pulses were monitored with an oscilloscope (TPS2014 by Tektronix, Inc., Beaverton, Oregon, USA); not shown in figure 1.

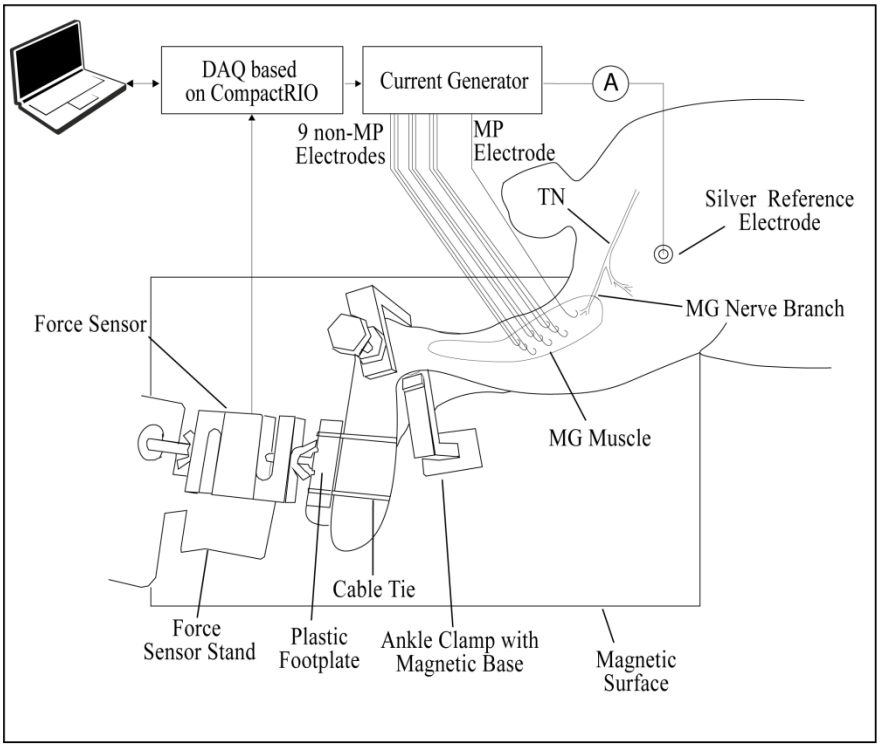


**Figure 8 Experimental set-up used for electrical stimulation and recording of evoked force responses. TN (tibial nerve), MG (medial gastrocnemius muscle).**

## 3.3.3 Electrical stimulation assays

### 3.3.3.1 Recruitment curves

Individual muscle twitches were produced by delivering 250 µs cathodic monophasic pulses with varying amplitude that increased from 0 to 4 mA in steps of 0.1 mA through each of the ten implanted electrodes. These pulses were automatically delivered in series by the stimulator/recorder at a rate of 1 pulse per second. The peak forces of the evoked muscle twitches were automatically determined for each pulse magnitude and plotted to construct the recruitment curve for each stimulation site.

Intermediate plateaus in the recruitment curves were identified whenever twitch peak forces increased by less than 5% over 2 or more increments in current for MP electrodes and 3 or more increments in current for the non-motor point electrodes [138]. Three parameters were extracted from the recruitment curves collected for each electrode; 1) maximal force defined as the force generated by the muscle in response to maximum stimulation allowed by our generator (4 mA), 2) plateau force defined as the mean force value at the first intermediate plateau region of the recruitment curve, 3) plateau width defined as the difference between the current value at the end of the first linear segment and the beginning of the second linear segment of the recruitment curve. As later explained in the discussion section, we conjecture that the plateau width and force are parameters that can be used to understand the organization of the motor unit groups within the muscle.

A peak twitch force of 0.3 N (approximately 10% of twitch force produced with maximum stimulation through MP electrode) was chosen as an adequate force level at which both overlap and fatigue were tested. This force level was selected because it was attainable even with stimulation of distalmost sites that generated relatively weak responses. Before performing the stimulation overlap test described below, the current amplitude was adjusted for all nine non-motor point intramuscular electrodes such that the magnitudes of their evoked twitch forces were matched to the predefined target value (0.3 N). Such adjustment was performed with the help of another algorithm that consisted of sequentially, at a rate of 4 pulses per second, delivering pulses through each electrode. The peak magnitudes of the resulting twitches were graphically displayed and the pulse amplitude on each electrode was manually programmed whenever the peak magnitude of its corresponding twitch significantly deviated from the desired target value. This step was repeated on a trial and error basis until the peak twitch forces obtained from all the electrodes were approximately equ

### 3.3.3.2 Stimulation overlap

Non-motor point electrodes that selectively accessed independent motor unit groups were identified by quantifying the stimulation overlap amongst all of them using the refractory technique [134], [135], [144]. This technique measures overlap between an electrode pair by comparing the sum of the twitch forces evoked when the two electrodes are stimulated separately with the twitch force generated when both electrodes fire with an interpulse interval of 750 μs between them as shown in Figure 9. This time delay ensures that the second stimulus is delivered during the refractory period of the motor axons excited by the first stimulus. If the two electrodes were independent, the forces evoked in response to stimulating one electrode immediately right after the other should be the same as the sum of the forces evoked when the two electrodes are stimulated individually. Contrastingly, if the two electrodes were overlapping, then forces evoked when both electrodes are stimulated in rapid succession would be lower than the sum of their individual responses. This is explained as a fraction of the motoneurons depolarized by the stimulus delivered through the first electrode would still be refractory and would be unable to respond to the stimulus passed through the second electrode.

The degree to which the magnitude of the integrated force deviates from the linear sum of the forces obtained when both electrodes are stimulated separately is proportional to the size of the overlapped region. Overlap was expressed as a percentage with values ranging from 0% to 100% whereby 0% corresponded to no overlap and a 100% indicated full overlap. % overlap was calculated for each electrode pair using the following equation:

$$Overlap = \frac{F_1 + F_2 - F_{1\&2}}{F_1} \times 100 \quad (1)$$

$F_1$ = Force evoked by stimulation through Electrode1
$F_2$ = Force evoked by stimulation through Electrode 2
$F_{1\&2}$ = Force evoked by stimulation through Electrode1 and 2

To analyze the stimulation overlap amongst all nine non-motor point electrodes in the array, eighty-one individual sets of pairwise electrode comparisons were performed, seventy-two of which were a result of testing each electrode against all other electrodes twice (stimulation was delivered in one order during the first test and the sequence was reversed in the second test) and nine of which are due to testing each electrode against itself (self-overlap). Thus, the overlap analysis generated a $9 \times 9$ matrix of overlap values which was further analyzed by a k-means clustering algorithm implemented in MATLAB (MathWorks, Natick, MA, USA) to determine the groups of electrodes that were stimulating the same muscle region (high overlap) and those activating the different muscle regions (low overlap) [145].

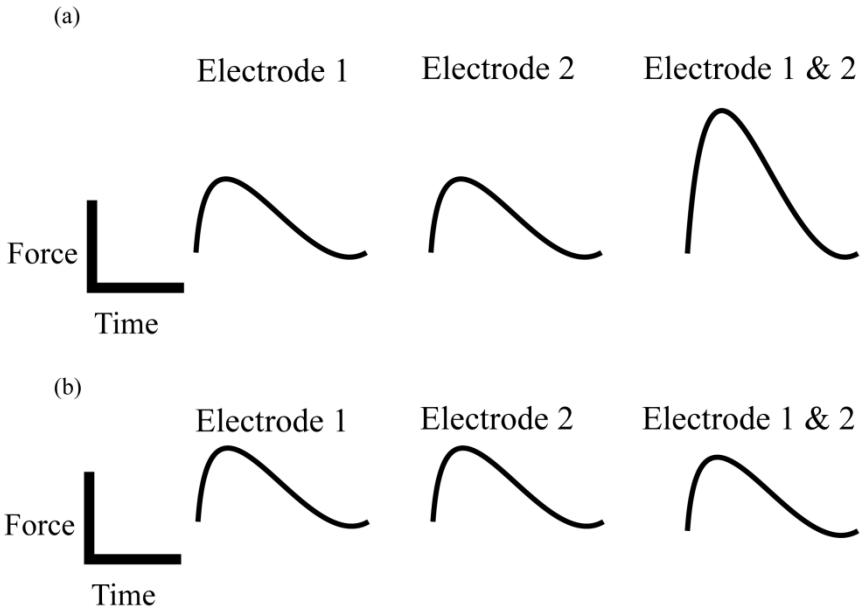

**Figure 9 Magnitudes of the twitch forces when electrode 1 and electrode 2 fire separately and when both fire with a short interpulse delay. (a) no overlap (b) full overlap.**

To our knowledge, there were no previous reports that showed how overlap amongst multiple intramuscular electrodes can be influenced by their location in the muscle and their arrangement with respect to each other. To investigate this, we analyzed the overlap for each row and each column of electrodes in the 3×3 electrode matrix (as shown in Figure 7(b)). Since each row and each column of electrodes (when considered in isolation) represented a unique electrode placement, we could thus readily demonstrate the effect that electrode positioning has on overlap. The row and column electrodes are referred to herein as horizontal and vertical triads (a combination of three adjacent electrodes) respectively.
The mean overlap for each triad was calculated by first averaging across the six overlap numbers generated from the six different pairwise test permutations possible with three electrodes within a triad (six permutations per three electrodes). At the end of this step, there was a single overlap value for each triad per rabbit. Then, the overlap values for the same triads in the different rabbits were pooled and averaged. Overlap amongst the electrodes used in interleaved stimulation was calculated in the same way.

## 3.3.3.3 Fatigue test

For the three rabbits, the clustering algorithm indicated that the nine non-motor point electrodes were grouped into three sets of highly overlapping electrodes. Out of each of the three sets identified, a single optimal electrode that ensured the lowest overlap when combined with electrodes from the other two sets was selected and was subsequently employed in the interleaved protocol.

Two procedures were performed before the commencement of the actual fatigue test. The goal of the first procedure was to deliver single pulses to check if equal twitch forces could be generated from the three selected electrodes when their corresponding current amplitudes—those previously determined from the overlap test—were applied. If the twitch forces from the three electrodes had different magnitudes, current amplitude was adjusted (only fine adjustments were needed). This careful force matching was crucial for minimizing the ripple in the force produced with interleaved stimulation (combining twitches of unequal amplitude results in a tetanic force with high ripple).

The aim of the second procedure was to determine the current amplitude required for the synchronous protocol to elicit a force similar to that produced by the interleaved protocol. First, the force produced with the interleaved protocol was determined by measuring the force response to delivering a 20 s pulse train of interleaved stimulation using the currents amplitudes determined in the first procedure (check following paragraph for stimulation features). Once the force generated with interleaved protocol was known, a series of 20 s pulse trains of 20 Hz synchronous stimulation was applied to the MP electrode and used to adjust the current intensity until the force achieved with the synchronous protocol was very similar to (but slightly lower than[1]) the one produced by the interleaved protocol. During these pulse trains, force signal was acquired at 500 samples per second and low pass filtered by an 8th order Bessel filter with a cutoff frequency of

[1] Since it was very difficult to perfectly match the synchronous force to the interleaved force, we decided to intentionally generate a synchronous force that was very similar to, but slightly lower than, the interleaved force. This ensured that not only were the forces in both protocols matched in terms of absolute ripple, but also that the relative ripple for synchronous protocol was slightly higher compared to the interleaved protocol as a way to set up a worst case scenario for testing our hypothesis.

50 Hz. The average force magnitude and the RMS force ripple over the last 5 s of the pulse trains were computed automatically by the algorithm. (It was not necessary to adjust the frequency of the synchronous protocol to match ripple as in preliminary assays it was found that synchronous stimulation at 20 Hz consistently produced similar ripple, or higher, than that produced by the interleaved protocol at 30 Hz).

The actual fatigue tests had a duration of 5 minutes. Muscle fatigue produced during interleaved and synchronous stimulation was assessed by examining the evolution of a quasi-tetanic contraction (i.e. almost fully fused twitches) over time. To produce a quasi-tetanic contraction with interleaved stimulation, 250 μs monophasic pulses were delivered through the three independent electrodes at 10 Hz each, with a small time shift (33.33 ms) amongst them, resulting in a composite frequency of 30 Hz (Int 30-Hz). The current value determined in the first procedure for each electrode was used. To obtain a contraction with synchronous stimulation that is equivalent (in terms of magnitude and ripple) to that achieved with interleaved stimulation, a continuous train of 250 μs monophasic pulses was applied on the MP electrode at 20 Hz (Syn 20-Hz) using the current amplitude determined in the second procedure.
All the fatigue tests lasted for five minutes and were separated by a ten minute period of rest to prevent fatigue/potentiation from influencing results from the subsequent tests. Force signal was acquired at 50 samples per second and low pass filtered by a 4th order Bessel filter with a cutoff frequency of 5 Hz. The order of testing of the different stimulation protocols was randomized. The difference in the patterns of stimulation between interleaved and synchronous protocols is illustrated in Figure 10. Electrical stimulation activated only the MG muscle and no signs of spread of stimulation to other muscles were observed.

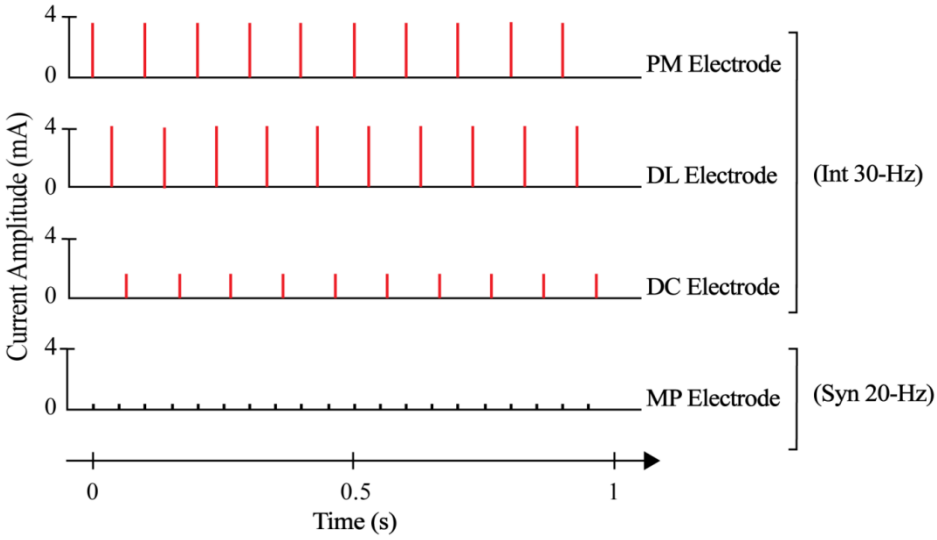


**Figure 10 Example of patterns of stimulus pulses delivered to the MG muscle of rabbit 1 during Int 30 Hz and Syn 20 Hz protocols to obtain forces with the same initial force and ripple value. Notice that the total frequency delivered to the muscle during interleaved protocol was higher than the synchronous protocol in order to match the ripple. Stimuli (indicated by the vertical lines) were delivered to a single intramuscular electrode at 20 Hz and to three independent intramuscular electrodes at 10 Hz each during Syn 20 Hz and Int 30 Hz protocols respectively. For the interleaved protocol, a time delay of 33.33 ms was implemented between the firing of one electrode and the next resulting in a composite frequency of 30 Hz. The height of the vertical lines represents the current amplitude used for each electrode. In this example, current amplitudes for MP, PM, DL and DC electrodes were 0.37 mA, 3.6 mA, 4 mA and 1.6 mA respectively to produce the same twitch force value of ~ 0.3 N.**

To determine the type of the motor units activated during the synchronous and interleaved stimulation, the durations of the twitches, recorded with the synchronous and each of the interleaved electrodes for creating the recruitment curves, were analyzed. Individual twitches evoked over current steps between threshold (current strength at which twitch force was first detected) and the

strength used to fatigue the muscle were analyzed for each electrode, The twitches were normalized to their peak values, and their duration defined as the time from the outset of the twitch until the force decayed to 10% of its peak value were measured[61]. Muscle fatigability was assessed by measuring the fatigue index (FI) and fatigue time (FT). FI was defined as the ratio between the peak force and the force at 100 s into the test, while FT was defined as the time it took for peak force to drop to 80% of its value. The peak force was defined as the maximum force value reached during the first 100 s into the test. This specific time window (from 0-100 s) was used to determine the peak force because, in one of the fatigue tests, force was recorded up to a 100 s and this allowed us to be consistent in our analysis of data obtained from different tests.

## 3.3.4 Sihler stain

Following the protocol outlined in [115], at the conclusion of the experiment, rabbits were euthanized with an overdose of sodium pentobarbital (120 mg/kg) and the MG muscle along with the intramuscular electrodes remaining in situ were excised and immediately fixed in 10% formalin for one month. Thereafter, muscles were then depigmented by maceration in a solution of 3% potassium hydroxide and 3% hydrogen peroxide (0.04 ml of $H_2O_2$ per 100 ml of KOH) for four weeks. The muscles were decalcified in Sihler's solution I (one part glacial acetic acid, one part glycerin, and six parts 1% aqueous chloral hydrate) for three weeks till the muscles were transparent. The nerves were stained by immersing the muscle in Sihler's solution II (two part Mayer's hematoxylin, one part glycerin, and six parts 1% aqueous chloral hydrate) for two weeks, followed by destaining step (in Sihler's solution I) lasted for six hours to remove excess stain. The stained muscles were neutralized in 0.05% lithium carbonate solution for one hour and cleared in glycerin at increasing concentrations (40%, 60%, 80%,

and 100%; for one week in each concentration). After clearing, the muscles were stored in pure glycerin in the dark.

### 3.3.5 Statistical Analysis

Two-way analysis of variance without interaction (treatment and animal) was performed to compare the twitch durations obtained from the different stimulation sites. The animal was used as a blocking factor to account for any variability caused by inter-animal differences [146]. A similar approach was used to test for statistically significant difference in mean overlap amongst the different triads as well as to analyze FI, FT and RMS ripple for the synchronous and interleaved protocols. Linear regression analysis was used to analyze how plateau force and width changed as a function of electrode-motor point distance. All results are presented as the mean ± standard error of the mean (SEM). All statistical tests were carried out at a significance level of $\alpha = 0.05$ using SPSS statistical package (IBM, Chicago, IL, USA).

## 3.4 Results

### 3.4.1 Recruitment characteristics as a function of electrode position

12/30 (40%) of the recruitment curves obtained in this experiment lacked intermediate plateaus while the remaining ones (60%) contained two or more linear regions of recruitment separated by intermediate plateau(s). Examples are shown in the insets of Figure 11(a)-(c). Figure 11 (b)-(d) shows the maximum force elicited from the MG muscle in response to maximum stimulation (4 mA) via each electrode. The bold horizontal lines in the bars correspond to the mean force value at the plateau region(s) of the recruitment curve obtained from each electrode. Stimulation with the MP

electrodes evoked the strongest responses out of all the implanted electrodes. Peak twitch forces produced with a 4 mA stimulus pulse delivered through the MP electrodes were 3.89 N, 3.92 N, and 4.31 N in rabbits 1, 2, and 3 respectively. Responses became weaker as the distance between the electrode and the motor point increased.

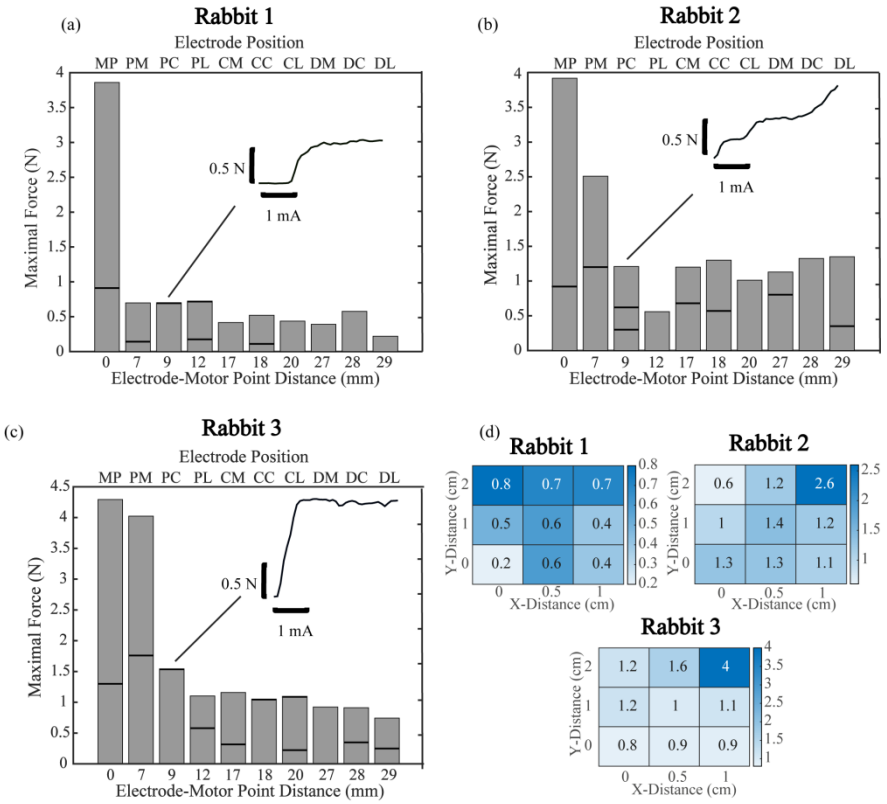


**Figure 11 Recruitment characteristics of ten intramuscular electrodes inserted at different distances from the MP with MP electrode lying the closest to and the DL electrode the farthest from it.. (a), (b), and (c) are bar charts displaying the force generated by the muscle when maximal stimulation (4 mA) was delivered as a function of the distance between each intramuscular electrode and the MP for rabbits 1, 2, and 3 respectively. The electrode ID corresponding to each distance value on the bottom x axis is shown on the top x axis. Bold**

**horizontal lines indicate the force value at the plateau region of the recruitment curve. The bold horizontal lines are lacking for electrode positions where force did not reach a plateau value. Insets depict the shape of the recruitment curves produced by PC electrode in all three rabbits. (d) Heat map of the peak force evoked by intramuscular stimulation as a function of x and y positions of the electrodes for the three rabbits.**

A heat map of the peak forces evoked with IM electrical stimulation as a function of the x and y positions of the IM electrodes are shown in (d) for each rabbit. Larger forces (i.e. darker color) were recorded from electrodes that were located closer to the nerve entry point compared to those that were farther from it (i.e. lighter color). Figure 12 (a) shows a stem plot of three recruitment curves obtained from rabbit 3 using IM electrodes located at successively more distal locations. Two aspects about the shape of the first plateau in the recruitment curves are noticeably changing as the IM is moved more distally: 1) the force magnitude at the first plateau is decreasing and its width is increasing. The possibility that by placing the IM electrode distally, finer neuromuscular compartment can be accessed is shown in Figure 12 (b). Linear regression analysis showed that the plateau force significantly decreased as the distance separating the electrode from the motor point increased ($p < 0.05$), as shown in Figure 12 (c) while Figure 12 (d) shows that the plateau width significantly increased as the distance between the electrode and the nerve entry point increased ($p < 0.05$).

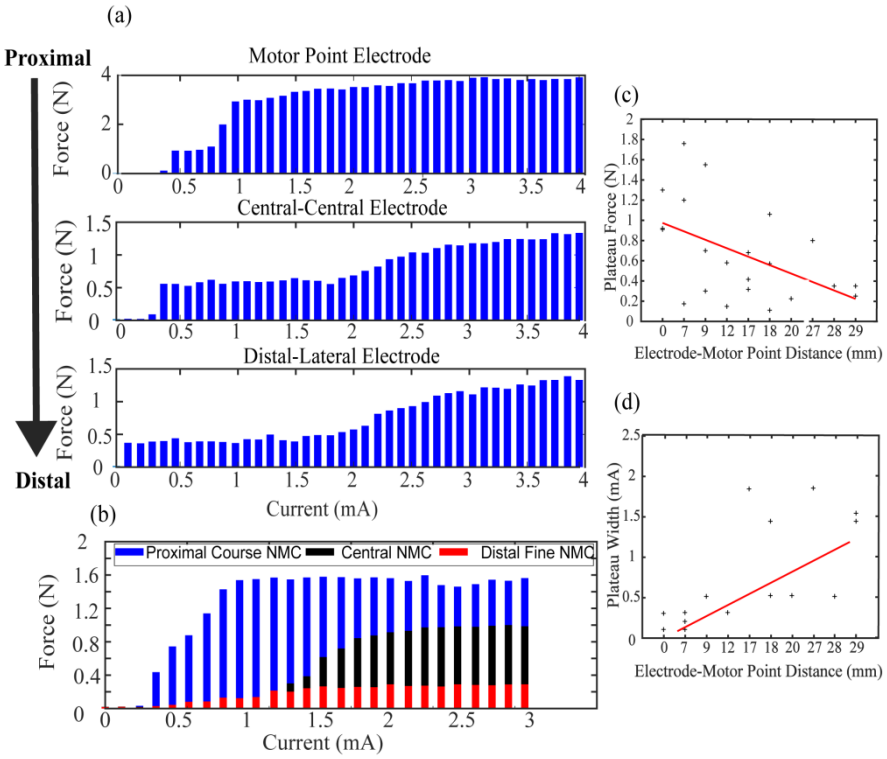


**Figure 12 Recruitment curve analysis. (a) Recruitment curves collected from three IM electrodes inserted at successively more distal locations. Notice how plateau force decreased and plateau width increased as IM electrode location changed from a proximal to a more distal location (black arrow). (b) Comparison of the maximum force outputs from neuromuscular compartments of different sizes. Evidence of high order compartmentalization; proximally placed IM electrodes accessed large compartments with large force outputs, while distally placed accessed fine compartments with fine force outputs. (c) Significant ($p < 0.05$) negative relationship between the plateau force and distance from the MP ($R = 0.5$). (d) Significant ($p < 0.05$) positive relationship between plateau width and distance from the MP ($R = 0.7$).**

### 3.4.2 Selectivity of stimulation with intramuscular electrodes

The ability of three adjacent intramuscular electrodes (triad) to selectively activate independent regions of the muscle was assessed as a function of their location in the intramuscular nerve pathway and their arrangement with respect to each other. The light gray, gray, and dark gray horizontal triads shown in Figure 13 (a) occupied the proximal, central and distal regions of the intramuscular nerve pathway respectively and the stimulation overlap amongst electrode members of each horizontal triad is depicted in Figure 13 (b).

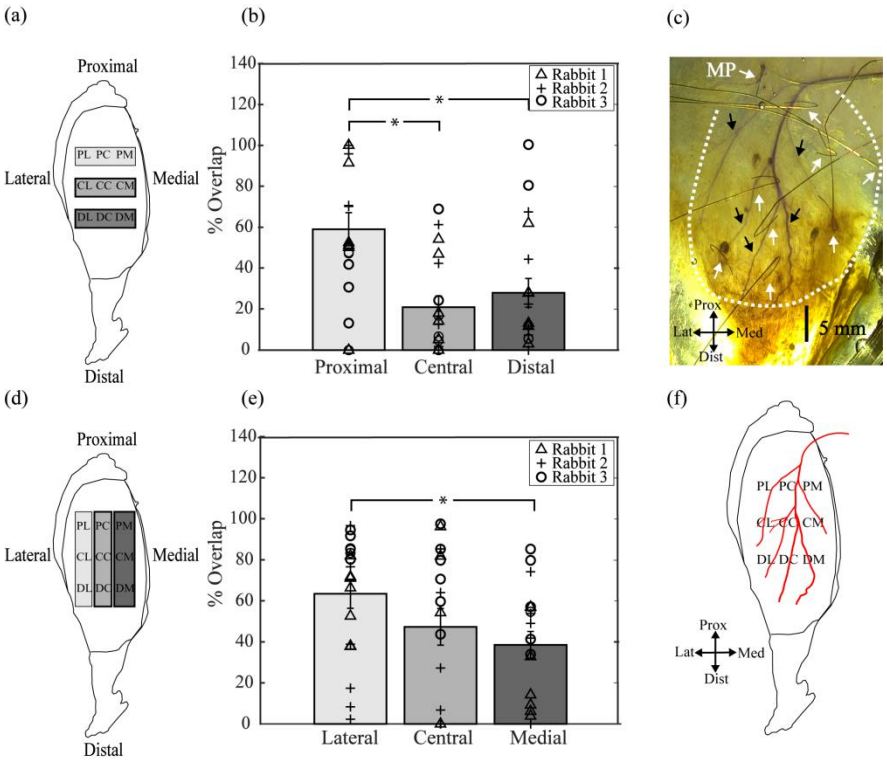


**Figure 13 Stimulation overlap produced by a combination of three adjacent electrodes (triad) as a function of their locations**

**in the intramuscular nerve pathway. The overlap produced by each horizontal and vertical triad was separately calculated and presented. Separation distance of electrodes in each horizontal and vertical triad was 5 mm and 10 mm respectively. (a) The triads in the proximal (light gray), central (gray) and distal (dark gray) regions of the muscle. (b) the mean % overlap ± SEM for the horizontal triads shown in (a). Individual data points collected from each rabbit are shown; (△), (○), and (+) for rabbits 1, 2, and 3 respectively. (c) Intramuscular innervation pattern on the outer surface of the MG muscle as revealed by Sihler staining. White dotted line circumscribes the muscle region containing the intramuscular electrodes. White arrows indicate the hooks of eight intramuscular electrodes, while black arrows show the locations of the five primary intramuscular nerve branches. Note that there are only eight intramuscular electrodes instead of nine as some were dislodged during the staining process. (d) Triad in the medial (dark gray), central (gray) and lateral (light gray) parts of the muscle. (e) Mean % overlap ± SEM of vertical triads shown in (d). (f) Tracing of the branching patterns of intramuscular nerves shown in (c) combined with the assumed locations of the electrodes. Note how overlap was minimum in regions where electrodes were aligned with different nerve branches and maximum when they were aligned with the same nerve branch. (*) indicates statistical significance ($p < 0.05$).**

Stimulation overlap produced by the proximal triad (59.1% ± 8.1%, mean ± SEM) was significantly higher than the overlap generated by the central (21% ± 5.5%,) and distal triad (28% ± 7%). The fact that the same horizontal triad produced lower stimulation overlap when placed more distally than proximally highly correlated to the wider separation of the primary intramuscular trunks due to their branching as revealed by Sihler staining in Figure 13 (c). The light gray, gray, and dark gray vertical triads shown in Figure 13 (d) were located in the medial, central and lateral regions of the intramuscular nerve pathway respectively and the stimulation

overlap amongst the electrode members of each vertical triad is presented in Figure 13 (e). Post-hoc analysis revealed that the overlap amongst electrodes in lateral triad was significantly higher (63.4% ± 7) than overlap amongst electrodes in the medial triad (38.5% ± 6.5%), but was not statistically different compared to overlap amongst electrodes in the central triad (47.3% ± 9%). The substantially high overlap measured for the lateral triad could be because, according to the Sihler stain, electrode members of this triad lied in the same region as and in alignment with a single primary nerve branch, which was not the case for other vertical triads that happened to align with different nerve branches. A tracing of the branching pattern shown in Figure 13 (c) is displayed in Figure 13 (f) where the approximate locations of the electrodes with respect to the five main intramuscular branches are shown. Consistently, stimulation overlap produced by a triad was the lowest whenever its electrodes were aligned with different nerve branches.

### 3.4.3 Fatigue induced by interleaved vs synchronous stimulation

The matrices of overlap numbers and the results of applying the K-means clustering algorithm to the overlap data obtained from each rabbit are shown in Figure 14.

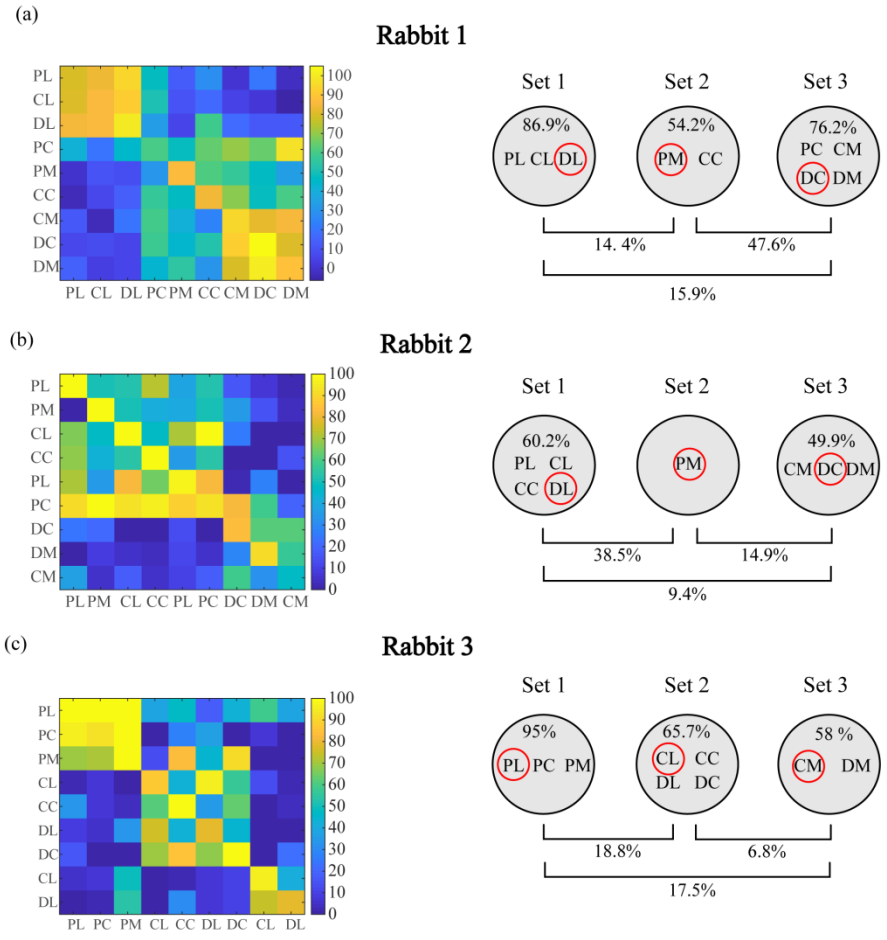


**Figure 14 Selection of the intramuscular electrodes that were used in interleaved stimulation. (a),(b), and (c) overlap matrices (left) and the classifcation results obtained by applying the clustering algorithm to overlap data (right) collected from**

**rabbit 1, 2, and 3 respectively. The clustering algorithm identified three different sets of highly overlapping intramuscular electrodes denoted as set 1, set 2 and set 3 for each rabbit. Each black circle represents an individual set and inside each circle are the IDs of the IM electrodes that are members of that specific set. Overlap number inside each back circle indicates the mean % overlap amongst its electrode members (i.e. intra-set % overlap) while the numbers outside the circle below the horizontal brackets indicate the mean inter-set % overlap. Note that for rabbit 2, PC electrode was excluded because it was an outlier (i.e. it highly overlapped with electrodes in both sets 1 and 2). This could be due to the possibility that it lied near a main nerve that branched out to a large region of the muscle and resulted in high overlap with several electrodes. Electrode ID encircled in red in each black circle indicates the electrode that was selected from each set and used in independent multisite interleaved stimulation.**

**Table 1. Summary of the electrodes, currents, and frequencies used in the synchronous (Syn 20-Hz) and interleaved (Int 30-Hz) stimulation protocols as well as the mean % overlap among the three electrodes used in the interleaved protocol for each rabbit.**

| Rabbit # | Protocol | Elec ID | Current (mA) | Freq (Hz) | Overlap (%) |
|---|---|---|---|---|---|
| | Syn 20 | MP | 0.37 | 20 | N/A |
| Rabbit 1 | | PM | 3.6 | 10 | |
| | Int30 | DL | 4 | 10 | 20.5 |
| | | DC | 1.6 | 10 | |
| | Syn20 | MP | 0.67 | 20 | N/A |
| Rabbit 2 | | PM | 0.3 | 10 | |
| | Int30 | DL | 0.5 | 10 | 24.6 |
| | | DC | 0.75 | 10 | |
| | Syn20 | MP | 0.48 | 20 | N/A |
| Rabbit 3 | | PL | 0.44 | 10 | |
| | Int30 | CL | 3.1 | 10 | 4.0 |
| | | CM | 1.5 | 10 | |

Electrodes that were found to be highly independent and were employed in interleaved stimulation were electrodes PM, DL, and DC for rabbits 1 and 2, and electrodes PL, CL, and CM for rabbit 3. The average overlap amongst the interleaved electrodes was 20.5%, 24.6%, and 4.0% in rabbits 1, 2, and 3 respectively. Electrode positions, currents and frequencies used in the synchronous and interleaved stimulation protocols for each rabbit are summarized in Table 1.

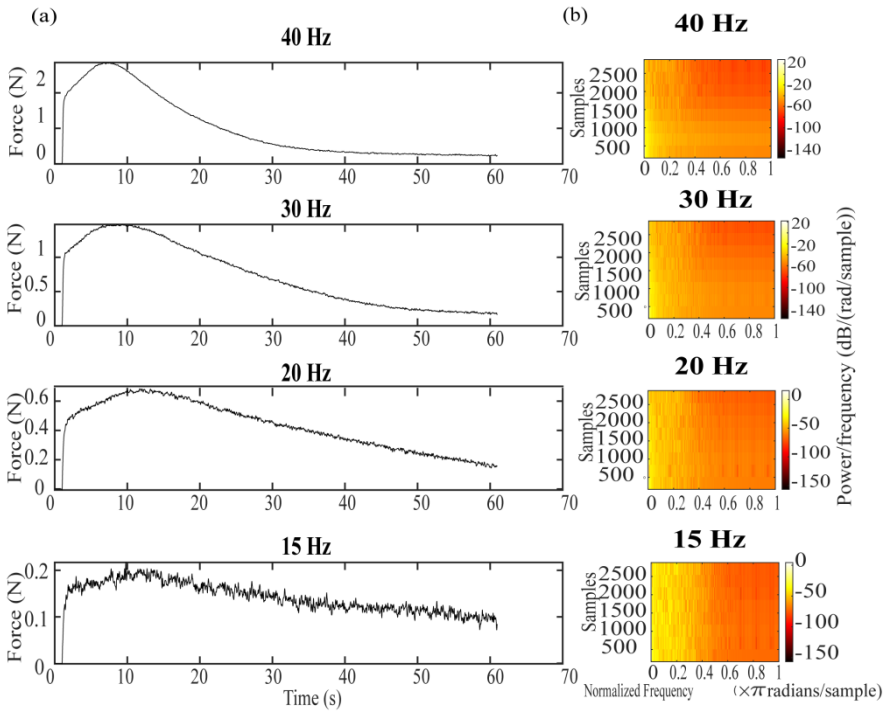


**Figure 15 . Dependency of muscle fatigue and maximum force on stimulation frequency. (a) Each plot corresponds to a single 60 s fatigue test obtained from GM of a WNZ rabbit. Stimulation was delivered through the single IM electrode with fixed current pulse amplitude of 0.67 mA at varying frequencies. Fatigue occurred at a higher rate with high frequencies than lower ones. (b) spectrograms of the each of the force signals shown in (a) to show that contraction ripple increased with decreasing stimulation frequency.**

The frequency by which stimulus pulses are delivered to a muscle to excite it influence the force output from the muscle in several ways. First, the higher the stimulation frequency that is used, the larger the magnitude of the evoked force as well as the smoother (more fused) it is, but the faster it fatigues. Those trends are captured in Figure 15 showing the muscle tension recorded from medial gastrocnemius (MG) muscle of a rabbit in response to stimulation delivered at different frequency using motor point stimulation with the MP electrode,

Figure 16 (a) shows the time course of force responses produced from a single trial performed in the MG muscle of rabbit 1 during both interleaved and synchronous stimulation protocols. Of the 14 fatigue trials performed across three rabbits, seven trials were Int 30-Hz and the rest were Syn 20-Hz. Force traces obtained from all 14 trials are provided in the supplementary material. It can be clearly seen that force evoked with interleaved stimulation could be maintained for a longer period of time compared to that generated by synchronous stimulation which decayed very rapidly soon after the beginning of the test. Figure 16 (b) displays the mean fatigue time (FT) calculated for each stimulation protocol. Mean FT for interleaved stimulation (111 s ± 17.7 s) was significantly longer than that measured for the synchronous protocol (12.6 s ± 3.7 s; $p<0.05$). Furthermore, the mean fatigue index (FI) of the interleaved protocol was significantly larger (0.86 ± 0.03) than that of the synchronous protocol (0.3 ± 0.06) as shown in Figure 16(c).

A summary of the ripple (i.e. smoothness) analysis of the force signals obtained with Int 30 Hz and Syn 20 Hz stimulation protocols is shown in Figure 17. Figure 17 (a) shows that the mean of the RMS ripple of forces produced during both stimulation protocols were not statistically different ($p = 0.96$) as expected. Figure 17 (b) is the Fourier analysis of the force signals obtained from both protocols. It shows that both force signals had nearly similar wave numbers that concentrated on the low-frequency end

of the spectrum. This indicates that force signals produced by both protocols had very similar frequency content and that both were free from any high frequency content (i.e. ripple). A time-frequency analysis of the force signals generated by each stimulation protocol was preformed and the resulting spectrograms are shown in Figure 17 (c). In agreement with Fourier analysis, both Int 30 Hz and Syn 20 Hz force signals had similar frequency content which did not significantly change with time.

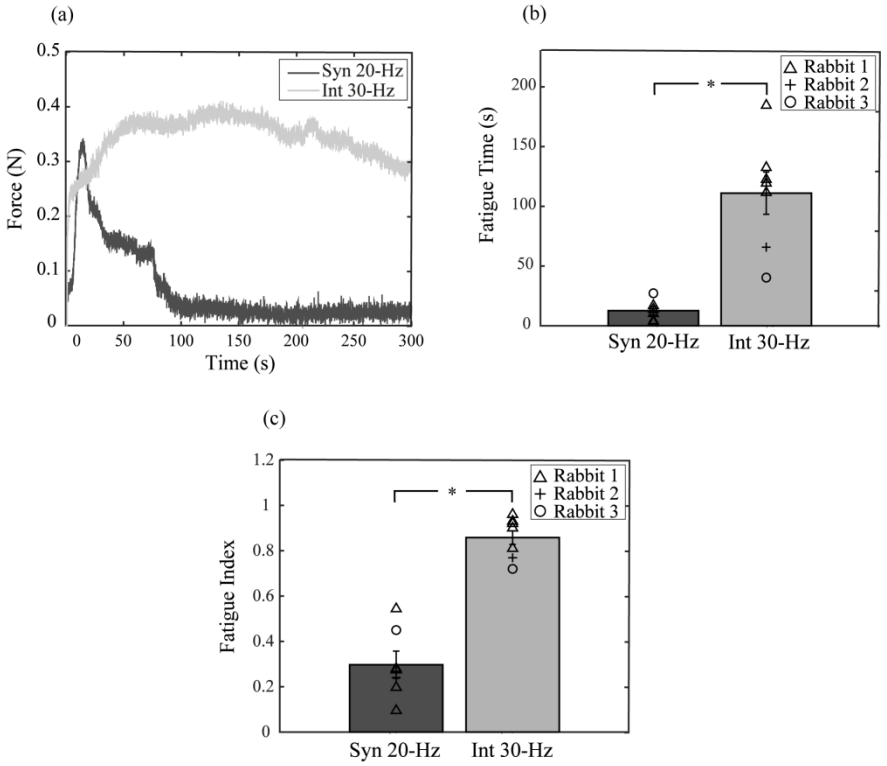


**Figure 16 Endurance of contractions evoked with minimally overlapping multisite interleaved (Int 30 Hz) vs synchronous stimulation (Syn 20 Hz). (a) Evolution of the quasi-tetanic force over time from a single trial in rabbit 1 elicited with Int 30 Hz (gray trace) and Syn 20 Hz (black trace), after forces were adjusted to have the same force magnitude and degree of ripple.**

**(b) Mean FT (s) ± SEM for Int 30 Hz (gray) and Syn 20 Hz (black) protocols. (c) Mean FI ± SEM for the Int 30 Hz (gray) and Syn 20 Hz (black) protocols. (*) indicates statistical significant results. Individual data points collected from each rabbit are shown; (△), (○), and (+) for rabbits 1, 2, and 3 respectively.**

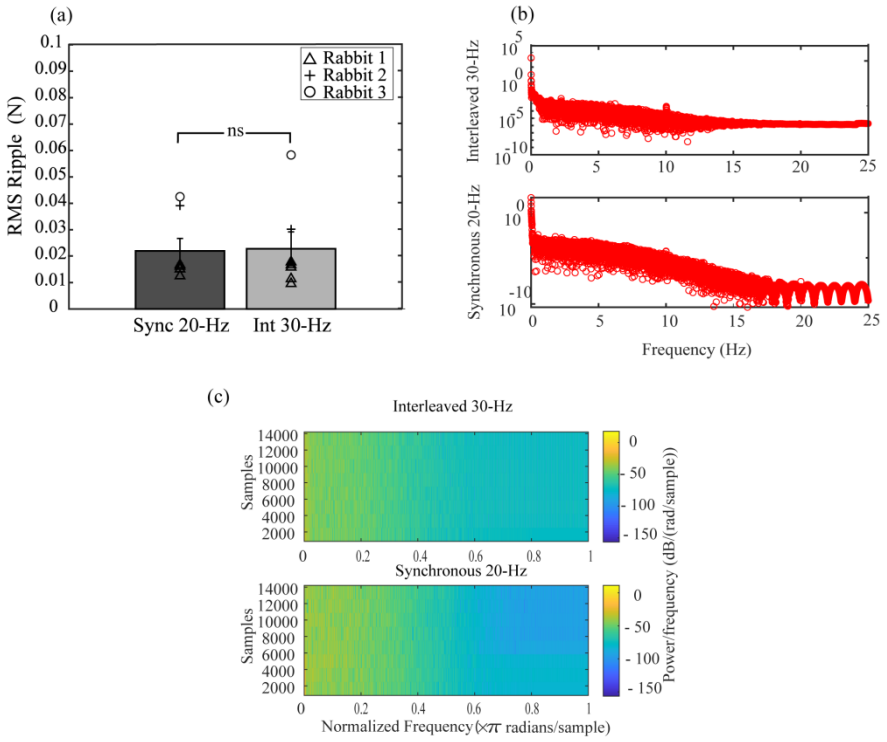


**Figure 17 Ripple analysis of force responses obtained with Int 30 Hz and Syn 20 Hz. (a) Mean RMS ripple in force evoked with Int 30 Hz (gray) and Syn 20 Hz (black) protocols. (ns) indicates non-statistically significant results. Individual data points collected from each rabbit are shown; (△), (○), and (+) for rabbits 1, 2, and 3 respectively. (b) Fourier transform of force signals obtained with Int 30 Hz (top) and Syn 20 Hz (bottom). (c) Spectrogram of of force signals obtained with Int 30 Hz (top) and Syn 20 Hz (bottom)**

### 3.4.4 Contractile properties of excited motor units

Twitch force recordings from different stimulation sites exhibited different timing features. Figure 18 (a), it is shown, for rabbit 3, the average of seven normalized twitches obtained at varying current amplitudes with the synchronous electrode and with the electrodes 1, 2, and 3 employed in the interleaved protocol. The durations of twitch waveforms collected from the synchronous electrode were longer than those obtained with the interleaved electrodes. These time profile of these twitches resemble those reported by other authors [147]. Figure 18 (b) displays a boxplot of the twitch durations of all the individual twitches collected at different current amplitudes obtained from the synchronous and interleaved electrodes across all rabbits. The duration of the twitches was significantly longer for the synchronous electrode (156 ms ± 1 ms) than interleaved electrode 1 (82 ms ± 2 ms), 2 (100 ms ± 2 ms) and 3 (75 ms ± 3 ms). Amongst the interleaved stimulation electrodes, electrode 2 had a significantly slower twitch than did electrodes 1 and 3.

By measuring the duration of the individual twitches that constituted the dynamic part of the recruitment curves, we were able to gain insight into the contractile properties of MUs that were recruited by each electrode. Sometimes, the spread (i.e. standard deviation (SD)) of the duration of force twitches obtained from a single site was narrow, as narrow as 5 ms, suggesting that the recruited nerve branch consisted entirely of one type of motor axons. Contrarily, there were other sites where the spread of the duration of the collected force twitches was broad (around 20 ms) reflecting that the nerve branch accessed by the electrode possessed a more mixed fiber type composition. Thus, this analysis was performed for electrodes from which twitches with large SD in their duration were recorded. We have found statistically significant

differences in the contractile properties of the recruited MUs at the different distal stimulation sites. An example of two stimulation sites exhibiting differential contractile properties in rabbit 3 is shown in Figure 18 (c). Figure 18 (c) shows the distribution of the durations of all the twitches collected from electrode CM and DM. The duration of the twitches collected with electrode DM distributed around higher

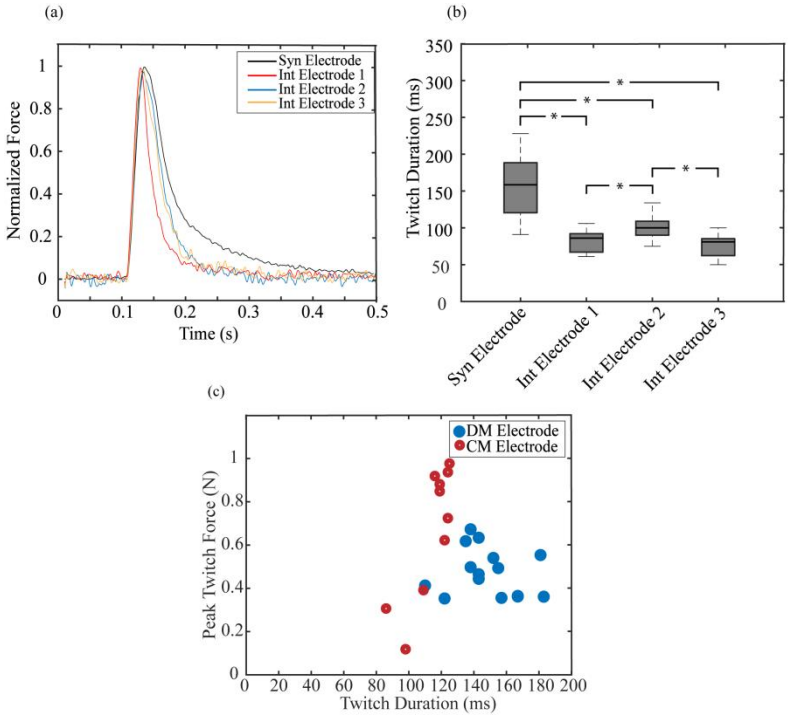


**Figure 18 Isometric twitch force recordings of motor units activated by synchronous stimulation electrode vs interleaved stimulation electrodes. (a) Average of seven twitches collected at varying current amplitudes from the synchronous electrode (black) and interleaved electrodes 1 (red), 2 (blue), and 3 (orange) in rabbit 1 after they were normalized to their peak twitch force. (b) Boxplot of the duration of the twitches pooled from all the rabbits for the synchronous and interleaved electrodes. (*) indicates statistical significance.(c) Scatter plot showing the distribution of the durations of all the twitches**

**collected from electrode CM and DM as a function of their corresponding peak twitch force.**

values compared to those collected from electrode CM. The results of the analysis of the MU contractile properties for the different electrodes are summarized in Table 2 for each rabbit as well as the results of the ANOVA procedure for testing statistical significance.

**Table 2 Summary contractile properties measured by the twitch width (TW) of the motor units stimulated by the different electrodes for all the rabbits.**

| Rabbit # | Electrode ID | Mean TW (ms) | SD (ms) | Significance (pairwise comparison) |
|---|---|---|---|---|
| 1 | PC | 99 | 15 | 2 vs 5, 4 vs 5, 5 vs 6, 5 vs 7, 5 vs 8, & 6 vs 9 |
| | Cl | 98 | 15 | |
| | CC | 60 | 16 | |
| | CM | 105 | 20 | |
| | DL | 97 | 17 | |
| | DC | 94 | 9 | |
| | DM | 83 | 14 | |
| 2 | PL | 59 | 16 | 1 vs 8 & 4 vs 8. |
| | CL | 65 | 5 | |
| | DC | 81 | 9 | |
| 3 | CL | 120 | 10 | 4 vs 9, 5 vs 9, & 6 vs 9 |
| | CC | 116 | 17 | |
| | CM | 114 | 13 | |
| | DM | 149 | 20 | |

## 3.4.5 Effect of motor unit type on muscle fatigue

Muscle fatigue associated with electrical stimulation depends on the frequency that is used to stimulate the muscle and the MU composition of that muscle. To assess which of the two factors is more important in influencing fatigue, we took advantage of the fact that different IM electrodes accessed MU with different fatigue

properties and we used this to compare the effect of MU type and stimulation frequency on muscle fatigue in the same experiment. Figure 19. Effect of MU type on electrical stimulation-induced muscle fatigue. (a) and (b) are results from rabbit 1. (a)Time course of the force produced by sustained stimulation of a slow MU group and a fast MU group at 10 Hz. (b) Plot of the width of the twitches obtained from the slow and fast MU groups fatigued in (a) as a function of current amplitude of the injected electric pulses. (b) confirms that the slow electrode accessed slow MUs since twitch widths collected from the slow electrode were longer than those collected from the fast electrode at most of the current values tested. (c) and (d) are results from rabbit 3. (c) Time course of the force produced by sustained stimulation of a slow MU group and a fast MU group at 40 Hz. (d) Plot of the width of the twitches obtained from the slow and fast MU groups fatigued in (c) as a function of current amplitude of the sequentially injected electric pulse. Each force series shown was normalized to its corresponding peak force value.Figure 19 shows the effect of MU type and stimulation frequency on electrical stimulation induced muscle fatigue. Figure 19 (a) and (c) show the evolution of muscle force over time produced by synchronously stimulating a region of the muscle that was mainly ‘slow’ i.e. consisted of mostly slow muscle fibers and another region that was mainly ‘fast’ at 10 Hz and 40 Hz respectively. There was no signifcant difference in the pattern of force decay when the slow or the fast MU groups were fatigued. Force decay was sensitive to the frequency of stimulation used (i.e. higher stimulation frequency resulted in a rapid loss in contractile strength), but not to the type of MUs recruited. To confirm the slow or the fast nature of the MUs that were fatigued, we generated a plot of the widths of the twitches obtained from each MU group as a function of the amplitude of the current pulses used to evoke them. Slow MU groups produced twitches that were significantly longer than those produced by the fast MU group across most of the current amplitude values tested as shown in Figure 19 (b) and (d).

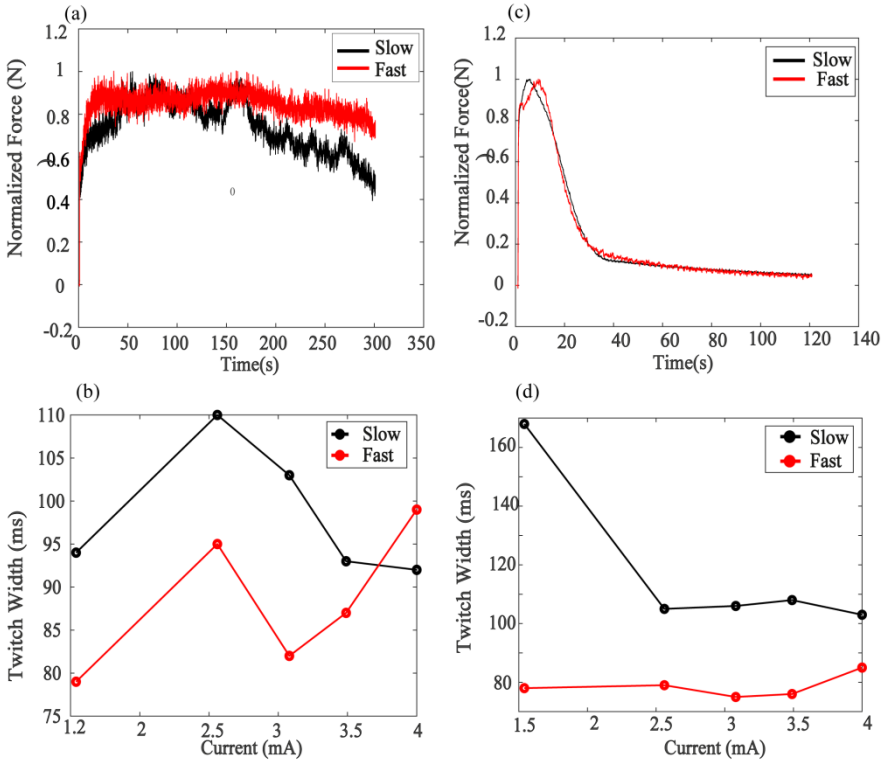


**Figure 19. Effect of MU type on electrical stimulation-induced muscle fatigue. (a) and (b) are results from rabbit 1. (a)Time course of the force produced by sustained stimulation of a slow MU group and a fast MU group at 10 Hz. (b) Plot of the width of the twitches obtained from the slow and fast MU groups fatigued in (a) as a function of current amplitude of the injected electric pulses. (b) confirms that the slow electrode accessed slow MUs since twitch widths collected from the slow electrode were longer than those collected from the fast electrode at most of the current values tested. (c) and (d) are results from rabbit 3. (c) Time course of the force produced by sustained stimulation of a slow MU group and a fast MU group at 40 Hz. (d) Plot of the width of the twitches obtained from the slow and fast MU groups fatigued in (c) as a function of current amplitude of the sequentially injected electric pulse. Each force series shown was normalized to its corresponding peak force value.**

## 3.4.6 Motor unit recruitment order with intramuscular electrodes

One way to measure the order of recruitment of MUs with electrical stimulation is to see what happens to the duration of the evoked muscle twitches as the amplitude of the injected current is increased. If short duration twitches are obtained at low current levels and longer ones are evoked at higher current levels, then order of MU recruitment is the opposite of that which occurs naturally. We used this approach to test the order of MUs recruitment with IM stimulation.

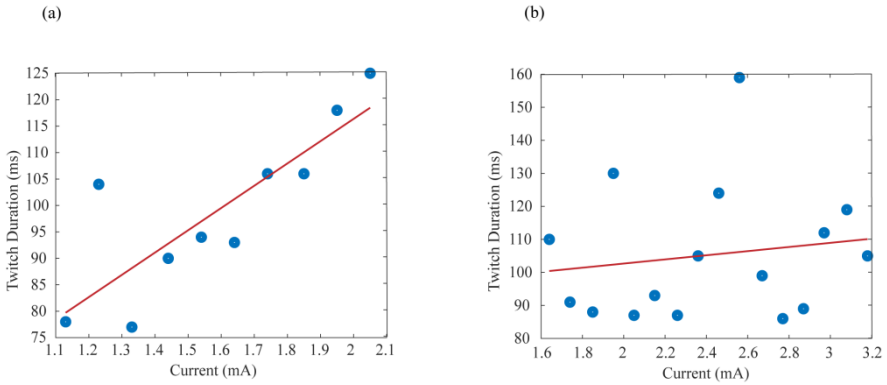


**Figure 20. Order of recruitment of MUs with IM stimulation depends on the location of the IM electrode. Linear regression analysis of how the duration of the evoked twitches changes with increasing the current amplitude of the electric pulses. (a) Inverse order of recruitment from the CC electrode. Slower MU are recruited at higher current levels (b) mixed order recruitment with DM electrode.**

**Table 3 Summary of the results of the analysis of recruitment order of MUs that was performed for a subset of implanted IM electrodes.**

| Rabbit # | Electrode ID | Slope | $R^2$ | p value | Order of recruitment |
|---|---|---|---|---|---|
| 1 | PC | 0.04 | 0.7 | 0.003 | Inverse |
| | CL | 0.02 | 0.4 | 0.0175 | Inverse |
| | CC | 0.03 | 0.7 | 0.004 | Inverse |
| | CM | 0.006 | 0.02 | 0.57 | Mixed |
| | DL | -0.002 | 0.001 | 0.95 | Mixed |
| | DM | -0.09 | 0.002 | 0.9 | Mixed |
| 2 | PL | 0.05 | 0.78 | 0.001 | Inverse |
| 3 | CC | -0.02 | 0.2 | 0.15 | Mixed |
| | CM | 0.03 | 0.57 | 0.012 | Inverse |
| | DM | -0.006 | 0.02 | 0.62 | Mixed |

The recruitment of MUs at the different stimulation sites in each rabbit appeared to follow either a mixed order where both slow and fast MU were equally likely to be activated by the next step increment in current amplitude, or an inverse order where the fast motoneurons were activated before the slow ones.

Figure 20 shows an example from two different stimulation sites (electrodes CC and DM) in the same muscle demonstrating inverse and mixed recruitment order of motor units respectively. The twitch duration was plotted against current amplitude as well as the linear regression line describing this relationship. Figure 20 (a) shows that the duration of the twitches significantly increased with higher current amplitudes ($p < 0.05$) indicating an inverse recruitment order of MU. Figure 20 (b) shows that twitch duration did not significantly depend on current amplitude suggesting a mixed recruitment order of motor units ($p > 0.05$). Only IM electrodes from which twitches with durations that had a standard deviation of

10 ms or above were collected were included in this analysis. A summary is presented in Table 3

## 3.5 Discussion

### 3.5.1 Recruitment characteristics as a function of electrode position

Recruitment properties were characterized for each intramuscular electrode by measuring three aspects of the generated recruitment curves: the maximum force, the plateau force, and the plateau width. We found that the maximum force decreased as the distance between the electrode and the nerve entry site increased. This can be explained by a reduction in the number of motor units that can be recruited as the stimulation electrode moves away from the main nerve branches. Sihler stain indeed revealed that nerve branches were progressively becoming thinner as they travelled distally thus innervating fewer motor units. Plateau width and force, on the other hand, are parameters that we conjecture can be used to understand the organization of the motor unit groups within the muscle. It has been reported previously that the hind limb muscles of mammals are divided by their primary (main) intramuscular nerve branches into discrete motor unit groups called neuromuscular compartments (NMCs) which can be activated independently of the other [106], [107], [148]. The organization of muscles into NMCs occurs because the axon populations in the different primary nerve branches are independent of each other. This is believed to occur because when a nerve trunk splits into different primary branches, each daughter (primary) nerve branch receives a unique subset of the axons present inside the nerve trunk. As a consequence, when one of these primary nerve branches is activated at low stimulation levels, only that nerve branch is recruited. Since the axons in the activated nerve branch do not have collaterals in the other unstimulated nerve

branches, there is no means by which action potential developed in the activated branch can antidromically invade the nerve branch point and excite the distant unstimulated nerve branches as explained in Figure 21.

Since the location of a nerve branch with respect to an intramuscular electrode affects its recruitment threshold, and because of the widespread distribution of the independent nerve branches, their recruitment with intramuscular stimulation occurs sequentially according to their distance from the electrode as current amplitude of the delivered pulses is increased. This piecewise recruitment of muscles with intramuscular stimulation has been linked to compartmentalization. The link is explained as follows: at moderately low current amplitudes, axons within the nerve branch closest to the electrode are the first to be activated. When the current amplitude is increased further, more axons within the same nerve branch become recruited causing force to rise linearly. Up until a certain current value beyond which any further increase in current does not produce additional force (i.e., plateau). At this point, the 'first' nerve branch is fully recruited and the current value is still below the activation threshold of the axons of a more distant neighboring branch. When current is further increased, fresh axons from the neighboring branch along with those in the firstly recruited branch are activated producing a second linear rise in force. Intermediate plateaus appeared in 60% of the recruitment curves collected in this study and corresponded to the consecutive activation of several independent spatially distributed NMCs. The step-wise activation of the MG muscle reported here is consistent with previous studies in which intramuscular electrodes were used to stimulate the soleus [149], ankle extensors [150], medial gastrocnemius [56] and biceps femoris [81] muscles of the cat, deltoid muscle of Rhesus monkeys [138], and the anterior tibialis muscle of humans [50]. Furthermore, the fact that our overlap test showed that we accessed three minimally overlapping regions further corroborates the compartmentalization hypothesis of muscle innervation.

The width of the intermediate plateaus in the recruitment curves represents the range of current values between the full activation of the 'firstly' recruited nerve branch and the threshold activation of 'secondly' recruited nerve branch. In other words, the wider the separation between two linear segments in a recruitment curve, the greater the degree to which one nerve branch can be activated in isolation without spillover to the other (i.e., selectivity of stimulation) [150].

The primary nerve branches (controlling the different NMCs) were closely packed together proximally but they became more widely spaced distally. And so, as the distance between the IM electrode and motor point increased, (i.e. the branches became more separated), the difference between the recruitment thresholds of neighboring nerve branches increased and so did the plateau width of the recruitment curves collected. Our results indicate that stimulation at sites near the motor point evoked strong responses but resulted in recruitment with narrow dynamic ranges (current range over which stimulation remained selective was narrow), while at more distal sites dynamic range of recruitment was broadened (high selectivity) yet lower forces were generated.

Only motor axons in the different primary nerve branches are known to be neurally segregated from each other and can be uniquely activated, and whether or not distal higher order nerve branches can be distinctly stimulated in a similar fashion is unknown [151]–[153]. For that reason, it is presumed that the smallest portion of a muscle that can be selectively activated is the one innervated by a primary nerve branch. In this study, we used the plateau force as a measure of the maximum force produced by the 'firstly' recruited nerve branch and quantified it for each electrode position. Remarkably, a linear regression analysis revealed that the plateau force decreased as the distance between the electrode and the motor point increased. This suggests that progressively smaller motor unit groups (NMCs) were selectively activated by the more

distal intramuscular electrodes. An interpretation of this is that NMCs innervated by primary nerve branches are further subdivided by the daughter nerve branches into smaller sub-compartments. If indeed the MG muscle is highly compartmentalized, this would mean that a large number of intramuscular electrodes (larger than the number of the primary nerve branches in the muscle) can be implanted without causing a significant loss in their independence which could be beneficial for producing finer, smoother and more fatigue-resistant contractions [24], [133].
Evidence of higher compartmentalization has never been reported possibly because the available techniques used to study compartmentalization of axons like glycogen depletion or EMG recording are suitable for extramuscular nerves but not for intramuscular ones. This is because, while extramuscular nerves are readily accessible and can be individually stimulated, access to intramuscular nerves to stimulate them requires surgical dissection which can be so extensive that it could ultimately lead to the destruction of the muscle. We believe that the analysis of plateaus offers a non-destructive approach to infer the segregation of axons especially in the nerves located in the distal regions of the intramuscular nerve pathway.

It was concluded that MUs inside the mammalian skeletal muscles seem to form independent functional modules called neuromuscular comparmens (NMCs) that organize into a well-defined hierarchical structure. In this thesis, we were able to partly demonstrate that this structure can be inferred from the branching pattern of the intramuscular nerve supply. We were able to infer that possibly each nerve segment on the intramuscular nerve tree corresponds to an individual NMC. The organization of motor units inside mammalian muscles is believed to be as follows: at each branching node in the IM nerve tree, a parent nerve branch and its corresponding coarse NMC is split into several sister nerve branches and their corresponding fine NMCs. This process is repeated at each level of branching giving rise to a larger number of

finer NMCs. In other words, it seems that mammalian skeletal muscle consists of a large number of fine NMCs disally that are nested within successively larger NMCs proximally. The force outputs of the distal fine NMCs are much smaller compared to the coarse proximal NMCs, and so, for applications where fine control over muscle force is needed, the distally located NMCs are preferred over their proximal counterparts as anatomical targets for electrical stimulation.

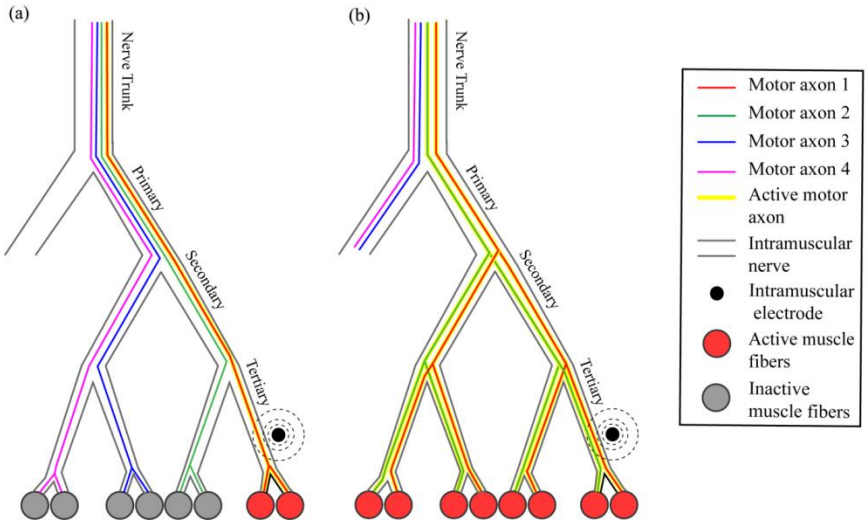


**Figure 21 Diagrammatic representation of how the behavior of motor axons (only four are shown for simplification) at the nerve branch points inside the intramuscular nerve pathway determines the compartmentalization pattern of the muscle. Primary, secondary, and tertiary labels on each segment of the intramuscular nerve tree indicate the nerve branch order. The yellow highlight over an axon indicates that it is active. Two possible axonal branching scenarios are illustrated: (a) Motor axon 1, 2,3, and 4 enter the same primary nerve branch but then axons 1 and 2 enter one secondary nerve branch while axons 3 and 4 enter the other secondary branch until eventually each axon enters a different tertiary nerve branch resulting in four independent tertiary nerve branches. Low intensity**

**stimulation by an intramuscular electrode placed near the 'red' tertiary branch will lead to highly restricted muscle fiber activation. Action potential developed in the 'red' tertiary nerve branch cannot invade the other tertiary nerve branches antidromically since the axons in activated branch are independent of axons in other nerve branches. This axon branching pattern results in a muscle with compartments about tertiary nerve branches. (b) Motor axon 1 and 2 exclusively enter one of the primary motor nerves but then they branch at each successive nerve branch point and send collaterals into all the secondary and tertiary nerve branches non-selectively. Low intensity stimulation by an intramuscular electrode placed near any tertiary nerve branch will lead to a widely spread muscle fiber activation. Action potential developed in the activated branch will spread to all the tertiary nerve branches antidromically since the axons in the activated nerve branch also have collaterals in the other tertiary nerve branches (i.e. they are dependent). This axon branching pattern results in a muscle with compartments about the primary nerve branches.**

## 3.5.2 Stimulation selectivity with intramuscular electrodes

The number and the locations of intramuscular electrodes required to perform multisite stimulation should be determined based on the number and the locations of the NMCs found in a muscle in order to achieve multisite stimulation with minimal overlap. However, knowledge of the compartment-specific nerve branches and their respective locations is almost impossible to obtain since there is no current imaging technique available that would allow visualization of intramuscular nerves *in vivo*. This problem is further complicated by the high variability in the branching patterns of intramuscular nerves and possibly compartmentalization patterns of axons inside the nerves for the same muscle across individuals. Thus, in an effort to help guide the selection of sites for the implantation of multiple IM electrodes to obtain relatively selective recruitment, we studied

the effect of varying the placements of the electrodes in the intramuscular nerve pathway on the selectivity of stimulation.
Overlap measured for the different triads highly correlated to the distribution of the intramuscular nerves and where the electrode members of the triad lied with respect to them. The horizontal central triad situated near the mid-belly exhibited far less stimulation interaction than did the same triad at a proximal location. As demonstrated via the Sihler stain, the nerve branches were more widely spaced at the mid-belly region than they were proximally and thus nerve branches were stimulated with less interaction. Likewise, the high overlap produced by the lateral triad strongly correlated to the presence of a large vertical primary nerve branch in the lateral region of the muscle. It seems that selectivity of stimulation was poor because members of this triad were aligned with the same nerve.

The results reported here, emphasize the roles of both the spatial arrangement of intramuscular electrodes with respect to each other and their locations relative to the intramuscular innervation in determining the selectivity of stimulation.

According to what we have exposed above in the first section of the discussion (i.e., possible existence of a large number of independent NMCs, well above what the primary nerve branches suggest) we would expect a large number of independent stimulation sites. Different reasons could explain why our overlap analysis did not turn over a high number of independent sites (the clustering algorithm only identified three independent groups of electrodes). One reason could be because of the arrangement of the nine electrodes used. We speculate that the proximal electrodes excited the parent nerves that gave off the daughter nerve branches which were being stimulated by the more distal electrodes leading possibly to a high degree of stimulation overlap. A single horizontal array of adequately spaced intramuscular electrodes spanning the mid-belly portion could have proven to be a more optimal configuration

resulting in less stimulation overlap. Another reason could be that because the pulse amplitudes were adjusted for a specific target twitch force (0.3 N) these amplitudes were either too high or too low to selectively stimulate minor NMCs (i.e., above or below the plateau forces).

### 3.5.3 Fatigue induced by interleaved vs synchronous stimulation

Interleaved stimulation has been shown to induce less muscle fatigue than synchronous stimulation with most types of electrode configurations in both human and animal subjects [15-30]. However, when intramuscular electrodes were used, fatigue reduction commonly seen with interleaved stimulation could not always be achieved. We reasoned that in those studies, overlap caused by the suboptimal placement of the intramuscular electrodes was another factor aside from interleaved stimulation that was simultaneously affecting fatigue. And so, to assess the effect of interleaved stimulation on fatigue without any bias, overlap had to be minimized. Moreover, it is established that although interleaved stimulation produces higher fatigue-resistance compared to synchronous stimulation, ripple was always worse off. This ripple is not just because of the low stimulus frequencies used during interleaved protocol, it is also due to the difficulty in obtaining equal force tension from different stimulation sites in the muscle or different muscles [13], [33]. In this study, we compared the fatigue of interleaved and synchronous stimulation after overlap in the former was minimized. At the same time, we wanted to see if the use of a higher total stimulation frequency during interleaved protocol to achieve a force with the same initial ripple as that obtained with the synchronous protocol would come at the cost of greater fatigue. The results presented here as well as some preliminary results obtained from rats (unpublished work due to

methodological limitations) showed that, for contractions of the same smoothness and magnitude, interleaved stimulation with minimally overlapping electrodes induced less fatigue compared to single site synchronous stimulation.
We conjecture that Buckmire et al. could not achieve fatigue reduction with interleaved stimulation because the electrodes that were employed highly overlapped (although overlap was not quantified, authors estimated up to 50% overlap between the two intramuscular electrodes) [138]. On the other hand, when a priori knowledge of the compartmentalization pattern of the muscle was used to guide the selection of sites for implanting the intramuscular electrodes, as was done by Liu et al. [116], independent compartments were successfully accessed. When those electrodes were employed in interleaved stimulation, fatigue was significantly reduced compared to synchronous stimulation [29].

During the first few seconds of the fatigue tests an enhancement (potentiation) in the force response was observed despite the delivery of pulses of fixed current amplitude, as reported by other authors in [23], [56]. [57]. As expected, the low frequency stimulation used in this study to fatigue the muscle produced potentiation [154]. Moreover, the low frequency fatigue induced by the interleaved and synchronous fatigue protocols might have been an additional factor that further contributed to potentiation [58], [59]. However, the magnitude of this potentiation did not vary between the fatigue trials and so it did not significantly interfere with our ability to match the magnitude of force to the same value at the beginning of the synchronous and interleaved protocols.

The motoneurons may be compartmentalized in the intramuscular nerve pathway not just based on their target compartment but also on their histochemical type. When motor units belonging to the same histochemical class spatially group in a localized region of a muscle, the muscle is referred to as exhibiting ‘regionalization’ [155]–[157]. The MG of the rabbit is a heterogeneous muscle made

up of different proportions of slow and fast motor units with the former being more fatigue-resistant than the latter [158]. Previous reports showed a tendency for slow and fast fibers to be spatially segregated in the MG muscle of the rabbit [159] and thus we were concerned that this would cause the electrodes located in different sites to produce contractions with different fatigue properties which could have confounded our fatigue assessment. Generally, the fatigue rate of contractions elicited with stimulation through an intramuscular electrode will depend on the fatigue properties of the predominant type of motor units activated by it. To confirm that the increased fatigue resistance obtained with interleaved stimulation was caused by interleaving stimulation *per se*, and not because the electrodes employed during interleaved stimulation were favorably inserted in regions consisting predominantly of slow (fatigue resistant) motor units, we measured and compared the contraction properties of motor units activated by the electrodes employed in both synchronous and interleaved protocols across all rabbits. The duration of the twitches elicited from stimulation at different current values with synchronous electrode were significantly longer than those evoked with interleaved electrodes (1, 2 & 3). This indicates that the synchronous electrode recruited more slow (fatigue-resistant) motor units than the interleaved electrodes that activated mostly fast (fatigable) ones. Despite the spatial bias created by the non-uniform distribution of slow and fast motor units which have caused the interleaved electrodes selectively activate fast (fatigable motor units), the fatigue resistance of interleaved stimulation was minimally affected. This suggests that the fatigue rate of an electrically evoked contraction depends more on the frequency of the stimulation pulses than on the type of MUs activated. Our finding is in agreement with results from Vroman et al. who showed that muscle fiber composition does not significantly affect fatigue [160]. Similarly, Bickel et al. observed no difference between the fatigue induced by repeatedly stimulating a slow and a fast muscle [161]. Evidence of the strong dependency of the rate of muscle fatigue on stimulation frequency has been reported before [118],

[162]. It was reported previously that intramuscular stimulation can elicit contractions that are more fatigue-resistant than those obtained with nerve cuff electrodes [54]. This was believed to be due to the fact that the difference between the diameters of the large and the small nerve fibers that underlies the inverse order of MU recruitment seen with electrical stimulation vanishes terminally (i.e. distally). The large motor nerve fibers branch more extensively as they approach the target muscle fibers compared to small nerve fibers. As a result, the nerve fibers that started off with large nerve fibers proximally end up having similar diameters distally to small nerve fibers. Therefore, inverse recruitment is expected to be less prominent when stimulating with an electrode placed distally than proximally. Thus, when stimulating at a distal/terminal location, the order of MU recruitment is expected to occur in either a random or physiological way. Even though our results show that some IM electrodes appeared to recruit MU in a random fashion, other IM electrodes (nearly 50%) recruited MUs in a reverse order. This challenges the claim that IM stimulation produces fatigue-resistant contractions because MUs are recruited in a more physiological way than nerve-based electrodes.

We had to increase the stimulation frequency of the interleaved protocol in order to achieve the same ripple as that of the synchronous protocol (30 Hz vs. 20 Hz). This did not adversely affect fatigue resistance. We believe that both the use of lower stimulation frequencies, minimally overlapping electrodes, and access to multiple independent motor unit populations during interleaved stimulation protocol were crucial to achieving such fatigue reduction [50]. Some of the limitations of this study were that the fatigue tests were conducted at a relatively low force level and not over a wide range of forces. Other limitations were the low number of rabbits studied and that the maximum capacity of our current generator was only 4 mA.

## 3.6 Conclusion

We showed that interleaved intramuscular stimulation with minimally overlapping electrodes produces less fatigue than single site synchronous stimulation for the same initial force and ripple. We also showed that overlap amongst the intramuscular electrodes appears to be related to the spatial distribution of the intramuscular nerves. A horizontal row of three electrodes in the central region of the intramuscular nerve pathway was the optimal placement that produced the least amount of overlap because nerve branches were most widely spread apart. Furthermore, we inferred that the MG muscle may be more extensively compartmentalized than previously thought in that motor axons are segregated not just in primary nerve branches but also in higher order nerve branches. The finding that the preferential activation of fast (fatigable) motor units during interleaved stimulation did not hinder its fatigue resistance lends evidence to support that the FES-induced muscle fatigue is caused primarily by the high frequency of stimulation used and to a lesser extent by the type of motor units recruited.

# Analysis of the neural stimulation efficiency and miniaturization potential of injectable wireless microstimulators based on volume conduction

CHAPTER 4

Part of this chapter was adapted from:
A. Eladly, B. Mercadal , M. Tudela-Pi, A. Ivorra. Analysis of the stimulation efficiency and miniaturization potential of injectable wireless microstimulators based on volume conduction.
[under preparation]

## 4.1 Abstract

Volume conduction is a wireless power transfer (WPT) method that, through bypassing the need to use bulky internal components, leads to thin injectable flexible wireless stimulators required for delivering safe selective multisite neuromuscular stimulation. Here, we report on the neural stimulation efficiency and miniaturization potential of two approaches for developing wireless injectable micro-stimulator based on volume conduction. In the first approach (rectifying method), the micro-stimulator is very thin (⌀ < 1mm), relies on the direct and instantaneous rectification of pulses of volume conducted high frequency (HF) currents for neurostimulation, and delivers half-rectified AC signals as a stimulus waveform. In the other approach (regular method), the microstimulator is bulkier (⌀ > 1 mm), contains a capacitor to store the energy received from the transmitted HF volume conducted current bursts, an onboard pulse generator, and delivers a square pulse as a stimulus waveform. In this study, we used a computational model of a myelinated axon to compare the efficiency of the stimulation associated with these two possible approaches by comparing the stimulation efficiency of the stimulus waveforms associated with each approach. The potential of the regular method to lead to thin implants was analyzed based on the computed neuronal activation thresholds. Our model predicts higher neural current, charge and energy thresholds with rectifying method than with the regular method. We also show that miniaturization potential of the microstimulators based on the regular method is limited, since the minimum energy required for neurostimulation was high (~50 μJ) and can only be provided by bulky capacitors (⌀ > 1mm). The choice of the approach in this case requires a trade-off between stimulation efficiency and miniaturization.

## 4.2 Introduction

Functional neuromuscular stimulation refers to the application of external electrical currents to the nerve supply of skeletal muscles to generate contractions for restoring functional movement to paralyzed limbs. Wireless miniature implantable neurostimulators offer a promising means by which electrical stimulation can be safely and selectively applied to the motor nerves to treat several neurological disorders that lead to motor deficiency e.g. spinal cord injury or stroke compared to their wired counterparts[2], [4], [163], [164]. Of those wireless miniature neuro-stimulators exists a special sub-class of devices, intended for interfacing with the peripheral nervous system, whose cylindrical shape allows for their implantation via simple injection[18], [36]. An example of such devices is the BIONs developed by G. E. Loeb *et al*[18]. The BIONs are wireless cylindrical single-channel microstimulators which incorporate both the pulse generator and the contact electrodes needed for stimulation on a single small injectable unit. It was envisioned that a multi-channel motor prosthetic system could be built from the individual BIONs to control multiple muscles for delivering electrical stimulation to generate complex movement patterns in motor-deficient patients[165], [166][167]. In this BION multi-channel motor prosthesis, each BION would target an individual muscle, but not the several fine independent compartments that exist inside each muscle. Such coarse electrical access to muscles provided by the BIONs (dictated by their large size) may not be enough for generating physiological contractions with electrical stimulation [168]. The BIONs are powered and controlled wirelessly by an external system through an inductive link or a rechargeable battery, thus it is a requirement that they incorporate bulky on-board coils/batteries that ultimately increase their overall size. The most compact version of the BIONs (2 mm wide ×1.5 cm long) is considered too bulky to provide fine access to the numerous small neural targets in skeletal muscles needed to

physiologically recruit muscles and evidently, is expected to cause significant damage to skeletal muscles if implanted in large numbers. As a result, thinner and more flexible wireless microstimulators are needed.

Miniaturization of wireless implantable electronics has been the focus of many research efforts[16], [17][36], [40], [41], [94], [169][98], [170], [171], since it could lead to devices that: 1) approach the size of their neural targets leading to very high spatial selectivity, 2) can be easily implanted in the body without causing significant trauma, and 3) possibly, allow for multi-channel operation by placing them in the body at distributed locations at the cost of little additional trauma.

Aside from the BIONs, other single channel wireless submillimeteric microstimulators that, owing to their small size and addressability, allow for multichannel stimulation in the form of a distributed microstimulator network include the FLAMES devices powered by light [16] and are intended for spinal cord stimulation[172], the StimDust devices powered by ultrasonic acoustic waves [170] for peripheral nerve stimulation, and the eAXONs undergoing development in our lab that are driven by pulses of ac volume conducted currents [41], [44] intended for intramuscular stimulation. FLAMES and StimDust would require a more invasive surgery for their implantation (despite their small size) compared to the eAXONs that can be introduced deep in the muscle with a simple injection. A challenging engineering aspect in obtaining submillimetric wireless microstimulators is to provide enough power to the electronics inside the implants needed for neural stimulation while ensuring that such electronics are small enough to fit inside miniature hermetic capsule.

To this end, volume conduction has been shown to wirelessly power and control microstimulators that have significantly less onboard components compared to those driven by other wireless

power transfer (WPT) methods, therefore allowing significant miniaturization [40], [173] in one dimension. Since, with volume conduction, the terminals (i.e. electrodes) of the microstimulators can be used to both capture the electrical energy to power the implant as well as to pass the stimulus pulse to nerves, bulky components (for example, antennas) can be excluded. Moreover, ideal receiver geometry in WPT based on volume conduction is an elongated thin cylinder. This geometry is highly advantageous for wireless implantable microstimulators to have as it permits their insertion in the body with simple injection or catheterization instead of open surgery.

Herein, two approaches for developing wireless injectable microstimulators based on volume conduction as a WPT method are investigated. The first approach (i.e. the rectifying method) leads to very thin implants that 1) do not incorporate a pulse generator, 2) rely on the direct and instantaneous rectification of bursts of volume conducted ac currents alone for neurostimulation, and 3) deliver non smooth half-rectified ac signals to excite the nerves. The other approach (i.e. the regular method) leads to bulky implants that 1) incorporate an internal pulse generator, 2) uses a capacitor to store the energy received from the volume conducted ac signals to power the onboard pulse generator, 3) delivers square pulses to the nerves. The regular approach has been proposed by others [91][90], but its miniaturization potential has not been yet tested.

The rectifying approach was first introduced in the 60s [36], [37], [160] and was based on implants whose electronic circuitry consisted only of a diode. Because these implants lacked addressability, this approach was only suitable for medical applications where a single target required stimulation. To allow for multichannel network operation, the rectifying method was further developed by our lab into the eAXON method by adding

the feature of digital addressability to the microstimulators [41], [44], [174]. It is important to note that the rectifying method was used by others recently to develop wireless non-addressable nerve cuff stimulators [175][99]. The externally applied HF currents (>1 MHz) are unable to directly induce neural excitation because the frequency of these currents is too high compared to the response dynamics of voltage-gated ion channels underlying action potentials[176][177]. In the rectifying as well as the eAXON method, the temporal features of the stimulus pulses delivered by the microstimulator are set by the temporal features of the externally applied AC fields.

A clear advantage of the rectifying over the regular method is that wirelesss microstimulators with a submillimetric cross-section can be achieved. However, it is not well-studied how the stimulation efficiency of the half-rectified ac stimulus waveforms associated with the rectifying method compares to that of the square waveforms associated with the regular method. It was reported that nerve fibers respond to the half-rectified ac signals in the similar way as they would to a square pulse with an amplitude equal to the dc value of that rectified pulse [44], [94]. However, in the only *in-vivo* study (conducted with a nerve cuff electrode on a sciatic nerve preparation in rats) where such comparison was held in a cursory way, the rectified signals were found to be associated with higher current neural excitation thresholds (19.6 μA) compared to the square pulse with an equivalent dc amplitude (17 μA) for a 1 ms pulse [175]. Since the shape of the stimulus waveforms can have a significant impact on the excitation thresholds of neurons[178][179], we were interested in examining the stimulation efficiency (i.e. current, charge, and energy consumption) of the half-rectified ac stimulus waveforms associated with the rectifying method over a broader range of clinically relevant pulse widths to see how it compared to the stimulation efficiency of the square waveforms associated with regular method.

We used a computational model of a myelinated axon to compare the stimulation efficiency of the non-smooth half-rectified ac signals and conventional square pulses with an amplitude equal to the dc component of those rectified signals associated with the rectifying and regular methods respectively. We also determined the miniaturization potential of the microstimulators based on the regular method by using their predicted energy requirements for neurostimulation to estimate the size of internal storage capacitor.

## 4.3 METHODS

### 4.3.1 Axon model

The temporal dynamics of the transmembrane voltage of an excitable myelinated axon at the nodes of Ranvier in response to the application of an external current was simulated using the cable model described in [180] based on the work of [181] via the following equation:

$$\frac{dV_n}{dt} = \frac{1}{C_m}\left[G_a\left(V_{n-1} - 2V_n + V_{n+1} + V_{e,\,n-1} - 2V_{e,n} + V_{e,n+1}\right) - I_n\right] \qquad \textbf{(2)}$$

where $V_{e,n}$ is the extracellular voltage at each node, $C_m$ is the membrane capacitance, $G_a$ is the axial internodal conductance, and $I_n$ is the ionic current across the membrane at the node n. The ionic current was calculated as the summation of three separate types of ionic currents and a leakage current as in [182] (see Appendix). The parameters used in (2) are listed in Table 4. Assuming that no axial current can exit at the end of the fiber (sealed end assumption) [183], the voltage at the extreme nodes is calculated as:

$$\frac{dV_1}{dt} = \frac{1}{C_m}\left[G_a\left(-V_1 + V_2 - V_{e,1} + V_{e,2}\right) - I_{i,1}\right] \quad \textbf{(3)}$$

$$\frac{dV_N}{dt} = \frac{1}{C_m}\left[G_a\left(-V_N + V_{N-1} - V_{e,N} + V_{e,N-1}\right) - I_{i,N}\right] \quad \textbf{(4)}$$

.

**Table 4**

| Symbol | Value | Definition, justification or source |
|---|---|---|
| $D$ | $10\ \mu m$ | Axon diameter (i.e. external myelin diameter) |
| $L$ | $115 \cdot D$ | Internodal distance, [184] |
| $C_m$ | $c_m \pi d_n\ G$ | Membrane capacity |
| $G_a$ | $\frac{\pi d_a^2}{4\rho_a L}$ | Axial intermodal conductance |
| $d_a$ | $0.7 \cdot D$ | Axon diameter, [185] |
| $d_n$ | $0.33 \cdot D$ | Node diameter, [185] |
| $\rho_a$ | $70\ \Omega \cdot cm$ | Axoplasmic resistivity, [186] |
| $c_m$ | $2\ \mu F/cm^2$ | Nodal capacitance, [187] |
| $G$ | $1\ \mu m$ | Nodal length, [185] |
| $V_{rest}$ | $-80\ mV$ | Resting voltage |

Implicit backward Euler method was chosen as an appropriate integration scheme and a central finite difference formula was used. The simulation was implemented in MATLAB

## 4.3.2 Stimulation waveforms

We studied the response of the myelinated axon to external electrical stimulation with two different stimulus waveforms: 1) the half-rectified ac signals associated with the rectifying method

and 2) square waveforms associated with the regular method. Both monophasic and biphasic variants of each type of waveform was studied. A 1 mA peak to peak rectified signal and its corresponding square waveform with an amplitude equal to its dc average were constructed. A graphical illustration of such waveforms with a phase width of 200 µs is shown in Figure 22. The different stimulus waveforms were generated using MATLAB. The time step that was used was 0.05 µs and the simulation run time was 1.8 ms.

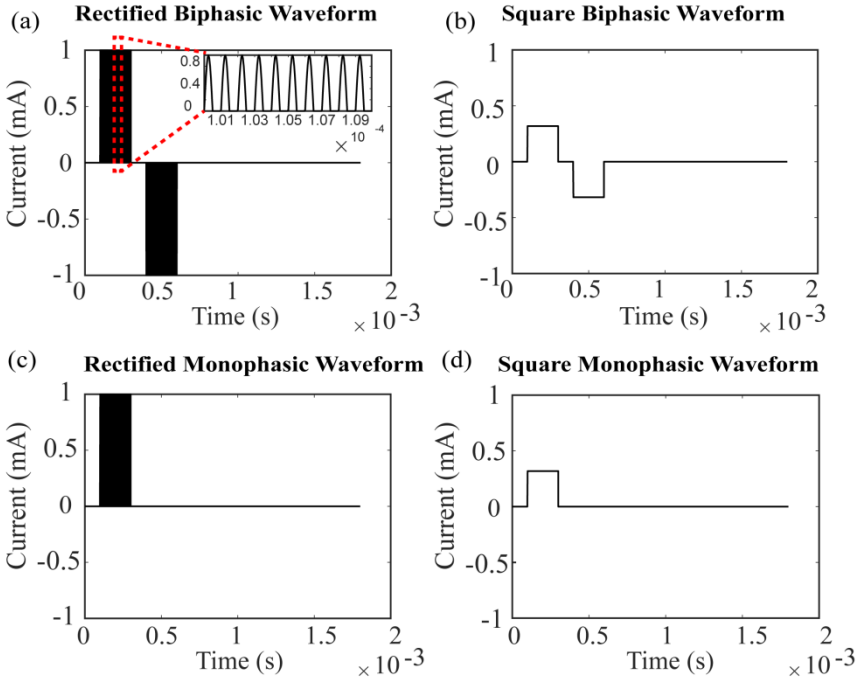


**Figure 22. Half-rectified ac signal (pulse width = 200 µs) delivered by the microstimulators based on the rectifying approach and their corresponding square waveforms delivered by microstimulators obtained with the regular approach. (a) Biphasic half-rectified waveform. Inset: the high frequency (1 MHz) component of the volume conducted HF current is still present in the pulses after half-rectification. (b)**

**Biphasic square pulse with an amplitude equal to the dc value of the rectified signal in (a). (c) Monophasic rectified waveform. (d) Monophasic square pulse.**

For each of the four different combinations (i.e. rectified or square and biphasic or monophasic), waveforms with different pulse widths spanning the range from 200 to 800 μs which corresponded to the range of pulse widths used clinically with similar wireless micro-stimulators [188]. For the biphasic variants of the waveforms, a constant interphase gap of 100 μs was used throughout the study as this ensured the lowest excitation thresholds (i.e. most efficient stimulation) [189].

## 4.3.3 Model Geometry

To simulate the extracellular stimulation of a myelinated axon, a single 10 cm long excitable axon was modelled. This length ensured that the axon was longer than the wireless microstimulators which are being considered in this study (Figure 23 (a & b))[39]. The modeled fiber had a diameter of 10 μm,(i.e. external myelin diameter) corresponding to a large motor fiber in the nerve supplying the medial gastrocnemius muscle of the cat [190]. Given an internodal distance of 1.15 mm, the 10 cm axon consisted of 87 nodes of Ranvier. To simulate the electrodes of a cylindrical bipolar wireless neuro-stimulator, two point sources of opposite polarity aligned parallel to the long axis of the nerve fiber were considered and equation (5) was used to analytically calculate the external voltage at each node of Ranvier under the assumption that our set-up lives in an isotropic and homogeneous medium [191].

$$V_e = \frac{\rho_e I_{el}}{4\pi r} \quad \textbf{(5)}$$

Where $\rho_e$ is the resistivity of the extracellular medium (i.e. muscle tissue) which was set to $2\ \Omega\cdot$m for rectified pulses [192] and $3\ \Omega\cdot$m for square pulses [193], $I_{el}$ is the current delivered by the electrode and $r$ is the distance between stimulating electrode and each node of Ranvier

The diameter of the electrodes and the nerve fiber-electrode distance were set to 1 mm and 10 mm respectively as shown in figure 23 (b). An electrode-nerve fiber distance of 10 mm was shown to be the maximum separation distance that ensured effective neural stimulation when an injectable wireless micro-stimulators of similar dimensions was used clinically [194]. Different interelectrode distances (i.e., length of the microstimulator) were studied to investigate how the length of the stimulator impacts its stimulation efficiency.

The extracellular voltage generated along the axon length by a 1 mA pulse is shown in figure 23 (c) and the response of the transmembrane voltage (TMV) to an 800 µs biphasic square – pulse applied at 15 mA is shown in figure 23(d).

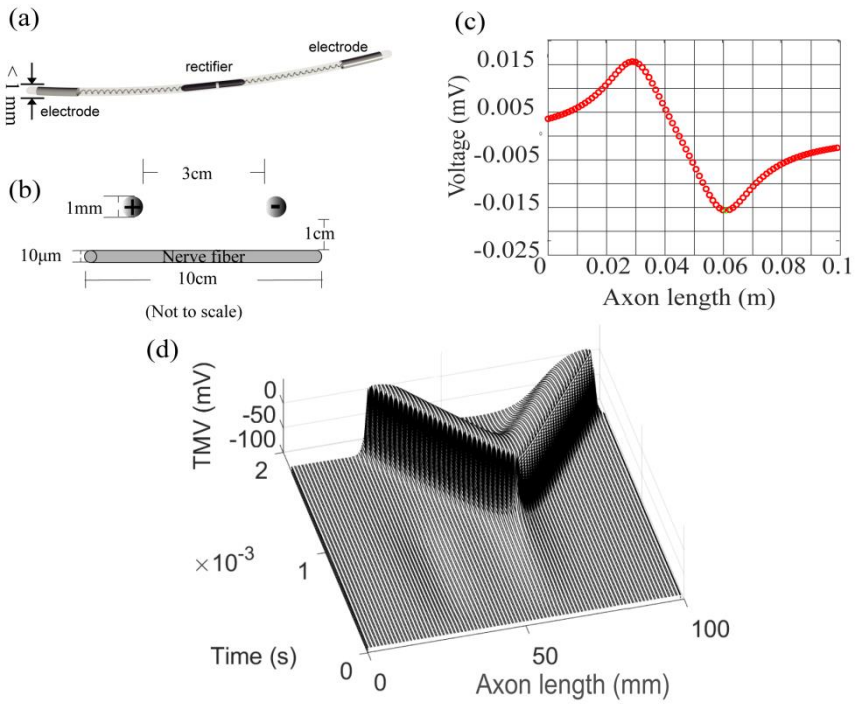


**Figure 23 . Model geometry. (a) depiction of the wireless extremely thin eAXON microstimulator developed in our lab based on the eAXON method (i.e. rectifying method + addressability for multichannel network operation) and delivers half rectified non-smooth stimulus wavefrms. (b) Geometry used to model extracellular stimulation of nerve fiber by a microstimulator like the eAXON. (c) Extacellular voltage generated along the length of the axon by a 1 mA pulse. (d) Transmembrane voltage (TMV) evoked in response to a 800 µs biphasic square pulse at 15 mA.**

## 4.3.4 Threshold calculation

To find the threshold current for a given waveform (i.e. the minimum current required to trigger an action potential), an algorithm was employed that tried to find a value above and a

value below the threshold. The interval between these two values was successively halved until the difference between them was within a given tolerance which in our case was set to 1%. Usually it took about 8 realizations for the algorithm to converge. The criteria used to determine if an action potential has been triggered was whether or not the value of the *m* gating variable corresponding to the activation of the fast sodium currents exceeded 0.8 on at least one of the nodes. The current thresholds values for the rectified stimulus ac signal were reported here in their RMS value.

To calculate the charge efficiency of the tested waveforms, threshold charge was computed as the time integral of the stimulus waveform using equation equation (2) For biphasic waveforms, the injected charge was computed by taking the integral over the leading phase only of the stimulus waveform.

$$Q = \int_0^t I(t)\,dt \qquad \textbf{(2)}$$

The percentage difference in the current and charge thresholds between square and rectified pulses were calculated using equation (7).

$$\%\,Difference = \frac{Threshold_{rectified} - Threshold_{square}}{Threshold_{square}} * 100 \qquad \textbf{(7)}$$

## 4.3.5 Miniaturization analysis

We determined the miniaturization potential of the microstimulators based on the regular method by computing the minimum amount of energy it needs to provide to produce neural

excitation. The higher the energy requirement for neurostimulation, the larger i.e. bulkier the onboard storage capacitor that would needed to be incorporated to ensure an adequate energy supply. The size of this storage capacitor is mainly determined by the energy required for threshold stimulation, the voltage amplitude of the pulse and the capacitor technology. The pulse energy is determined by

$$E = Pw \tag{8}$$

where $P$ (W) is the pulse power, and $w$ (s) is the pulse width. The pulse voltage, considering that the implant has spherical electrodes and is surrounded by homogeneous tissue, can be calculated as

$$V = IR = \frac{I}{\pi \sigma D} \tag{9}$$

where $\sigma$ (S/m) the tissue conductivity set to 0.5 S/m and $D$ (m) the electrode diameter set to 1 mm.

## 4.3.6 Neural stimulation efficiency analysis

To compare the energy efficiency of the stimulus waveforms associated with rectifying method with that of the square waveforms associated with the regular method, we calculated the energy $E_{stim}$ required to threshold activate the axon and the corresponding energy $E_{app}$ of the volume conducted ac field that needs to be applied externally in order to obtain $E_{stim}$ in the microstimulator. It is important to remember that throughout this study, the waveforms are being used as proxies for the approaches to evaluate their neural stimulation efficiency. For microstimulators based on the rectifying approach, we considered a device that produced local symmetrical bipolar rectification of

the volume conducted ac field. We assumed the presence of a quasi-ideal Schottky diode (figure 24 (a)) that produces a voltage drop of 0.2 V between the applied and the captured voltage.

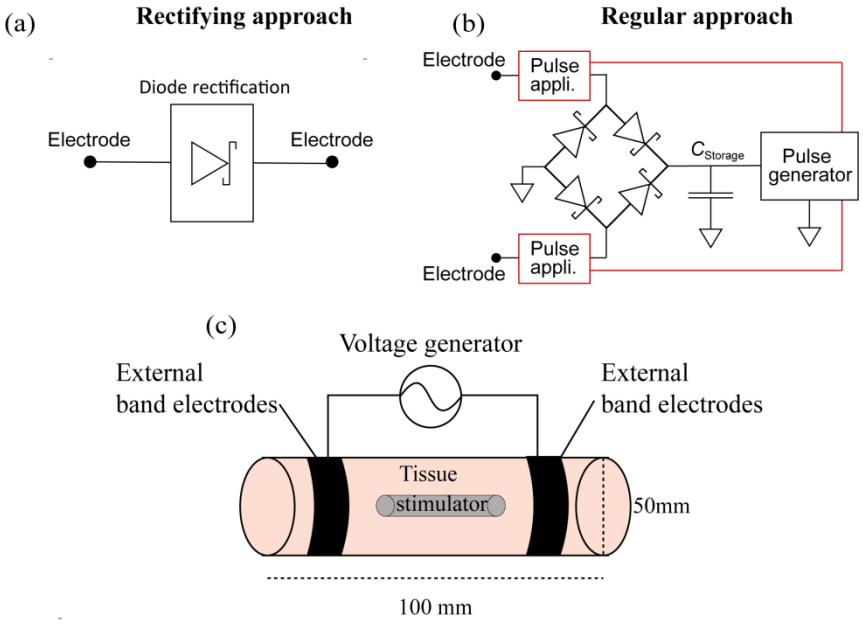


**Figure 24 Energy efficiency of neural stimulation provided by microstimulators based on the rectifying and regular approaches.(a) circuit architecture of the rectifying microstimulator.(b) circuit architecture of the regular microstimulator.(c) Geometry considered for computing the energy that is needed to be applied by the external system to obtain energy values needed to threshold activate the axon in the stimulator (axon is not shown).**

For microstimulators based on the regular method, we considered an architecture that consisted of a full-wave rectifier (in this case a Schottky diode bridge, with a voltage drop of 0.2 V per diode), a capacitor to store the energy, and a bipolar pulse generator with an efficiency of 90 % as shown in figure 24 (b). In order to be able to compute $E_{app}$, we assumed that the devices were enclosed by a homogeneous muscular tissue and that the electrodes used to pick

up the energy were the same as those used to deliver the stimulus pulse to the tissue. We considered devices with spherical electrodes that were 1 mm in diameter and inter-electrode spacing that ranged from 80 mm to 6 mm.

The electric field was applied using volume conduction and had a frequency of 6.78 MHz (to avoid undesired stimulation). We assumed that this field was applied uniformly over a cylindrical volume of homogeneous muscle tissue with a length of 100 mm and a diameter of 50 mm that surrounded the implants. So, the energy efficiency ($E_{\text{eff}}$) was determined as the ratio between the applied pulse energy ($E_{\text{stim}}$) and the total energy applied ($E_{\text{app}}$) in the described volume.

$$E_{\text{eff}} = \frac{E_{\text{stim}}}{E_{\text{app}}} \tag{10}$$

The resistance between electrodes, provided that the tissue that was assumed is homogeneous and the inter-electrode spacing was much larger than the diameter of the spherical electrodes, can be determined as

$$R(f) = \frac{1}{\pi\sigma(f)D} \tag{11}$$

where the conductivity is a function of the applied frequency. Here, we considered a conductivity of 0.6 S/m, 0.5 S/m 0.33 S/ for the applied external field (6.78 MHz), the squared pulses and the rectified signals respectively.

For microstimulators based on the rectifying method, the peak voltage that needed to be captured in order to induce neurostimulation was computed as

$$V_{elec} = I_{\text{stim}}R(f) + 0.2. \tag{12}$$

On the other hand, peak voltage that needs to be captured by microstimulators based on the regular approach to cause neurostimulation was calculated as

$$V_{elec} = \frac{I_{\text{stim}} R(f)}{0.9} + 0.4. \tag{13}$$

Thus, assuming a parallel alignment between both microstimulators and the electric field, the amplitude of the external field was computed using

$$E_{\text{amp}} = V_{\text{elec}} L. \tag{14}$$

And the energy dissipated at the tissue ($E_{\text{app}}$)

$$E_{\text{app}} = \frac{w}{2} \int_V E_{\text{amp}} J \, dV \tag{15}$$

where $J$ is the current density, and it can be calculated as

$$J = \sigma(f) E. \tag{16}$$

The energy used to stimulate is

$$E_{\text{stim}} = w \int i(t)^2 R(f) \, dt. \tag{17}$$

This analysis was performed for stimulation using biphasic pulses only since similar trends were obtained with monophasic pulses.

## 4.4 Results

### 4.4.1 Comparison between axonal excitation thresholds obtained with rectifying vs regular method: monophasic stimulation

In agreement with the experimental results [175], the current amplitudes required to threshold activate the axon were higher for half-rectified ac signals associated with the rectifying method compared to their corresponding square waveform with an equivalent dc amplitude associated with the regular method.. Figure25 (a) shows the strength duration curves obtained for the half-rectified ac signal and its respective square pulse with equivalent dc amplitude. For all the pulse width values tested, the difference between the current activation thresholds of the axon with a half-rectified ac signal and a square waveform remained constant (Figure25 (c)). Our model predicted that, for a given pulse width, nearly 50% more current would be needed to threshold activate an axon if a rectifying microstimulator is used than if a regular microstimulator is used.

The charge-duration curves were also obtained for both the half-rectified ac stimulus signal and the square waveform and used to generate Figure25 (b). Similar to the strength-duration curves, the charge-duration curve of the half-rectified ac signals was shifted to higher charge amplitudes compared to that of their dc equivalent square waveforms. The difference between the amount of charge required to reach activation threshold of the axon with half-rectified ac signal and its corresponding adjusted square waveform did not significantly change across the different pulse width tested.

Our model predicts that the square waveforms (associated with the regular approach) are more charge efficient compared to their corresponding rectified signals (associated with the rectifying approach). Figure25 (d) shows that using rectified signals instead of their corresponding dc equivalent square signals results in nearly 50% increase in charge injection.

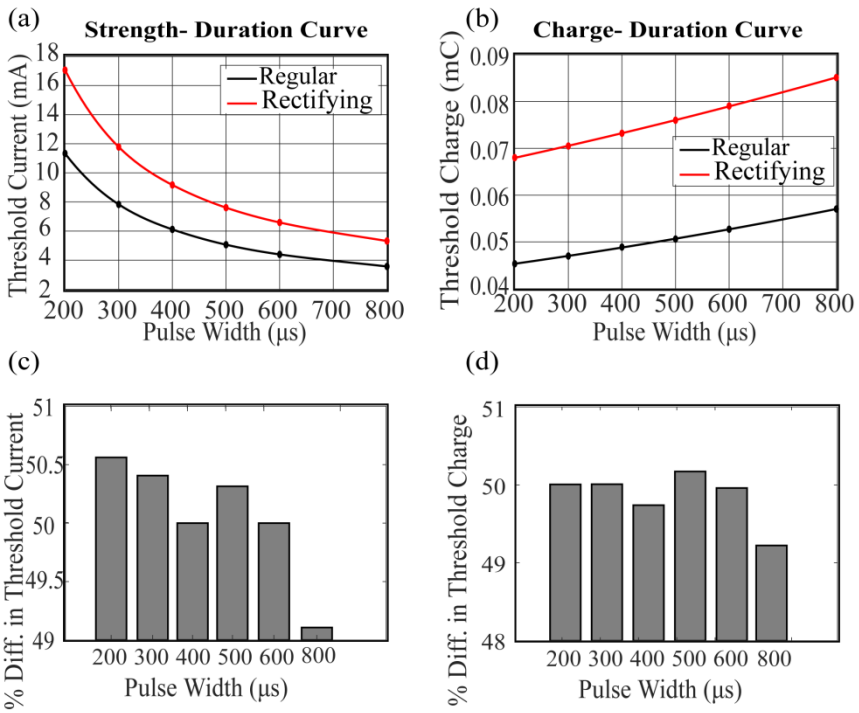


**Figure25 Monophasic stimulation. Current and charge efficiency of stimulation delivered by microstimulators based on the rectifying and regular approaches measured indirectly through their corresponding stimulus signals. (a) Strength-duration curves. (b) Charge-duration curves. (c) % Difference between the amplitude of the current thresholds obtained with microstimulators based on rectifying and regular approaches**

**as a function of pulse width. (d) % Difference between the amplitude of the charge thresholds obtained with microstimulators based on rectifying and regular approaches as a function of pulse width.**

### 4.4.2 Comparison between axonal excitation thresholds obtained with rectifying and regular approaches: Biphasic stimulation

Similar to the monophasic stimulation case, the current amplitudes needed to reach the activation threshold of the axon were higher for rectified signals (i.e. rectifying microstimulators) compared to their corresponding square waveform with equivalent dc amplitude (i.e. regular microstimulators). The same trends for current and charge thresholds that were seen with monophasic stimulation were also observed for biphasic stimulation with the only difference being that current and charge thresholds were higher for biphasic compared to monophasic stimulation. Figure 26 (a) shows the strength duration curves obtained for the rectified signal and a square pulse with equivalent dc amplitude when biphasic stimulation was used. Similar to the monophasic case, for all the pulse width values tested, the difference between the current amplitude needed to threshold activate the axon with a rectified signal and a square waveform did not seem to vary significantly (i.e. it was pulse width- independent, Figure 26 (c)). The difference between the current efficiencies of rectified signal or square waveforms was also independent of whether monophasic or biphasic stimulation was used.

Under biphasic stimulation, charge-duration curves for rectified signals and their corresponding square waveforms are plotted in Figure 26 (c). The charge required to threshold activate an axon with a rectified stimulus signal was approximately 50% higher

than that needed if its square wave counterpart was used. This was true for all pulse widths tested as seen in Figure 26 (d).

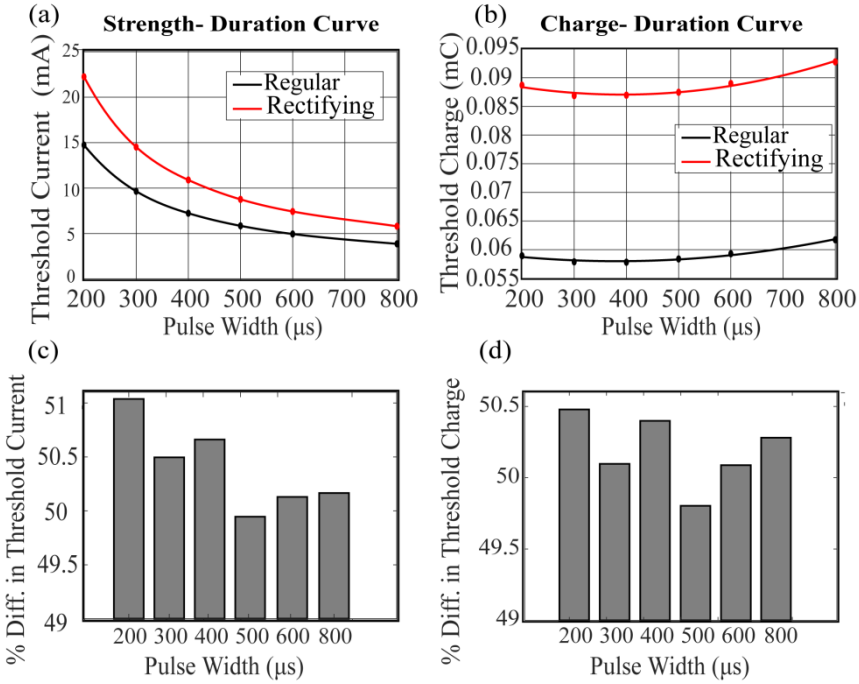


**Figure 26 Biphasic stimulation. Current and charge efficiency of stimulation delivered by microstimulators based on the rectifying and regular approaches measured indirectly through their corresponding stimulus signals. (a) Strength-duration curves. (b) Charge-duration curves. (c) % Difference between the amplitude of the current thresholds obtained with microstimulators based on rectifying and regular approaches as a function of pulse width. (d) % Difference between the amplitude of the charge thresholds obtained with microstimulators based on rectifying and regular approaches as a function of pulse width**

### 4.4.3 Effect of the length of the microstimulator on thresholds

We studied the effect of varying the interelectrode spacing (i.e. length of the microstimulator) on the activation thresholdsobtained with rectifying and regular microstimulator. We wanted to see if the length of microstimulators can be optimized to maximize the stimulation efficiency. Figure 26 (a) shows the extracellular voltage generated at the nodes of Ranvier on the modelled axon by a stimulus current pulse of 1 mA for different interelectrode spacing. The larger the interelectrode spacing, the greater the magnitude of the peak voltage generated at the node closest to the electrode. The activation thresholds of the axon computed with either rectified signals or their corresponding square waveform of a 200 μs pulse width increased as the interelectrode spacing decreased as shown in Figure 26 (b) at nearly the same rate. Contour plots of the amplitude of excitation threshold computed for the rectifying and regular microstimulators when a 200 μs monophasic pulse is delivered as a function of pulse width and interelectrode spacing are shown in Figure 26 (c) and Figure 26 (d) respectively. It is clearly seen that the longer the microstimulators are, the more efficient they become in activating the axon.

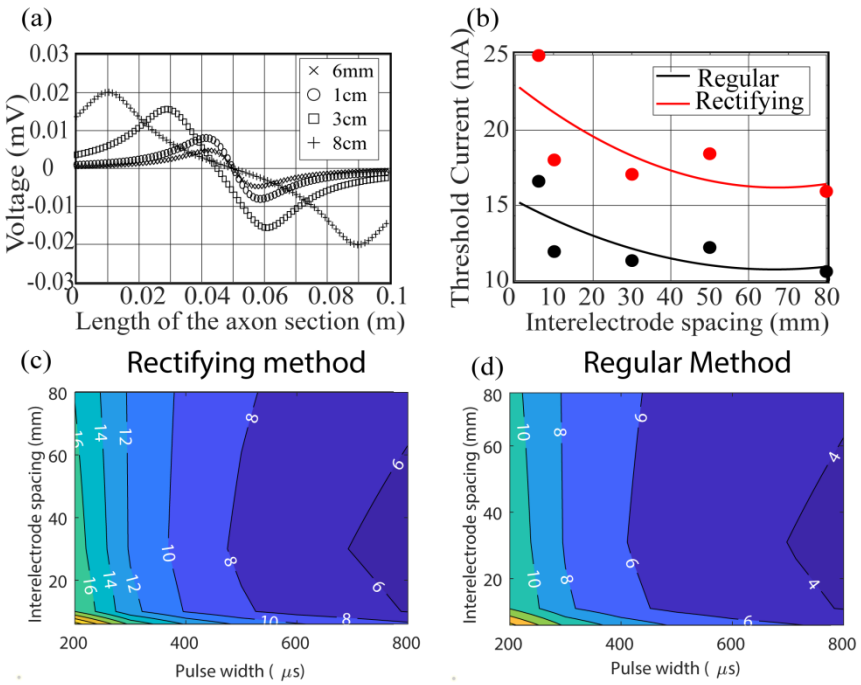


**Figure 27. Effect of interelectrode spacing on activation thresholds obtained with rectifying and regular microstimulator. (a) Extracellular voltage generated by a current pulse of 1 mA for different interelectrode spacing. (b) threshold-interelectrode spacing plot for the rectified signals and their square counterparts. (c) and (d) contour plots of the activation thresholds of an axons obtained with rectifying and regular microstimulators respectively when a 200 µs square monophasic waveform is delivered as a function of pulse width and interlectrode spacing.**

## 4.4.4 Miniaturization potential of regular microstimulators

The diameter of wirelessly powered microstimulators is determined by the largest onboard electronic component. In the regular microstimulator, the largest component is the capacitor needed for energy storage. Thus, the higher the energy

requirements for neurostimulation, the larger this storage capacitor need be in order to cope with the higher neural stimulation energy demands. We were able to assess the miniaturization potential of the regular microstimulators by using the computed current excitation thresholds to estimate the voltage and energy requirements for neurostimulation under biphasic and monophasic stimulation. Figure 28 (a) and (b) show the threshold voltage amplitudes needed to activate the axon at different stimulus pulse widths for monophasic and biphasic stimulation respectively when very short (6 mm) and long (8 mm) microstimulators are used. The corresponding threshold energy amplitudes were computed for monophasic and biphasic stimulation and used to create figure 28 (c) and (d) respectively. For the case where long microstimulators, long pulse widths and monophasic stimulation are used (i.e., best case scenario, in other words, energy required for stimulation is the lowest), the energy needed for stimulation was still significantly higher than the energy storage capacity of a capacitor that is 1 mm in its smallest dimension (see discussion). Therefore achieving submillimetric microstimulator with the regular approach is very difficult.

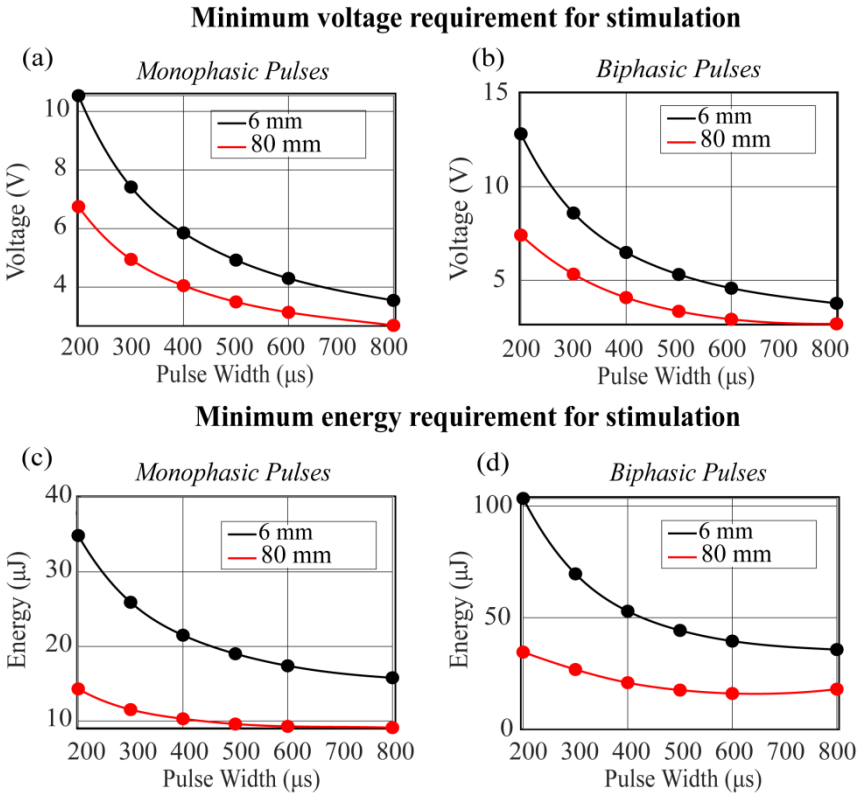


**Figure 28. Miniaturization potential of the regular microstimulator.(a) and (b)The minimum voltage required to activate the axon with monophasic and biphasic stimulation respectively provided by a regular microstimulator that is either 6 mm or 80 mm long. (c) and (d)The minimum energy required to activate the axon with monophasic and biphasic stimulation respectively provided by a regular microstimulator that is either 6 mm or 80 mm long. A conductivity of 0.5 S/m, and an electrode diameter of 1 mm is assumed to obtain the voltage and energy values.**

### 4.4.5 Comparison of the energy efficiency of stimulation provided with rectifying vs regular microstimulators

The energy efficiency of stimulation achieved with either the rectifying or the regular microstimulators was estimated by computing the ratio between the amplitude of the energy required to achieve threshold activation of the axon and the amplitude of the energy of the ac field that needs to be externally applied in order to obtain sufficient energy in the implanted device for neurostimulation. Figure 29 (a) shows the energy efficiency of biphasic stimulation performed with a 3 cm long rectifying and regular microstimulator as a function of the pulse widths. Stimulation performed by regular microstimulators was approximatley more than twice as energy efficient as the stimulation delivered by the rectifying microstimulators. Figure 29 (b) shows the difference between the energy efficiency of biphasic stimulation delivered by rectifying and a regular microstimulator as a function pulse width and interelectrode spacing. It can be seen that this difference was independent of pulse width, but it heavily depended on the microstimulator length. At long microstimulator lengths the difference between the energy efficiency of stimulation provided by the rectifying and regular microstimulator was maximized. As the microstimulator length increased, the energy efficiency of the stimulation increased at a much faster rate for the regular than the rectifying microstimulators. Because of the higher activation thresholds associated with the rectifying method, energy efficiency was lower.. Figure 29 (c) and (d) are mesh plots of the energy efficiency of biphasic stimulation when regular and rectifying microstimulators are used respectively as a function of pulse width and interelectrode spacing.

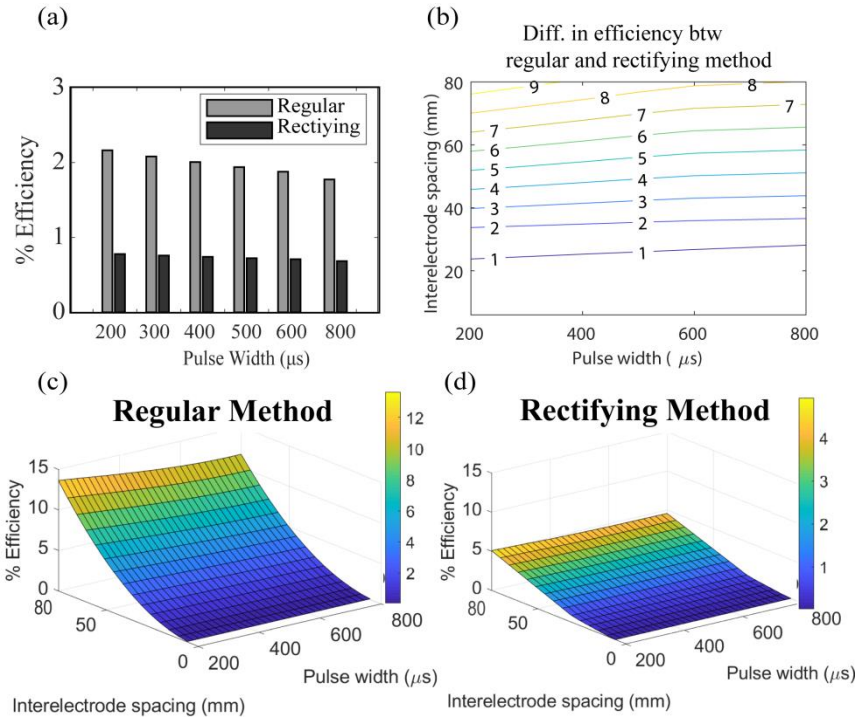


**Figure 29 Energy efficiency of the stimulation delivered by rectifying and regular microstimulators. (a) Bar graph showing the energy efficiency of biphasic stimulation provided by a 3 cm long rectifying and regular microstimulators as a function of pulse width. (b) Contour plot of the difference between the energy efficiency of biphasic stimulation performed by the rectifying and regular microstimulators as the pulse width and microstimulator length are varied. (c) mesh plot of the energy efficiency of the biphasic stimulation provided by regular microstimulators. (d) mesh plot of the energy efficiency of the biphasic stimulation provided by rectifying microstimulators.**

## 4.5 Discussion

Injectable single channel wirelessly powered micro-stimulators represent an attractive neural interface in functional neuromuscular stimulation applications because they can provide access to multiple points in the neuromuscular system for stimulation while causing minimal trauma since they can be implanted in a minimally invasive way i.e. via injection. To the best of our knowledge, the only injectable wireless micro-stimulators ever used for neuromuscular stimulation to restore function in patients with motor deficiencies are the BIONs system [18]. The BIONs are either driven by an external inductive link (i.e. magnetic fields) or rechargeable batteries [85], and thus they must incorporate bulky and mechanically rigid internal components that ultimately lead to increasing their overall volume as well as their stiffness. Such bulky microstimulators cannot be used to perform asynchronous selective activation of skeletal muscles required for physiological recruitment of muscles, since 1) they are physically large to fit several of them inside a single muscle and 2) they are large compared to their neural targets [168] and thus unable to selectively activate them.

In neurostimulation applications where space at the stimulation site is limited, wirelessly powering implanted microstimulators with volume conducted currents may be a viable and promising option. This is because volume conduction can transfer sufficient power required for neurostimulation from the external system to the implanted stimulator, while bypassing the need to incorporate bulky components inside the implanted microstimulator for successful coupling i.e. very thin implants can be realized.

With volume conduction used as WPT method, two approaches for developing wireless injectable microstimulator are being investigated in this study: the rectifying and the regular approach.

It was not clear to us which of these two approaches would be more preferable for developing microstimulators for performing multisite selective neural stimulation in neurorehabilitation applications. Therefore we carried out an assessment based on two important performance criteria: stimulation efficiency and miniaturization potential.

We evaluated the stimulation efficiency of the microstimulators based on the rectifying and regular approach through the stimulation efficiency of their corresponding stimulation waveforms. The rectifying microstimulator cannot generate the stimulus pulses by itself and relies on the instantaneous rectification of externally applied pulses of volume conducted ac currents to provide neurostimulation. Due to this mechanism of neurostimulation, the stimulus pulse that rectifying microstimulator delivers to the nerves has a shape of a non-smooth half-rectified ac signal. On the other hand, the regular microstimulator produces conventional square waveforms, since it has an onboard pulse generator that receives power from the transmitted ac fields through a storage capacitor. Even though it was reported that nerves respond to the 'half-rectified signals' (associated with the rectifying approach) as they would to conventional square waveforms with equivalent dc amplitude (those associated with the regular approach)[90],[94],[101],[44], experimental results from the only study where this was explored in superficial way in rat sciatic nerve preparation reported higher threshold current for stimulus signals created by direct rectifcation (19.6 μA) than its corresponding square waveforms (17 μA) for a 1 ms pulse [175].

When we used our myelinated axon model to compare the activation threshold of the axon when the stimulus waveform created by rectifying microstimulator was applied vs when it corresponding square waveform produced by the regular microstimulator was applied, our model predicted that

approximately 50% more current would be needed to trigger an action potential from the axon if the former was used than if the latter was used. Similarly, the the stimulus waveform associated with rectifying microstimulators were found to be approximally 50% less charge efficient than their corresponding square waveform with an equivalent dc amplitude associated with the regular microstimulators. High charge thresholds have important implications, especially for very small implants, where the charge injection limits can be easily exceeded because the electrodes have smaller surface areas. If the safe charge injection limit is exceeded, electrode corrosion and tissue damage due the release of toxic electrochemical products at the electrode-tissue interface can occur [11]. As expected, monophasic stimulation delivered by the microstimulators was associated with lower excitation thresholds than biphasic stimulation. This is because in the monophasic case, there is no second phase of opposite polarity to counteract the depolarization induced by first phase [189][55] [59]. Nonetheless, the stimulation efficiency of biphasic pulses can be improved by using trailing phases with very low amplitudes, but of longer durations (i.e. asymmetric pulses) [195] [196] [197].

The energy efficiency of the stimulation provided by the rectifying microstimulator was lower than that of the stimulation achieved by the regular microstimulator. In other words, ac fields of higher amplitude will be required to perform threshold excitation of the axon with rectifying microstimulator than with the regular microstimulator. Since higher electric fields are required, for more realistic scenarios where trains of pulses will be delivered, it is necessary that a thermal analysis is performed to validate that the applied electric fields are below the maximum specific absorption (SAR) limits provided by IEEE standards [198]. We did not compute the SAR values required to perform threshold neural stimulation with either microstimulator approaches, since only single stimulus pulses were considered in

this study.We then determined the miniaturization potential of the regular microstimulator by determining the minimum energy that it needs to deliver to produce neural stimulation. The energy requirements for neurostimulation associated with the regular microstimulators were in the order of a several tens of μJs. A capacitor with a volume of 1 $mm^3$ (i.e. 1mm×1mm×1mm) that has an energy density of around 5000 $J/m^3$ similar to that of a multilayered ceramic X7R capacitor [199] could only store 5 $\mu$J. This value is several times lower than the values needed to produce neurostimulation. For this reason, incorporating an internal storage capacitor can impede the miniaturization of the regular microstimulators.

## 4.6 Conclusion

The stimulation delivered by the rectifying microstimulators appears to be less current, charge and energy efficient than that provided by regular microstimulators. This is believed to be due to the shape of the waveform created by the rectifying microstimulator that is used to stimulate the nerves. It could be that the axon membrane is unable to efficiently respond to the pulsation or oscillations in those half-rectified ac waveforms. It is possible that the inclusion of smoothing capacitor in the circuit to rid that stimulus signal of the oscillation before it is delivered to the nerves can increase the efficiency of stimulation delivered by the rectifying microstimulators. The miniaturization of the regular microstimulators is limited by the large size of the onboard storage capacitor needed to ensure a sufficient power supply for neurostimulation. It appears that the choice of the microstimulator approach to be used requires a tradeoff between miniaturization and stimulation efficiency.

## 4.7 Appendix

The equations describing the ionic currents at the axon's membrane were taken from [182]. The membrane current in this model is that of a mammalian motor neuron being excited at 36 ºC and composed of three individual ionic currents and a leakage current. Thus the total ionic current at each node is calculated as the sum of 4 different currents:

$$I_i = I_{Naf} + I_{Nap} + I_{Ks} + I_{Lk}$$

The equations used to compute each current and the dynamics of the gating variable controlling each current are as follows (expressed in mV and ms):

Fast sodium current:

$$I_{Naf} = g_{Naf} m^3 h (V_m - E_{Na})$$

$$\frac{dm}{dt} = \alpha_m (1 - m) - \beta_m m$$

$$\alpha_m = 6.57 \frac{V_m + 20.4}{1 - \exp[-(V_m + 20.4)/10.3]}$$

$$\beta_m = 0.304 \frac{-(V_m + 25.7)}{1 - \exp[(V_m + 25.7)/9.16]}$$

$$\frac{dh}{dt} = \alpha_h (1 - h) - \beta_h h$$

$$\alpha_h = 0.34 \frac{-(V_m + 114)}{1 - \exp[(V_m + 114)/11]}$$

$$\beta_h = \frac{12.6}{1 + \exp[-(V_m + 31.8)/13.4]}$$

Persistent sodium current

$$I_{Nap} = g_{Nap} p^3 (V_m - E_{Na})$$

$$\frac{dp}{dt} = \alpha_p (1 - p) - \beta_p p$$

$$\alpha_p = 0.0353 \frac{V_m + 27}{1 - \exp[-(V_m + 27)/10.2]}$$

$$\beta_p = 0.000883 \frac{-(V_m + 34)}{1 - \exp[(V_m + 34)/10]}$$

Slow potassium current

$$I_{Ks} = g_{Ks} s (V_m - E_K)$$

$$\frac{ds}{dt} = \alpha_s (1 - s) - \beta_s s$$

$$\alpha_s = \frac{0.3}{1 + \exp[-(V_m + 53)/5]}$$

$$\beta_s = \frac{0.03}{1 + \exp[-(V_m + 90)/1]}$$

Leakage current

$$I_{Lk} = g_{Lk} (V_m - E_{Lk})$$

Where the values $g_i$ are the maximum conductance values for the individual ion channels, *m*, *h*, *p* and *s* are the channel gating variables that range from 0 to 1 and $E_i$ are the ionic Nernst potentials.

Values of the parameters used to model the ionic currents:
$g_{Naf} = 3\,S/cm^2$, $g_{Nap} = 0.01\,S/cm^2$, $g_{Ks} = 0.08\,S/cm^2$, $g_{Lk} = 0.007\,S/cm^2$, $E_{Na} = 50\,mV$, $E_K = -90\,mV$, $E_{Lk} = -90\,mV$.

# Conclusion

CHAPTER 5

## 5.1 General conclusions

The work carried out in this PhD is the first of many steps that need to be taken before a motor prosthetic system based on high density selective electrical stimulation of skeletal muscles is fully developed and can be used to drive the neural circuits of skeletal muscles to restore function to paralyzed limbs in a physiological wat. This work showed that a neuroprosthetic system like the BIONs and eAXONs designed to provide a network of widely distributed IM microstimulators bodes well with the compartmentalized nature of the muscle and would provide the hardware required to perform interleaved electrical stimulation through relatively safe implantation procedures (injection). The work carried out in this PhD helped shed some light on the importance of the selection of implantation sites for these microstimulators in skeletal muscles. The choice of the implantation site controls the amount of electrical overlap between the microstimulators and, in turn, the efficacy of interleaved stimulation in delaying ES-induced fatigue. Even though the ability of interleaved stimulation with minimally overlapping electrodes to achieve smooth and fatigue-resistant contractions was previously demonstrated using nerve electrodes (for example, Utah Slanted Electrode Array) by other authors, such interfaces could not be easily translated to the clinics for use in humans, since they require invasive surgeries for their implantation. In this PhD we demonstrated that the same smooth and fatigue-resistant forces obtained with these invasive nerve electrodes can be potentially produced by injectable IM interfaces like eAXONS. Because the eAXONs can be implanted via injection at an out-patient clinic they have a much higher potential for clinical translation compared to their invasive nerve counterparts.

In this PhD, we also inferred the functional organization of MUs inside the MG muscle of WNZ rabbits. Prior to the work carried out in this PhD, it was thought that mammalian skeletal muscles are coarsely compartmentalized (i.e. NMCs occurred about the primary intramuscular branches only). However, we inferred from our work that the mammalian skeletal muscles are more finely compartmentalized about the higher order IM nerve branches. These fine compartments require finer neural interfaces to control them. Such knowledge about the neuromuscular organization of MUs is important when it comes to developing devices to electrically interface with skeletal muscles.

We also showed that there are two possible approaches for developing microstimulators based on volume conduction; the rectifying and regular method. We showed that while stimulus waveforms delivered by microstimulators based on the rectifying approach (created by direct rectification of external ac signals instead of produced by an onboard pulse generator) are less current, charge, and energy efficient than the square waveforms associated with the regular microstimulators in exciting an axon, the rectifying method can lead to very thin implants whereas the regular method cannot.
Therefore, the benefits of using direct rectification of volume conducted ac currents as a means of neurostimulation to achieve thinner microstimulators should be cautiously weighed against its lower stimulation efficiency.

## 5.2 Future work

As explained previously, in this PhD we were only able to infer the extensive compartmentalization of mammalian muscles, but we were not able to show enough evidence to prove it. Thus another study is warranted to investigate the compartmentalization of motor axons in the primary, secondary, and tertiary IM nerve branches by testing the independence of their response to electrical stimulation. This multi-level compartmentalization which we believe exists can also be studied by comparing the magnitude of the plateau force evoked when a parent IM nerve branch is stimulated with the sum of the magnitudes of the plateau forces obtained following the stimulation of each of the daughter branches alone. It is not yet known whether or not the individual nerve branches on an intramuscular nerve tree can respond independently of each other when electrically stimulated.

Once the existence of these multi-level compartments with different maximum force outputs is confirmed in skeletal muscles, the ability to recruit them in different patterns and combinations to achieve fine control over skeletal muscle force should also be studied. For example, fine NMCs should be engaged to produce low level forces needed to execute daily activities (humans use 25% of the maximum strength available to their muscles when performing daily activities) and large NMCs should be engaged when large forces are needed.

# References

[1] M. Granat, J. F. Keating, A. C. Smith, M. Delargy, and B. J. Andrews, “The use of functional electrical stimulation to assist gait in patients with incomplete spinal cord injury.,” *Disabil. Rehabil.*, vol. 14, no. 2, pp. 93–97, 1992.

[2] E. B. Marsolais and R. Kobetic, “Functional electrical stimulation for walking in paraplegia.,” *JBJS*, vol. 69, no. 5, 1987.

[3] D. Guiraud, T. Stieglitz, K. P. Koch, J.-L. Divoux, and P. Rabischong, “An implantable neuroprosthesis for standing and walking in paraplegia: 5-year patient follow-up,” *J. Neural Eng.*, vol. 3, no. 4, pp. 268–275, Sep. 2006.

[4] E. Hardin *et al.*, “Walking after incomplete spinal cord injury using an implanted FES system: a case report.,” *J. Rehabil. Res. Dev.*, vol. 44, no. 3, pp. 333–346, 2007.

[5] B.-C. Son, D.-R. Kim, I.-S. Kim, and J. T. Hong, “Phrenic nerve stimulation for diaphragm pacing in a quadriplegic patient,” *J. Korean Neurosurg. Soc.*, vol. 54, no. 4, pp. 359–362, Oct. 2013.

[6] J. S. Walter, R. D. Wurster, Q. Zhu, C. Staunton, and F. Laghi, “Stimulating multiple respiratory muscles with intramuscular permaloc electrodes,” *J. Spinal Cord Med.*, vol. 33, no. 2, pp. 135–143, 2010.

[7] J. S. Walter, R. B. Dunn, R. D. Wurster, and F. Laghi, “Microstimulators and intramuscular hook electrodes for the stimulation of respiratory muscles,” *J. Spinal Cord Med.*, vol. 30, no. 4, pp. 338–345, 2007.

[8] C. Godec, A. S. Cass, and G. F. Ayala, “Electrical stimulation for incontinence: Technique, selection, and results,” *Urology*, vol. 7, no. 4, pp. 388–397, 1976.

[9] A. Esa, H. Kiwamoto, T. Sugiyama, Y. C. Park, S. Kaneko, and T. Kurita, “Functional electrical stimulation in the management of incontinence: Studies of urodynamics,” *Int. Urol. Nephrol.*, vol. 23, no. 2, pp. 135–141, 1991.

[10] A. L. Burnett, P. E. Teloken, A. Briganti, T. Whitehurst, and F. Montorsi, “Intraoperative assessment of an implantable electrode array for cavernous nerve stimulation.,” *J. Sex. Med.*, vol. 5, no. 8, pp. 1949–1954, Aug. 2008.

[11] P. E. Crago, P. H. Peckham, J. T. Mortimer, and J. P. Van Der Meulen, “The choice of pulse duration for chronic electrical stimulation via surface, nerve, and intramuscular electrodes,” *Ann. Biomed. Eng.*, vol. 2, no. 3, pp. 252–264, 1974.

[12] J. T. Mortimer and N. Bhadra, “Peripheral Nerve and Muscle Stimulation,” in *Neuroprosthetics: Theory and Practice*, 2004, pp. 1–48.

[13] J. T. Naples G, Mortimer, A. Scheiner, and J. D. Sweeney, “A spiral nerve cuff electrodes for peripheral neve stimulation,” *IEEE Trans. Biomed. Eng.*, vol. 35, no. 8823295, 1988.

[14] W. D. Memberg, P. H. Peckham, and M. W. Keith, “A surgically-implanted intramuscular electrode for an implantable neuromuscular stimulation system,” *IEEE Trans. Rehabil. Eng.*, vol. 2, no. 2, pp. 80–91, Jun. 1994.

[15] P. A. Grandjean and J. T. Mortimer, “Recruitment properties of monopolar and bipolar epimysial electrodes,” *Ann. Biomed. Eng.*, vol. 14, no. 1, pp. 53–66, 1986.

[16] A. Abdo, M. Sahin, D. S. Freedman, E. Cevik, P. S. Spuhler, and M. S. Unlu, “Floating light-activated microelectrical stimulators tested in the rat spinal cord,” *J. Neural Eng.*, vol. 8, no. 5, p. 056012, Oct. 2011.

[17] M. Sahin and V. Pikov, “Wireless microstimulators for neural prosthetics,” *Crit. Rev. Biomed. Eng.*, vol. 39, no. 1, pp. 63–77, 2011.

[18] G. E. Loeb, R. A. Peck, W. H. Moore, and K. Hood, “BION system for distributed neural prosthetic interfaces.,” *Med. Eng. Phys.*, vol. 23, no. 1, pp. 9–18, Jan. 2001.

[19] X. Navarro, T. B. Krueger, N. Lago, S. Micera, T. Stieglitz, and P. Dario, “A critical review of interfaces with the peripheral nervous system for the control of neuroprostheses and hybrid bionic systems.,” *J. Peripher. Nerv. Syst.*, vol. 10, no. 3, pp. 229–258, Sep. 2005.

[20] R. A. Normann *et al.*, “Coordinated, multi-joint, fatigue-resistant feline stance produced with intrafascicular hind limb nerve stimulation.,” *J. Neural Eng.*, vol. 9, no. 2, p. 26019, Apr. 2012.

[21] M. A. Frankel, V. J. Mathews, G. A. Clark, R. A. Normann, and S. G. Meek, “Control of dynamic limb motion using fatigue-resistant asynchronous intrafascicular multi-electrode stimulation,” *Front. Neurosci.*, vol. 10, no. SEP, pp. 1–12, 2016.

[22] D. McDonnall, G. A. Clark, and R. A. Normann, “Selective motor unit recruitment via intrafascicular multielectrode stimulation,” *Can. J. Physiol. Pharmacol.*, vol. 82, no. 8–9, pp. 599–609, 2004.

[23] D. McDonnall, G. A. Clark, and R. A. Normann, “Interleaved, multisite electrical stimulation of cat sciatic nerve produces fatigue-resistant, ripple-free motor responses,” *IEEE Trans. Neural Syst. Rehabil. Eng.*, vol. 12, no. 2, pp. 208–215, 2004.

[24] A. R. Lind and J. Scott Petrofsky, “Isometric tension from rotary stimulation of fast and slow cat muscles,” *Muscle Nerve*, vol. 1, no. 3, pp. 213–218, 1978.

[25] P. M. Rack and D. R. Westbury, “The effects of length and stimulus rate on tension in the isometric cat soleus muscle,” *J. Physiol.*, vol. 204, no. 2, pp. 443–460, Oct. 1969.

[26] R. Kobetic, R. J. Triolo, and E. B. Marsolais, “Muscle selection and walking performance of multichannel FES systems for ambulation in paraplegia,” *IEEE Trans. Rehabil. Eng.*, vol. 5, no. 1, pp. 23–29, 1997.

[27] S. FERRANTE, A. L. G. PEDROCCHI, and G. FERRIGNO, “Biomimetic neuroprostheses: Human-Like Control Strategies to Improve Training Rehabilitative Exercises Using Functional Electrical Stimulation,” in *Progress in Biological Cybernetics Research*, 2008, pp. 161–185.

[28] M. Bijak *et al.*, “Stimulation parameter optimization for FES supported standing up and walking in SCI patients.,” *Artif. Organs*, vol. 29, no. 3, pp. 220–223, Mar. 2005.

[29] P. H. Thomson, M., Veltink, “Influence of synchronous and sequential stimulation on muscle fatigue,” *Med.& Biol. Eng. Comput*, vol. 35, no. May, pp. 186–192, 1997.

[30] A. W. Monster and H. Chan, “Isometric force production by motor units of extensor digitorum communis muscle in man.,” *J. Neurophysiol.*, vol. 40, no. 6, pp. 1432–1443, Nov. 1977.

[31] C. W. Caldwell and J. B. Reswick, “A percutaneous wire electrode for chronic research use.,” *IEEE Trans. Biomed. Eng.*, vol. 22, no. 5, pp. 429–432, Sep. 1975.
[32] W. D. Memberg, P. H. Peckham, G. B. Thrope, M. W. Keith, and T. P. Kicher, “An Analysis of the Reliability of Percutaneous Intramuscular Electrodes in Upper Extremity FNS Applications,” *IEEE Trans. Rehabil. Eng.*, vol. 1, no. 2, pp. 126–132, 1993.
[33] Arthur Prochazka Lyle A. Davis, “Clinical experience with reinforced , anchored intramuscular electrodes for functional neuromuscular stimulation,” *J. Neurosci. Methods*, vol. 42, pp. 175–184, 1992.
[34] B. J. KuppT, Hochman P. Hale J, “Effect of motion on polymer implant capsule formation in muscle,” *Biomaterials*, 1980.
[35] V. Mendenhall and C. L. Van Kampen, “of Motion on the Tissue Fiber Implants,” vol. 15, pp. 37–41, 1994.
[36] B. Ziaie, M. D. Nardin, A. R. Coghlan, and K. Najafi, “A single-channel implantable microstimulator for functional neuromuscular stimulation.,” *IEEE Trans. Biomed. Eng.*, vol. 44, no. 10, pp. 909–920, Oct. 1997.
[37] A. Scheiner, G. Polando, and E. B. Marsolais, “Design and Clinical Application of a Double Helix Electrode for Functional Electrical Stimulation,” vol. 41, no. 5, 1994.
[38] Y. Shimada, K. Sato, H. Kagaya, N. Konishi, S. Miyamoto, and T. Matsunaga, “Clinical use of percutaneous intramuscular electrodes for functional electrical stimulation.,” *Arch. Phys. Med. Rehabil.*, vol. 77, no. 10, pp. 1014–1018, Oct. 1996.
[39] L. Becerra-Fajardo and A. Ivorra, “In Vivo Demonstration of Addressable Microstimulators Powered by Rectification of Epidermically Applied Currents for Miniaturized Neuroprostheses,” *PLoS One*, vol. 10, no. 7, p. e0131666, Jul. 2015.
[40] L. Becerra-Fajardo, M. Schmidbauer, and A. Ivorra, “Demonstration of 2 mm Thick Microcontrolled Injectable Stimulators Based on Rectification of High Frequency Current Bursts,” *IEEE Trans. Neural Syst. Rehabil. Eng.*, vol. 25, no. 8, pp. 1343–1352, 2017.
[41] A. Ivorra, L. Becerra-fajardo, and Q. Castellví, “In vivo demonstration of injectable microstimulators based on charge-balanced rectification of epidermically applied currents,” *J Neural Eng.*, vol. 12, no. 6, 2015.
[42] K. Famm, B. Litt, K. J. Tracey, E. S. Boyden, and M. Slaoui, “Drug discovery: a jump-start for electroceuticals,” *Nature*, vol. 496, no. 7444, pp. 159–161, Apr. 2013.
[43] C. C. Horn, J. L. Ardell, and L. E. Fisher, “Electroceutical Targeting of the Autonomic Nervous System,” *Physiology (Bethesda).*, vol. 34, no. 2, pp. 150–162, Mar. 2019.
[44] A. Ivorra, “Remote electrical stimulation by means of implanted rectifiers,” *PLoS One*, vol. 6, no. 8, 2011.
[45] T. Cameron *et al.*, “Micromodular Implants to Provide Electrical Stimulation of Paralyzed Muscles and Limbs,” vol. 44, no. 9, pp. 781–790, 1997.
[46] R. E. Burke and P. Tsairis, “Anatomy and innervation ratios in motor units of cat gastrocnemius,” *J. Physiol.*, vol. 234, no. 3, pp. 749–765, 1973.

[47] J. C. Eccles and C. S. Sherrington, “Numbers and contraction-values of individual motor-units examined in some muscles of the limb,” *Proc. R. Soc. London. Ser. B, Contain. Pap. a Biol. Character*, vol. 106, no. 745, pp. 326–357, Jun. 1930.

[48] D. Mani, D. F. Feeney, and R. M. Enoka, “The modulation of force steadiness by electrical nerve stimulation applied to the wrist extensors differs for young and older adults.,” *Eur. J. Appl. Physiol.*, vol. 119, no. 1, pp. 301–310, Jan. 2019.

[49] A. J. Bergquist, J. M. Clair, O. Lagerquist, C. S. Mang, Y. Okuma, and D. F. Collins, “Neuromuscular electrical stimulation: implications of the electrically evoked sensory volley.,” *Eur. J. Appl. Physiol.*, vol. 111, no. 10, pp. 2409–2426, Oct. 2011.

[50] J. T. Mortimer, “Motor Prostheses,” *Comprehensive Physiology*. pp. 155–187, 01-Jan-2011.

[51] M. B. Laskowski and J. R. Sanes, “Topographic mapping of motor pools onto skeletal muscles,” *J. Neurosci.*, vol. 7, no. 1, pp. 252–260, 1987.

[52] D. R. McNEAL and J. B. RESWICK, “Control of Skeletal Muscle by Electrical Stimulation,” in *Advances in Biomedical Engineering*, J. H. U. BROWN and J. F. DICKSON, Eds. Academic Press, 1976, pp. 209–256.

[53] J. T. Mortimer, D. Kaufman, and U. Roessmann, “Intramuscular electrical stimulation: Tissue damage,” *Ann. Biomed. Eng.*, vol. 8, no. 3, pp. 235–244, 1980.

[54] K. Singh, F. J. R. Richmond, and G. E. Loeb, “Recruitment properties of intramuscular and nerve-trunk stimulating electrodes,” *IEEE Trans. Rehabil. Eng.*, vol. 8, no. 3, pp. 276–285, 2000.

[55] P. H. Gorman and J. T. Mortimer, “The Effect of Stimulus Parameters on the Recruitment Characteristics of Direct Nerve Stimulation,” *IEEE Trans. Biomed. Eng.*, vol. BME-30, no. 7, pp. 407–414, Jul. 1983.

[56] D. Popovic, T. Gordon, V. F. Rafuse, and A. Prochazka, “Properties of implanted electrodes for functional electrical stimulation,” *Ann. Biomed. Eng.*, vol. 19, no. 3, pp. 303–316, 1991.

[57] M. Laubacher, E. A. Aksöz, S. Binder-macleod, and K. J. Hunt, “Comparison of proximally versus distally placed spatially distributed sequential stimulation electrodes in a dynamic knee extension task,” vol. 26, no. 2, pp. 110–115.

[58] L. Edström and E. Kugelberg, “Histochemical composition, distribution of fibres and fatiguability of single motor units. Anterior tibial muscle of the rat.,” *J. Neurol. Neurosurg. Psychiatry*, vol. 31, no. 5, pp. 424–433, 1968.

[59] J. B. Ranck Jr, “Extracellular stimulation,” in *Electrical stimulation research techniques*, Elsevier, 1981, pp. 1–36.

[60] J. J. Denier and P. Physics, “Coordination and Inhomogeneous Activation of Human Arm Muscles During Isometric Torques,” vol. 60, no. 5, 1988.

[61] Z. P. Fang and J. T. Mortimer, “A Method to Effect Physiological Recruitment Order in Electrically Activated Muscle,” *IEEE Trans. Biomed. Eng.*, vol. 38, no. 2, pp. 175–179, 1991.

[62] R. Baratta, M. Ichie, S. K. Hwang, and M. Solomonow, “Orderly Stimulation of Skeletal Muscle Motor Units with Tripolar Nerve Cuff Electrode,” *IEEE Trans. Biomed. Eng.*, vol. 36, no. 8, pp. 836–843, 1989.

[63] C. Tai and D. Jiang, “Selective Stimulation of Smaller Fibers in a Compound Nerve Trunk with Single Cathode by Rectangular Current Pulses,” *IEEE Trans. Biomed. Eng.*, vol. 41, no. 3, pp. 286–291, 1994.

[64] L. Grimby and J. Hannerz, “Firing rate and recruitment order of toe extensor motor units in different modes of voluntary conraction.,” *J. Physiol.*, vol. 264, no. 3, pp. 865–879, 1977.

[65] C. S. Bickel, C. M. Gregory, and J. C. Dean, “Motor unit recruitment during neuromuscular electrical stimulation: A critical appraisal,” *Eur. J. Appl. Physiol.*, vol. 111, no. 10, pp. 2399–2407, 2011.

[66] J. S. Petrofsky, “Control of the recruitment and firing frequencies of motor units in electrically stimulated muscles in the cat,” *Med. Biol. Eng. Comput.*, vol. 16, no. 3, pp. 302–308, 1978.

[67] P. E. Crago, P. H. Peckham, and G. B. Thrope, “Modulation of Muscle Force by Recruitment During Intramuscular Stimulation,” *IEEE Trans. Biomed. Eng.*, vol. BME-27, no. 12, pp. 679–684, 1980.

[68] W. M. Grill and J. T. Mortimer, “The effect of stimulus pulse duration on selectivity of neural stimulation,” *IEEE Trans. Biomed. Eng.*, vol. 43, no. 2, pp. 161–166, Feb. 1996.

[69] M. Solomonow, “External Control of the Neuromuscular System,” *IEEE Trans. Biomed. Eng.*, vol. BME-31, no. 12, pp. 752–763, 1984.

[70] H. B. K. Boom, A. J. Mulder, and P. H. Veltink, “Fatigue during functional neuromuscular stimulation,” in *Natural and Artificial Control of Hearing and Balance*, vol. 97, Elsevier, 1993, pp. 409–418.

[71] B. Dreibati, C. Lavet, A. Pinti, and G. Poumarat, “Influence of electrical stimulation frequency on skeletal muscle force and fatigue,” *Ann. Phys. Rehabil. Med.*, vol. 53, no. 4, pp. 266–277, 2010.

[72] W. M. Grill and J. T. Mortimer, “Quantification of recruitment properties of multiple contact cuff electrodes,” *IEEE Trans. Rehabil. Eng.*, vol. 4, no. 2, pp. 49–62, 1996.

[73] A. Branner, R. B. Stein, and R. A. Normann, “Selective stimulation of cat sciatic nerve using an array of varying-length microelectrodes,” *J. Neurophysiol.*, vol. 85, no. 4, pp. 1585–1594, 2001.

[74] P. H. P. M. W. K. A. A. Freehafer, “Restoration of functional control by electrical stimulation in the upper extremity of the quadriplegic patient.,” *J. Bone Jt. Surgery. Br. Vol. J. Bone Jt. Surgery.*, vol. 70, no. 1, pp. 144–148, 1988.

[75] J. S. Knutson, G. G. Naples, P. H. Peckham, and M. W. Keith, “Electrode fracture rates and occurrences of infection and granuloma associated with percutaneous intramuscular electrodes in upper-limb functional electrical stimulation applications.,” *J. Rehabil. Res. Dev.*, vol. 39, no. 6, pp. 671–683, 2002.

[76] B. J. U. E. Bagge, “Displacement and deformation of wire electrodes in electromyography. A roentgenologic study" Electromyography. May-Jul;9(2):201-211. 1968.

[77] B. J. and S. Reichman, “Displacement deformation and fracture of wire electrodes for electromyography.” Electromyography. Nov-Dec;8(4):329-47. 1968.

[78] G. E. Loeb, R. A. Peck, W. H. Moore, and K. Hood, “BION □ system for distributed neural prosthetic interfaces,” vol. 23, pp. 9–18, 2001.

[79] A. D. Salter, F. J. R. Richmond, and G. E. Loeb, “Prevention of Muscle Disuse Atrophy by Low-Frequency Electrical Stimulation in Rats,” vol. 11, no. 3, pp. 218–226, 2003.

[80] T. Cameron, T. L. Liinamaa, G. E. Loeb, and F. J. R. Richmond, “Long-term biocompatibility of a miniature stimulator implanted in feline hind limb muscles,” *IEEE Trans. Biomed. Eng.*, vol. 45, no. 8, pp. 1024–1035, 1998.

[81] T. Cameron, F. J. R. Richmond, and G. E. Loeb, “Effects of Regional Stimulation Using a Miniature Stimulator Implanted in Feline Posterior Biceps Femoris,” *IEEE Trans. Biomed. Eng.*, vol. 45, no. 8, pp. 1036–1043, 1998.

[82] R. Davis *et al.*, “Poststroke Upper-Limb Rehabilitation Using 5 to 7 Inserted Microstimulators : Implant Procedure , Safety , and Efficacy for Restoration of Function,” *Arch Phys Med Rehabil*. vol. 89, no. October, pp. 1907–1912, 2008..

[83] V. W. H. Lin, X. Deng, Y. S. Lee, and I. N. Hsiao, “Stimulation of the expiratory muscles using microstimulators,” *IEEE Trans. Neural Syst. Rehabil. Eng.*, vol. 16, no. 4, pp. 416–420, 2008.

[84] R. Carbunaru, T. Whitehurst, K. Jaax, J. Koff, and J. Makous, “Rechargeable battery-powered bion microstimulators for neuromudulation.,” *Conf. Proc. IEEE Eng. Med. Biol. Soc.*, vol. 6, no. February 2004, pp. 4193–4196, 2004.

[85] D. Chung and Z. Ayyoub, “Feasibility Study of the Bioness Battery-Powered Microstimulator ( BBPM ) to Treat Post-Stroke Shoulder Pain in Chronic Post-Stroke Subjects,” *J Neurol Disord Stroke*, vol. 2, no. 1, p. 1030., 2014.

[86] T. L. Trentman, D. M. Rosenfeld, B. B. Vargas, T. J. Schwedt, R. S. Zimmerman, and D. W. Dodick, “Greater occipital nerve stimulation via the Bion microstimulator: implantation technique and stimulation parameters. Clinical trial: NCT00205894.,” *Pain Physician*, vol. 12, no. 3, pp. 621–8, 2009.

[87] A.F. von Recum, “New aspects of biocompability: Motion at the interface.,” in *Clinical implant materials, advances in biomaterials.*, E. Heimke G, Soltesz U, Lee AJC, Ed. Amsterdam: : Elsevier Science Publishers BV.

[88] K. L. Helton, B. D. Ratner, and N. A. Wisniewski, “Biomechanics of the sensor-tissue interface - Effects of motion, pressure, and design on sensor performance and the foreign body response - Part I: Theoretical framework,” *J. Diabetes Sci. Technol.*, vol. 5, no. 3, pp. 632–646, 2011.

[89] Y. Wang, S. Vaddiraju, B. Gu, F. Papadimitrakopoulos, and D. J. Burgess, “Foreign Body Reaction to Implantable Biosensors: Effects of Tissue Trauma and Implant Size.,” *J. Diabetes Sci. Technol.*, vol. 9, no. 5, pp. 966–977, Aug. 2015.

[90] R. Erfani, F. Marefat, A. M. Sodagar, and P. Mohseni, “Modeling and Experimental Validation of a Capacitive Link for Wireless Power Transfer to Biomedical Implants,” *IEEE Trans. Circuits Syst. II Express Briefs*, vol. 65, no. 7, pp. 923–927, Jul. 2018.

[91] R. Sedehi *et al.*, “A Wireless Power Method for Deeply Implanted

Biomedical Devices via Capacitively Coupled Conductive Power Transfer," *IEEE Trans. Power Electron.*, vol. 36, no. 2, pp. 1870–1882, Feb. 2021.

[92] Y. PALTI, "Stimulation of muscles and nerves by means of externally applied electrodes," *Bull. Res. Counc. Isr. Sect. E. Exp. Med.*, vol. 10, p. 54—56, Jun. 1962.

[93] J. C. Schuder and H. Stoeckle, "The silicon diode as a receiver for electrical stimulation of body organs," *Trans. Am. Soc. Artif. Intern. Organs*, vol. 10, p. 366—370, 1964.

[94] B. C. Towe, P. J. Larson, and D. W. Gulick, "A microwave powered injectable neural stimulator.," *Annu. Int. Conf. IEEE Eng. Med. Biol. Soc. IEEE Eng. Med. Biol. Soc. Annu. Int. Conf.*, vol. 2012, pp. 5006–5009, 2012.

[95] D. W. Gulick and B. C. Towe, "Characterization of simple wireless neurostimulators and sensors.," *Annu. Int. Conf. IEEE Eng. Med. Biol. Soc. IEEE Eng. Med. Biol. Soc. Annu. Int. Conf.*, vol. 2014, pp. 3130–3133, 2014.

[96] Y. Palti, "Stimulation of internal organs by means of externally applied electrodes.," *J. Appl. Physiol.*, vol. 21, no. 5, pp. 1619–1623, Sep. 1966.

[97] A. Ivorra and L. Becerra-fajardo, "Flexible Thread-like Electrical Stimulation Implants Based on Rectification of Epidermically Applied Currents which Perform Charge Balance," *Replace. Repair, Restore, Reli. – Bridg. Clin. Eng. Solut. Neurorehabilitation*, 2014.

[98] D. K. Freeman *et al.*, "A Sub-millimeter, Inductively Powered Neural Stimulator," *Front. Neurosci.*, vol. 11, p. 659, 2017.

[99] S. Ha, M. L. Khraiche, G. A. Silva, and G. Cauwenberghs, "Direct inductive stimulation for energy-efficient wireless neural interfaces.," *Annu. Int. Conf. IEEE Eng. Med. Biol. Soc. IEEE Eng. Med. Biol. Soc. Annu. Int. Conf.*, vol. 2012, pp. 883–886, 2012.

[100] B. C. Towe, T. Graber, D. Gulick, and R. Herman, "Wireless microstimulators for treatment of peripheral vascular disease," in *2013 6th International IEEE/EMBS Conference on Neural Engineering (NER)*, 2013, pp. 1485–1488.

[101] P. J. Larson and B. C. Towe, "Miniature ultrasonically powered wireless nerve cuff stimulator," in *2011 5th International IEEE/EMBS Conference on Neural Engineering*, 2011, pp. 265–268.

[102] D. P. Lindsey, E. L. McKee, M. L. Hull, and S. M. Howell, "A new technique for transmission of signals from implantable transducers.," *IEEE Trans. Biomed. Eng.*, vol. 45, no. 5, pp. 614–619, May 1998.

[103] B. C. Towe, P. J. Larson, and D. W. Gulick, "Wireless ultrasound-powered biotelemetry for implants.," *Annu. Int. Conf. IEEE Eng. Med. Biol. Soc. IEEE Eng. Med. Biol. Soc. Annu. Int. Conf.*, vol. 2009, pp. 5421–5424, 2009.

[104] S. Malik *et al.*, "Injectable Sensors Based on Passive Rectification of Volume-Conducted Currents," *IEEE Trans. Biomed. Circuits Syst.*, vol. 14, no. 4, pp. 867–878, Aug. 2020.

[105] H. N. Schwerdt *et al.*, "A Fully-Passive Wireless Microsystem for Recording of Neuropotentials using RF Backscattering Methods," *J. Microelectromech. Syst.*, vol. 20, no. 5, pp. 1119–1130, Oct. 2011.

[106] A. W. English, S. L. Wolf, and R. L. Segal, “Compartmentalization of muscles and their motor nuclei: The partitioning hypothesis,” *Phys. Ther.*, vol. 73, no. 12, pp. 857–867, 1993.
[107] S. W. Herring, F. C. Anapol, and L. E. Wineski, “Neural organization of the masseter muscle in the pig,” *J. Comp. Neurol.*, vol. 280, no. 4, pp. 563–576, 1989.
[108] C. G. M. Hammond, D. C. Gordon, J. T. Fisher, and F. J. R. Richmond, “Motor unit territories supplied by primary branches of the phrenic nerve,” *J. Appl. Physiol.*, vol. 66, no. 1, pp. 61–71, 1989.
[109] E. D. H. Zonnevijlle *et al.*, “Sequential segmental neuromuscular stimulation: An effective approach to enhance fatigue resistance,” *Plast. Reconstr. Surg.*, vol. 105, no. 2, pp. 667–673, 2000.
[110] W. D. Letbetter, “Influence of intramuscular nerve branching on motor unit organization in medial gastrocnemius muscle.,”Anat Rec 178:402, 1974.
[111] J. A. Hoffer, G. E. Loeb, N. Sugano, W. B. Marks, M. J. O’Donovan, and C. A. Pratt, “Cat hindlimb motoneurons during locomotion. III. Functional segregation in sartorius,” *J. Neurophysiol.*, vol. 57, no. 2, pp. 554–562, 1987.
[112] C. G. Widmer, D. I. Carrasco, and A. W. English, “Differential activation of neuromuscular compartments in the rabbit masseter muscle during different oral behaviors,” *Exp. Brain Res.*, vol. 150, no. 3, pp. 297–307, 2003.
[113] C. B. Olson, D. O. Carpenter, and E. Henneman, “Orderly Recruitment of Muscle Action Potentials: Motor Unit Threshold and EMG Amplitude,” *Arch. Neurol.*, vol. 19, no. 6, pp. 591–597, Dec. 1968.
[114] Arthur W English Steven L Wolf Richard L Segal, “Compartmentalization of Muscles and Their Motor Nuclei: The Partitioning Hypothesis,” *Phys. Ther.*, vol. 73, no. 12, pp. 857–867, 1993.
[115] K. J. Shin *et al.*, “Anatomical study of the nerve regeneration after selective neurectomy in the rabbit: Clinical application for esthetic calf reduction,” *Anat. Cell Biol.*, vol. 48, no. 4, pp. 268–274, 2015.
[116] J. Liu, V. P. Kumar, H. K. Lau, B. P. Pereira, V. Shen, and R. W. H. Pho, “Neuromuscular compartments in the long head of triceps: A morphological study in rabbits,” *Muscle and Nerve*, vol. 20, no. 7, pp. 897–899, 1997.
[117] S. G. Carroll, R. J. Triolo, H. J. Chizeck, R. Kobetic, and E. B. Marsolais, “Tetanic responses of electrically stimulated paralyzed muscle at varying interpulse intervals,” *IEEE Trans. Biomed. Eng.*, vol. 36, no. 11, p. 1143, 1989.
[118] C. Scott Bickel, C. M. Gregory, and A. Azuero, “Matching initial torque with different stimulation parameters influences skeletal muscle fatigue,” *J. Rehabil. Res. Dev.*, vol. 49, no. 2, pp. 323–332, 2012.
[119] A. S. Gorgey, C. D. Black, C. P. Elder, and G. A. Dudley, “Effects of electrical stimulation parameters on fatigue in skeletal muscle,” *J. Orthop. Sports Phys. Ther.*, vol. 39, no. 9, pp. 684–692, 2009.
[120] C. Vila-Chã, D. Falla, and D. Farina, “Motor unit behavior during submaximal contractions following six weeks of either endurance or strength training,” *J. Appl. Physiol.*, vol. 109, no. 5, pp. 1455–1466, 2010.

[121] F. Bellemare, J. J. Woods, R. Johansson, and B. Bigland Ritchie, “Motor-unit discharge rates in maximal voluntary contractions of three human muscles,” *J. Neurophysiol.*, vol. 50, no. 6, pp. 1380–1392, 1983.
[122] M. Pournezam, B. J. Andrews, R. H. Baxendale, G. F. Phillips, and J. P. Paul, “Reduction of muscle fatigue in man by cyclical stimulation,” *J. Biomed. Eng.*, vol. 10, no. 2, pp. 196–200, 1988.
[123] H. M. Franken, P. H. VeItink, M. Fidder, and H. B. K. Boom, “Fatigue of intermittently stimulated quadriceps during imposed cyclical lower leg movements,” in *1992 14th Annual International Conference of the IEEE Engineering in Medicine and Biology Society*, 1992, vol. 4, pp. 1341–1342.
[124] J. S. Petrofsky, “Sequential motor unit stimulation through peripheral motor nerves in the cat,” *Med.& Biol. Eng. Comput*, vol. 17, no. January, pp. 87–93, 1979.
[125] J. S. Petrofsky and A. R. Lind, “Isometric endurance in fast and slow muscles in the cat,” *Am. J. Physiol. - Cell Physiol.*, vol. 5, no. 3, 1979.
[126] T. I. H. Brown, Y. Huang, D. L. Morgan, U. Proske, and A. Wise, “A new strategy for controlling the level of activation in artificially stimulated muscle,” *IEEE Trans. Rehabil. Eng.*, vol. 7, no. 2, pp. 167–173, 1999.
[127] S. C. K. Lee, D. W. Russ, and S. A. Binder-Macleod, “Force-Frequency Relation of Skeletal Muscle,” in *Encyclopedia of Neuroscience*, M. D. Binder, N. Hirokawa, and U. Windhorst, Eds. Berlin, Heidelberg: Springer Berlin Heidelberg, 2009, pp. 1608–1611.
[128] E. D. H. Zonnevijlle *et al.*, “Sequential Segmental Neuromuscular Stimulation Reduces Fatigue and Improves Perfusion in Dynamic Graciloplasty,” *Ann. Plast. Surg.*, vol. 45, no. 3, pp. 292–7, 2000.
[129] L. Z. P. Maneski, N. M. Malešević, A. M. Savić, T. Keller, and D. B. Popović, “Surface-distributed low-frequency asynchronous stimulation delays fatigue of stimulated muscles,” *Muscle Nerve*, vol. 48, no. 6, pp. 930–937, 2013.
[130] N. M. Malešević, L. Z. Popović, L. Schwirtlich, and D. B. Popović, “Distributed low-frequency functional electrical stimulation delays muscle fatigue compared to conventional stimulation,” *Muscle and Nerve*, vol. 42, no. 4, pp. 556–562, 2010.
[131] D. G. Sayenko, R. Nguyen, M. R. Popovic, and K. Masani, “Reducing muscle fatigue during transcutaneous neuromuscular electrical stimulation by spatially and sequentially distributing electrical stimulation sources,” *Eur. J. Appl. Physiol.*, vol. 114, no. 4, pp. 793–804, 2014.
[132] R. J. Downey, M. J. Bellman, H. Kawai, C. M. Gregory, and W. E. Dixon, “Comparing the Induced Muscle Fatigue Between Asynchronous and Synchronous Electrical Stimulation in Able-Bodied and Spinal Cord Injured Populations,” *IEEE Trans. Neural Syst. Rehabil. Eng.*, vol. 23, no. 6, pp. 964–972, 2015.
[133] M. Thomsen and P. H. Veltink, “Influence of synchronous and sequential stimulation on muscle fatigue,” *Med. Biol. Eng. Comput.*, vol. 35, no. 3, p. 186—192, May 1997.
[134] K. Yoshida and K. Horch, “Reduced fatigue in electrically stimulated

muscle using dual channel intrafascicular electrodes with interleaved stimulation," *Ann. Biomed. Eng.*, vol. 21, no. 6, pp. 709–714, 1993.
[135] K. Yoshida and K. Horch, "Selective Stimulation of Peripheral Nerve Fibers using Dual Intrafascicular Electrodes," *IEEE Trans. Biomed. Eng.*, vol. 40, no. 5, 1993.
[136] H. K. Lau, J. Liu, B. P. Pereira, V. P. Kumar, and R. W. Pho, "Fatigue reduction by sequential stimulation of multiple motor points in a muscle.," *Clin. Orthop. Relat. Res.*, no. 321, pp. 251–258, Dec. 1995.
[137] P. H. Peckham, J. P. Van Der Meulen, and J. B. Reswick, "Electrical Activation of Skeletal Muscle by Sequential Stimulation," in *The Nervous System and Electric Currents: Proceedings of the Third Annual National Conference of the Neuro-Electric Society, held in Las Vegas, Nevada, March 23--25, 1970*, N. L. Wulfsohn and A. Sances, Eds. Boston, MA: Springer US, 1970, pp. 45–49.
[138] A. J. Buckmire, D. R. Lockwood, C. J. Doane, and A. J. Fuglevand, "Distributed stimulation increases force elicited with functional electrical stimulation," *J. Neural Eng.*, vol. 15, no. 2, 2018.
[139] M. J. Wiest, A. J. Bergquist, H. L. Schimidt, K. E. Jones, and D. F. Collins, "Interleaved neuromuscular electrical stimulation: Motor unit recruitment overlap," *Muscle and Nerve*, vol. 55, no. 4, pp. 490–499, 2017.
[140] M. Tate, "Characterizing the Ripple in Force Output during Asynchronous and Conventional Stimulation," BSc thesis University of Florida, 2013.
[141] R. J. Downey, M. Tate, H. Kawai, and W. E. Dixon, "Comparing the force ripple during asynchronous and conventional stimulation," *Muscle and Nerve*, vol. 50, no. 4, pp. 549–555, 2014.
[142] A. C. Hughes, L. Guo, and S. P. Deweerth, "Interleaved multichannel epimysial stimulation for eliciting smooth contraction of muscle with reduced fatigue.," *Conf Proc IEEE Eng Med Biol Soc*, vol. 2010, pp. 6226–6229, 2010.
[143] T. Stieglitz, M. Schuettler, A. Schneider, E. Valderrama, and X. Navarro, "Noninvasive Measurement of Torque Development in the Rat Foot: Measurement Setup and Results from Stimulation of the Sciatic Nerve with Polyimide-Based Cuff Electrodes," *IEEE Trans. Neural Syst. Rehabil. Eng.*, vol. 11, no. 4, pp. 427–437, 2003.
[144] W. L. C. Rutten, H. J. Van Wier, and J. H. M. Put, "Sensitivity and Selectivity of Intrneural Stimulation using a Silicon Electrode Aray," *IEEE Trans. Biomed. Eng.*, vol. 38, no. 2, pp. 192–198, 1991.
[145] D. Arthur and S. Vassilvitskii, "K-means++: The advantages of careful seeding," *Proc. Annu. ACM-SIAM Symp. Discret. Algorithms*, vol. 07-09-Janu, pp. 1027–1035, 2007.
[146] M. F. W. Festing, "Randomized block experimental designs can increase the power and reproducibility of laboratory animal experiments," *ILAR J.*, vol. 55, no. 3, pp. 472–476, 2014.
[147] N. J. M. Rijkhoff and T. Sinkjaer, "Orderly recruitment of motoneurons in an acute rabbit model," in *Proceedings of the 20th Annual International Conference of the IEEE Engineering in Medicine and Biology Society. Vol.20 Biomedical Engineering Towards the Year 2000*

*and Beyond (Cat. No.98CH36286)*, 1998, vol. 5, pp. 2564–2565 vol.5.
[148] G. E. Loeb, C. A. Pratt, C. M. Chanaud, and F. J. R. Richmond, "Distribution and innervation of short, interdigitated muscle fibers in parallel-fibered muscles of the cat hindlimb," *J. Morphol.*, vol. 191, no. 1, pp. 1–15, 1987.
[149] P. E. Crago, P. H. Peckham, and G. B. Thrope, "Modulation of Muscle Force by Recruitment During Intramuscular Stimulation," *IEEE Trans. Biomed. Eng.*, vol. BME-27, no. 12, pp. 679–684, 1980.
[150] J. A. Gruner and C. P. Mason, "Nonlinear muscle recruitment during intramuscular and nerve stimulation," *J. Rehabil. Res. Dev.*, vol. 26, no. 2, pp. 1–16, 1989.
[151] T. Gordon and J. E. T. de Zepetnek, "Motor unit and muscle fiber type grouping after peripheral nerve injury in the rat," *Exp. Neurol.*, vol. 285, pp. 24–40, 2016.
[152] V. F. Rafuse and T. Gordon, "Self-reinnervated cat medial gastrocnemius muscles. II. Analysis of the mechanisms and significance of fiber type grouping in reinnervated muscles," *J. Neurophysiol.*, vol. 75, no. 1, pp. 282–297, 1996.
[153] O. I. Weeks and A. W. English, "Cat triceps surae motor nuclei are organized topologically," *Exp. Neurol.*, vol. 96, no. 1, pp. 163–177, 1987.
[154] B. R. MacIntosh and C. C. Kupsh, "Staircase, fatigue, and caffeine in skeletal muscle in situ.," *Muscle Nerve*, vol. 10, no. 8, pp. 717–722, Oct. 1987.
[155] D. Kernell, "Muscle regionalization," *Can J Appl Physiol.*, vol. 23, no. 1, pp. 1–22, 1998.
[156] P. E. Galvas and W. J. Gonyea, "Motor-end-plate and nerve distribution in a histochemically compartmentalized pennate muscle in the cat," *Am. J. Anat.*, vol. 159, no. 2, pp. 147–156, 1980.
[157] S. Vanden Noven, P. F. Gardiner, and K. L. Seburn, "Motoneurons innervating two regions of rat medial gastrocnemius muscle with differing contractile and histochemical properties," *Acta Anat. (Basel).*, vol. 150, no. 4, pp. 282–293, 1994.
[158] A. L. Kost and G. J. Kost, "A comparison of fiber types and measurement techniques in the medial gastrocnemius and soleus muscles of the rabbit.," *Microsc. Acta*, vol. 86, no. 1, pp. 25–36, 1982.
[159] L. C. Wang and D. Kernell, "Proximo-distal organization and fibre type regionalization in rat hindlimb muscles," *J. Muscle Res. Cell Motil.*, vol. 21, no. 6, pp. 587–598, 2000.
[160] M. Vromans and P. Faghri, "Electrical Stimulation Frequency and Skeletal Muscle Characteristics: Effects on Force and Fatigue," *Eur. J. Transl. Myol.*, vol. 27, no. 4, pp. 239–245, 2017.
[161] C. S. Bickel, J. M. Slade, G. L. Warren, and G. A. Dudley, "Fatigability and Variable-Frequency Train Stimulation of Human Skeletal Muscles," *Phys. Ther.*, vol. 83, no. 4, pp. 366–373, 2003.
[162] S. A. Binder-Macleod and T. Guerin, "Preservation of force output through progressive reduction of stimulation frequency in human quadriceps femoris muscle," *Phys. Ther.*, vol. 70, no. 10, pp. 619–625, 1990.
[163] R. Kobetic *et al.*, "Implanted functional electrical stimulation system for

mobility in paraplegia: A follow-up case report," *IEEE Trans. Rehabil. Eng.*, vol. 7, no. 4, pp. 390–398, 1999.

[164] P. Smith Keith Roscoe, "An externally powered, multichannel, implantable stimulator for versatile control of paralized muscle," *IEEE Trans. Biomed. Eng.*, vol. BME-34, n°, no. 4, pp. 499–508, 1987.

[165] G. E. Loeb *et al.*, "BION/sup TM/. Bionic neurons for functional and therapeutic electrical stimulation," in *Proceedings of the 20th Annual International Conference of the IEEE Engineering in Medicine and Biology Society. Vol.20 Biomedical Engineering Towards the Year 2000 and Beyond (Cat. No.98CH36286)*, 1998, vol. 5, pp. 2305–2309 vol.5.

[166] R. Davoodi, M. Hauschild, J. Lee, P. T. Montazemi, and G. E. Loeb, "Biomimetic control of FES reaching," in *Proceedings. 2005 First International Conference on Neural Interface and Control, 2005.*, 2005, pp. 177–181.

[167] G. E. Loeb, "Reanimating paralyzed limbs coping with spatially distributed, multimodal systems," in *Proceedings of the Second Joint 24th Annual Conference and the Annual Fall Meeting of the Biomedical Engineering Society] [Engineering in Medicine and Biology*, 2002, vol. 3, pp. 2066–2067 vol.3.

[168] A. Eladly *et al.*, "Interleaved intramuscular stimulation with minimally overlapping electrodes evokes smooth and fatigue resistant forces," *J. Neural Eng.*, vol. 17, no. 4, 2020.

[169] B. K. Thurgood, D. J. Warren, N. M. Ledbetter, G. A. Clark, and R. R. Harrison, "A Wireless Integrated Circuit for 100-Channel Charge-Balanced Neural Stimulation," *IEEE Trans. Biomed. Circuits Syst.*, vol. 3, no. 6, pp. 405–414, 2009.

[170] D. K. Piech *et al.*, "A wireless millimetre-scale implantable neural stimulator with ultrasonically powered bidirectional communication," *Nat. Biomed. Eng.*, vol. 4, no. 2, pp. 207–222, 2020.

[171] T. Kim, P. R. Troyk, and M. Bak, "Active Floating Micro Electrode Arrays (AFMA)," in *2006 International Conference of the IEEE Engineering in Medicine and Biology Society*, 2006, pp. 2807–2810.

[172] A. Ersen, S. Elkabes, D. S. Freedman, and M. Sahin, "Chronic tissue response to untethered microelectrode implants in the rat brain and spinal cord.," *J. Neural Eng.*, vol. 12, no. 1, p. 16019, Feb. 2015.

[173] M. Tudela-Pi, L. Becerra-Fajardo, A. García-Moreno, J. Minguillon, and A. Ivorra, "Power Transfer by Volume Conduction: In Vitro Validated Analytical Models Predict DC Powers Above 1 mW in Injectable Implants," *IEEE Access*, vol. 8, pp. 37808–37820, 2020.

[174] L. Becerra-fajardo, S. Member, M. Schmidbauer, and A. Ivorra, "Demonstration of 2 mm Thick Microcontrolled Injectable Stimulators Based on Rectification of High Frequency Current Bursts," vol. 25, no. 8, pp. 1343–1352, 2017.

[175] A. Sridharan, S. Chirania, B. C. Towe, and J. Muthuswamy, "Remote Stimulation of Sciatic Nerve Using Cuff Electrodes and Implanted Diodes," *Micromachines*, vol. 9, no. 11, p. 595, Nov. 2018.

[176] M. Slovak, A. T. Barker, and C. R. Chapple, "The assessment of a novel electrical stimulation waveform recently introduced for the treatment of overactive bladder.," *Physiol. Meas.*, vol. 34, no. 5, pp. 479–486, May

2013.
[177] L. E. Medina and W. M. Grill, “Nerve excitation using an amplitude-modulated signal with kilohertz-frequency carrier and non-zero offset,” *J. Neuroeng. Rehabil.*, vol. 13, no. 1, p. 63, 2016.
[178] M. Sahin and Y. Tie, “Non-rectangular waveforms for neural stimulation with practical electrodes.,” *J. Neural Eng.*, vol. 4, no. 3, pp. 227–233, Sep. 2007.
[179] W. M. Grill, “Waveforms for Neural Stimulation,” in *Neuromodulation*, Second Edi., E. S. Krames, P. H. Peckham, and A. R. B. T.-N. (Second E. Rezai, Eds. Academic Press, 2018, pp. 95–102.
[180] B. Mercadal, C. B. Arena, R. V Davalos, and A. Ivorra, “Avoiding nerve stimulation in irreversible electroporation: a numerical modeling study.,” *Phys. Med. Biol.*, vol. 62, no. 20, pp. 8060–8079, Oct. 2017.
[181] D. R. McNeal, “Analysis of a Model for Excitation of Myelinated Nerve,” *IEEE Trans. Biomed. Eng.*, vol. BME-23, no. 4, pp. 329–337, Jul. 1976.
[182] C. C. McIntyre, A. G. Richardson, and W. M. Grill, “Modeling the Excitability of Mammalian Nerve Fibers: Influence of Afterpotentials on the Recovery Cycle,” *J. Neurophysiol.*, vol. 87, no. 2, pp. 995–1006, Feb. 2002.
[183] K. W. Altman and R. Plonsey, “Analysis of excitable cell activation: relative effects of external electrical stimuli,” *Med. Biol. Eng. Comput.*, vol. 28, no. 6, pp. 574–580, 1990.
[184] C.-H. Berthold and M. Rydmark, “Electron microscopic serial section analysis of nodes of Ranvier in lumbosacral spinal roots of the cat: ultrastructural organization of nodal compartments in fibres of different sizes,” *J. Neurocytol.*, vol. 12, no. 3, pp. 475–505, 1983.
[185] M. Rydmark, “Nodal axon diameter correlates linearly with internodal axon diameter in spinal roots of the cat,” *Neurosci. Lett.*, vol. 24, no. 3, pp. 247–250, Jul. 1981.
[186] J. N. Barrett and W. E. Crill, “Specific membrane properties of cat motoneurones,” *J. Physiol.*, vol. 239, no. 2, pp. 301–324, Jun. 1974.
[187] B. Frankenhaeuser and A. F. Huxley, “The action potential in the myelinated nerve fiber of Xenopus Laevis as computed on the basis of voltage clamp data,” *J. Physiol.*, vol. 171, no. 2, pp. 302–315, Jun. 1964.
[188] D. Popovic, L. L. Baker, and G. E. Loeb, “Recruitment and Comfort of BION Implanted Electrical Stimulation: Implications for FES Applications,” *IEEE Trans. Neural Syst. Rehabil. Eng.*, vol. 15, no. 4, pp. 577–586, Dec. 2007.
[189] C. van den Honert and J. T. Mortimer, “The response of the myelinated nerve fiber to short duration biphasic stimulating currents,” *Ann. Biomed. Eng.*, vol. 7, no. 2, pp. 117–125, 1979.
[190] A. M. Mcphedran, R. B. Wuerker, and E. Henneman, “Properties of motor units in a heterogeneous pale muscle (M. Gastrocnemius) of the cat.,” *J. Neurophysiol.*, vol. 28, pp. 85–99, Jan. 1965.
[191] R. Malmivuo, Jaakko; Plonsey, “Functional electrical stimulation,” in *Bioelectromagnetism: Principles and Applications of Bioelectric and Biomagnetic Fields*, Oxofrd University Press, 1995, pp. 493–508.
[192] S. Gabriel, R. W. Lau, and C. Gabriel, “The dielectric properties of

biological tissues: III. Parametric models for the dielectric spectrum of tissues," *Phys. Med. Biol.*, vol. 41, no. 11, pp. 2271–2293, Nov. 1996.

[193] S. RUSH, J. A. ABILDSKOV, and McFEER, "Resistivity of body tissues at low frequencies.," *Circ. Res.*, vol. 12, pp. 40–50, Jan. 1963.

[194] R. B. Stein, D. J. Weber, K. M. Chan, G. E. Loeb, R. Rolf, and S. L. Chong, "Stimulation of peripheral nerves with a microstimulator: experimental results and clinical application to correct foot drop," in *In Proceedings of the 9th annual conference of the International FES Society.*, 2004.

[195] C. A. Miller, P. J. Abbas, K. V Nourski, N. Hu, and B. K. Robinson, "Electrode configuration influences action potential initiation site and ensemble stochastic response properties.," *Hear. Res.*, vol. 175, no. 1–2, pp. 200–214, Jan. 2003.

[196] MCNEAL and DR., "Effect of electrode placement on threshold and initial site of excitation of a myelinated nerve fiber," *Funct. Electr. Stimul. Appl. Neural Prostheses.*, pp. 405–412, 1977.

[197] D. R. McNeal, L. L. Baker, and J. T. Symons, "Recruitment data for nerve cuff electrodes: implications for design of implantable stimulators," *IEEE Trans. Biomed. Eng.*, vol. 36, no. 3, pp. 301–308, Mar. 1989.

[198] D. Ahn and M. Ghovanloo, "Optimal Design of Wireless Power Transmission Links for Millimeter-Sized Biomedical Implants," *IEEE Trans. Biomed. Circuits Syst.*, vol. 10, no. 1, pp. 125–137, Feb. 2016.

[199] L. Dai, F. Lin, Z. Zhu, and J. Li, "Electrical characteristics of high energy density multilayer ceramic capacitor for pulse power application," in *IEEE Transactions on Magnetics*, 2005.

# List of publications

## Peer-reviewed journal articles

1) **A. Eladly** *et al.*, "Interleaved intramuscular stimulation with minimally overlapping electrodes evokes smooth and fatigue resistant forces," *J. Neural Eng.*, vol. 17, no. 4, 2020.

2) **A. Eladly**, B. Mercadal , M. Tudela-Pi, A. Ivorra. Analysis of the stimulation efficiency and miniaturization potential of injectable wireless microstimulator based on volume conduction . [**under preparation**]

3) B. Mercadal, J. M. Phillips, **A. Eladly**, A. Ivorra "Innervation model for the study of the recruitment patterns in intramuscular electrical stimulation" [**To be submitted**]

4) Aracelys García-Moreno, Laura Becerra-Fajardo, **Ahmed Eladly**, Marc Tudela-Pi, Georgia Sarquella-Brugada and Antoni Ivorra 'Leadless Pacemakers Based on Rectification of Volume Conducted High Frequency Currents for Intrapericardial Pacing' **[under preparation]**

## Abstracts in conference proceedings

1) A**hmed Eladly**, Antoni Ivorra PhD "The Need for Studying the Biocompatibility and Safety of Biomimetic eAXON Neuro-prosthetic Systems" 2018 Summer School on Neurorehabilitation Workshop 10-14 September, 2018, Baiona, Spain.